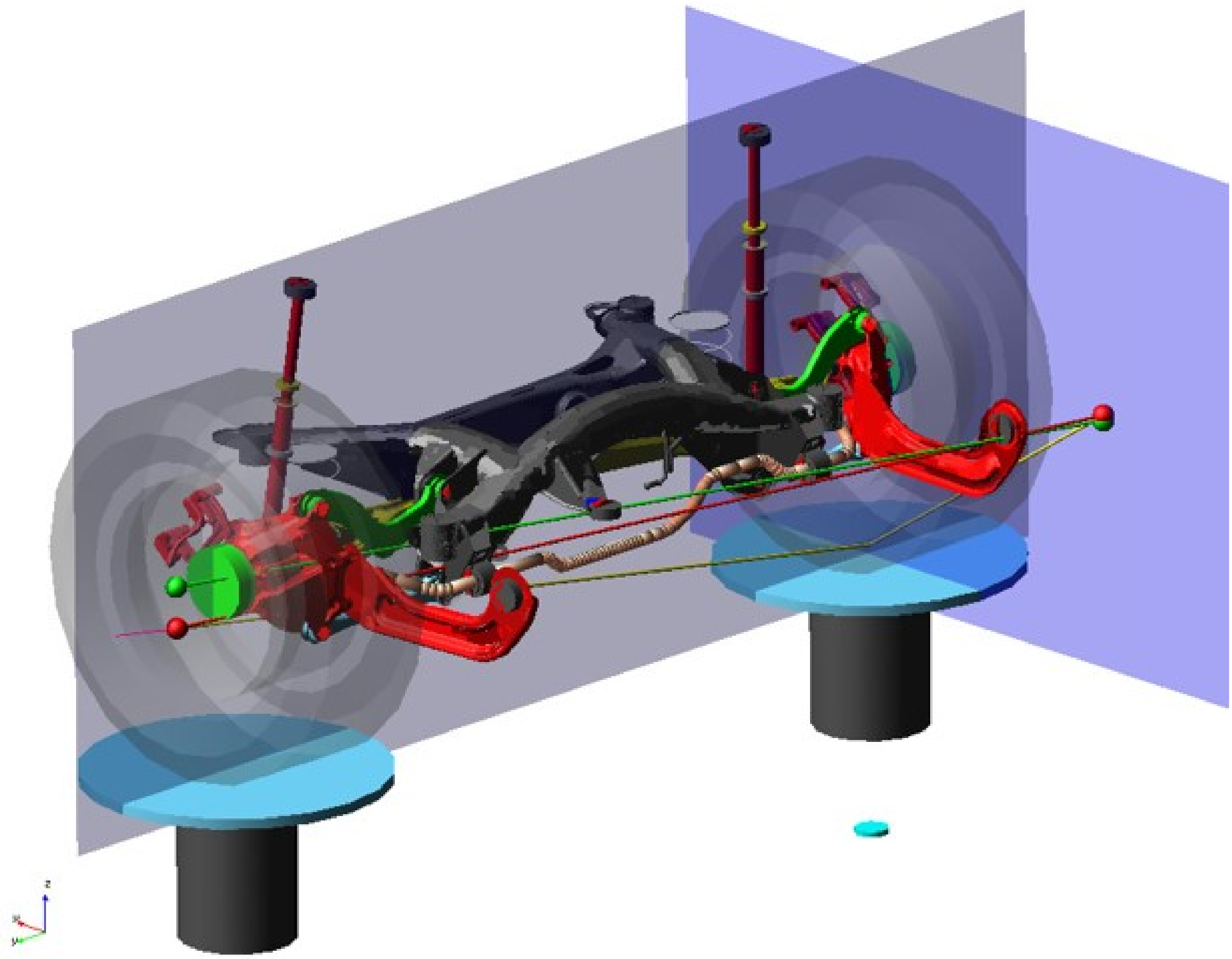

Development of Kinematic Analysis Methods for Spatial Multi-link Road Vehicle Suspensions

Master's thesis in Automotive Engineering and Applied Mechanics

RON GEORGE
SIDHANT RAY

Department of Mechanics and Maritime Sciences
CHALMERS UNIVERSITY OF TECHNOLOGY
Göteborg, Sweden 2018

MASTER'S THESIS IN AUTOMOTIVE ENGINEERING AND APPLIED MECHANICS

Development of Kinematic Analysis Methods for Spatial Multi-link Road Vehicle Suspensions

RON GEORGE
SIDHANT RAY

Department of Mechanics and Maritime Sciences
Division of Vehicle Engineering and Autonomous Systems
CHALMERS UNIVERSITY OF TECHNOLOGY

Göteborg, Sweden 2018

Development of Kinematic Analysis Methods for Spatial Multi-link Road Vehicle Suspensions
RON GEORGE
SIDHANT RAY

Master's thesis 2018:71
Department of Mechanics and Maritime Sciences
Division of Vehicle Engineering and Autonomous Systems
Chalmers University of Technology
SE-412 96 Göteborg
Sweden
Telephone: +46 (0)31-772 1000

Cover:
Spatial Suspension of a production vehicle on MSC ADAMS [Image courtesy of CEVT AB]

Chalmers Reproservice
Göteborg, Sweden 2018

Development of Kinematic Analysis Methods for Spatial Multi-link Road Vehicle Suspensions
Master's thesis in Automotive Engineering and Applied Mechanics
RON GEORGE
SIDHANT RAY
Department of Mechanics and Maritime Sciences
Division of Vehicle Engineering and Autonomous Systems
Chalmers University of Technology

Abstract

The fast moving, globalized vehicle industry has put extreme pressures to be able to develop new vehicles at a quicker rate while still being able to keep a high quality of the product. This has made the need for complete understanding of vehicle systems more important while having easy to use tools to make decisions crucial to be able to perform efficiently in this market.

The focus of this thesis is to find and compare various methods of analyzing complex spatial multi-link suspensions and to get a better understanding of these. It also looks into the various parameters of suspension design that affect vehicle dynamic behaviour. These parameters are studied and methods to analyze them for spatial suspension are discussed. The differences between planar suspensions and spatial suspensions in analysis methods are also reviewed. Instantaneous Screw axis is an important concept that is explained and used to understand the behaviour of the spatial suspension and its complex three dimensional motion. The instantaneous screw axis for the chassis is also considered in a specific case.

Basic graphical methods based on Kennedy's theorem are applied for simple planar suspension analysis and to find the roll center. It is found that these simple methods cannot be used for spatial suspensions which do not have a motion in one plane. Thus, $\Delta Y/\Delta Z$ method, Virtual Position Method and Screw Axis Offset Method are found to be accurate methods to find the roll centers for these types of suspensions. They all give the value for the roll center which is defined as Moment Center (MC) of the chassis in this thesis and a force passing through it does not rotate the chassis. These methods define the spatial motion of the suspensions in a plane (wheel planes) for analysis. The Screw Axis Offset Method gives a clear understanding and reasoning for the differences of the roll center in spatial suspensions compared to one that can be erroneously found through approaches similar to those used in planar methods. These are also verified using various multibody models and a model of a production vehicle suspensions.

Finally the instantaneous screw axis for a chassis is also looked into in brief. The instantaneous screw axis of the chassis with and without steering input is studied and a difference in instantaneous screw axis between the two is found.

Keywords: multi-link, suspension, screw axis, spatial suspension, instant screw theory, kinematics, roll center, instantaneous center, Arnold Kennedy theorem, suspension design

Acknowledgements

First of all we would like to thank our supervisors at the Department of Mechanics and Maritime Sciences, Chalmers University of Technology, Prof. Mathias Lidberg, Division of Vehicle Engineering and Autonomous Systems and Prof. Peter Folkow, Division of Dynamics, who have supported us on a daily basis throughout the entire project.

We would also like to thank Jan Hellberg at CEVT AB, Jonas Alfredsson at DsenseD Technology AB and Gunnar Olsson at ÅF Automotive AB for their guidance and invaluable suggestions. The superb image representing MSC Adams Car model of rear subframe and suspension system has also been provided by Jan.

We would like to express our sincere gratitude to administrators and non-teaching staffs at VEAS division, Chalmers University of Technology in providing us a better work place.

We are also grateful to Prof. Bengt Jacobson for granting us opportunity for poster presentation at the SVEA seminar, Model Fidelity for Vehicle Motion Predictions, held in Johanneberg Science Park, Gothenburg.

Finally, we are fortunate to meet our hearty colleagues at VEAS project room catering to explore an efficient work-life balance.

Nomenclature

List of Symbols

α	Slip angle
ΔF_{zi}	Vertical load transferred between wheels of the chosen axle
δ	Steer angle
δ_l	Left steering angle
δ_r	Right steering angle
$\dot{s}$	Rate of pitch
γ	Camber angle
ϕ	Roll angle for vehicle level
σ_i	Load transfer coefficient of the chosen axle
$\boldsymbol{\omega}$	Angular velocity of a rigid body
$pl_{\boldsymbol{n}}\boldsymbol{r}$	Projection vector $\boldsymbol{r}$ on plane with normal vector $\boldsymbol{n}$
$\widehat{\boldsymbol{\omega}}$	Direction of instantaneous screw axis or angular velocity vector of a rigid body
$\boldsymbol{a}$	Offset vector in screw axis offset method
$\boldsymbol{e}_x$	Orthogonal unit vector along X-axis
$\boldsymbol{e}_y$	Orthogonal unit vector along Y-axis
$\boldsymbol{e}_z$	Orthogonal unit vector along Z-axis
$\boldsymbol{F}$	Force vector
$\boldsymbol{I}$	Moment of inertia tensor
$\boldsymbol{L}$	Angular momentum
$\boldsymbol{o}$	Direction of link vector
$\boldsymbol{p}$	Linear momentum
$\boldsymbol{r}$	Position vector
$\boldsymbol{r}_{IA}$	Displacement vector from point I to point A
$\boldsymbol{r}_I$	Position vector of point I in global co-ordinate system
$\boldsymbol{t}$	Pitch velocity vector
$\boldsymbol{u}$	Circumferential velocity vector
$\boldsymbol{u}_A$	Circumferential velocity vector at point A
$\boldsymbol{v}$	Velocity vector
$\boldsymbol{v}_M$	Translational velocity of wheel carrier
a	Longitudinal distance of front axle from center of gravity
a_y	Component of offset vector along Y-axis
a_z	Component of offset vector along Z-axis
a_{centri}	Centrifugal acceleration
b	Longitudinal distance of rear axle from center of gravity
c_α	Cornering stiffness of tire
C_{ϕ_i}	Roll stiffness of the chosen axle
c_ψ	Steering torsional stiffness
e	Caster trail

f	Mobility
F_x	Longitudinal force
F_y	Lateral force
F_z	Vertical force
f_{rot}	Rotational mobility
f_{scr}	Screw mobility
f_{tran}	Translational mobility
h	Height of CoG
h'	Perpendicular distance between roll axis and center of gravity
h_{RC}	Roll center height in center of gravity plane
I_{01}	Instant centers of rotation of link s_1 with respect to link s_0
I_{IA}	Moment of inertia scalar of point mass at point A around center I perperdicular to the plane
j	Number of joints
K	Movability of an unconstrained system
L	Wheelbase of the vehicle
l_f	Distance of CoG from front axle
m	Mass of a body or vehicle
M_{ϕ_i}	Roll moment on the chosen axle
n	Number of rigid bodies
P	Power
P_{yz}	Point of zero velocity for a rigid body on the YZ plane
r	Yaw angle
R_e	Effective rolling radius of the tire
S	Link (in a four bar linkage)
s	Pitch length along instantaneous screw axis
s_i	Track width of the chosen axle
s_x	Longitudinal slip ratio
t	Simulation time
t_x	Pitch velocity component along x-axis
t_y	Pitch velocity component along y-axis
t_z	Pitch velocity component along z-axis
u_x	Circumferential velocity component along x-axis
u_y	Circumferential velocity component along y-axis
u_z	Circumferential velocity component along z-axis
w	Track width

Acronyms

Acronyms	Description
2D	Two-dimensional (Planar)
3D	Three-dimensional (Spatial)
CAE	Computer Aided Engineering
CoG	Center of Gravity
DoF(s)	Degree(s) of Freedom
IC(s)	Instantaneous/ Instant Center(s) of rotation
ISO	International Organization for Standardization
IST	Instant Screw Theory
Jt.	Joint
K & C	Kinematics and Compliance
LBJ	Lower Ball Joint
MBD	Multibody Dynamics
MC(s)	Moment Center(s)
MSC	MacNeal-Schwendler Corporation
RC	Roll Center
SAE	Society of Automotive Engineers
SPMM	Suspension Parameter Measurement Machine
SR	Slip Ratio
SVEA	Swedish Vehicular Engineering Association
TCP	Tire-road Contact Patch
TROJ	Tie-Rod Outer Joint
UBJ	Upper Ball Joint
UWT	Assembly of Upright, Wheel and Tire
WC	Wheel Center

Contents

List of Figures

List of Tables

1 Introduction

1.1 Background

The trend of globalization of the automotive industry continues. Development times are being reduced and product complexity is increasing. For chassis systems, this includes electrification of steering assistance and propulsion. For vehicle dynamics and control the refinement of the suspension is reaching new heights. The dawn of autonomous driving will also bring about new challenges in design and development of chassis systems. This leads to the separation of the design of different subsystems and mechanics and control becoming more challenging due to high interactions. Thus, better understanding of the vehicle is crucial to be able to make quick and efficient design choices and design realization, while still having superior quality in design.

In terms of vehicle dynamics, a lot of the work going on these days is the use of more mechatronic or electronic systems to control the vehicle. Technology has made it possible to create more complex control systems for vehicles and newer powertrain arrangements like separate electric motors for driven wheels with the easier and more powerful controllability of electric motors motivate these innovations which have greatly helped improve performance and safety. They also have major rooms for innovation in the future and thus are the area resources are being shifted. That being said, with all the interest going into these systems, basic mechanical systems and improving them has started to stagnate. The research for continuous better understanding of vehicle systems like the suspension and steering system on a base mechanical level can be useful to understand more complex systems of today. It can also go hand in hand with electrification of system and can also complement them to achieve better results.

1.2 Purpose

With the refinement in vehicle dynamics today and with tighter time constraints for development, efficient methods to understand complex suspensions are needed. Inadequate vehicle dynamics behaviour or properties are unacceptable to the consumer.

Most, if not all vehicle manufacturers rely on carrying over parts of design between their various platforms in order to efficiently use their resources and cut cost and lead times. This kind of platform thinking is essential from an economic standpoint but, smart design decisions are required to balance platform commonalities and vehicle specific performance requirements. For this, quick and easy to use tools are helpful to realize the amount and types of changes needed between platforms and to make educated decisions at early phases of the vehicle design.

Automobiles are some of the most complex pieces of machinery that are built, as they consist of large number of parts. A big challenge in the design of automobiles is the packaging of these numerous parts. Suspension parts are most affected by this for a few reasons. They are parts that move in space and require enough volume not only to fit, but also to move so as to be able to fulfill their functions appropriately. They are parts that are affected greatly by the location of other large components such as powertrain parts such as the engine and the drive shaft. But, the biggest challenge that exists, is that in the case of suspension design, packaging and performance have a very close interaction. The location or coordinates of the suspension hardpoints apart from affecting the packaging volume, also affect performance parameters such as roll center location, camber gain, motion ratio between spring travel and wheel travel and consequently the wheel rate. Thus, a compromise between hardpoint location for performance and packaging is necessary. Packaging issues may also occur at later stages leading to changes required in hardpoints and these need to be done while still fulfilling the vehicle performance requirements. Thus, intuitive tools and knowledge of complex suspensions is necessary here.

Finally, even with useful and accurate results available from commercial softwares, the lack of a proper understandable method to analyze complex suspensions for the designer, can make it difficult to quickly tune and adjust suspension points. Thus, the need is to understand complex suspensions, understand the effect of suspension parameters on the vehicle dynamics, analyze methods to develop complex suspensions and utilize the information in all stages of the vehicle development process.

Spatial suspensions are defined in Section 1.7. Spatial suspensions refer to wheel suspension systems which have complex motions in three-dimensional space and these are used in most vehicles today. The multi-link suspension, which in this thesis is considered the same as a five-link suspension is a suspension having spatial motion usually (*It is possible to have simpler 5-link suspensions as well but they are not seen in cars usually and are thus not considered in this thesis*). Use of complex multi-link suspensions by various car manufacturers on their premium cars points to a more refined vehicle characteristics from these types of suspensions. But, they can be difficult to visualize and analyze and easy to understand methods are not readily available in the public domain and have not been compared with other methods. This thesis aims to shed some light into this area as well.

1.3 Goal

The goal of this thesis is the following:

- To understand multi-link suspension for two axle passenger vehicles.

- To develop, analyze and compare various methods of suspension analysis including planar methods and three dimensional methods.

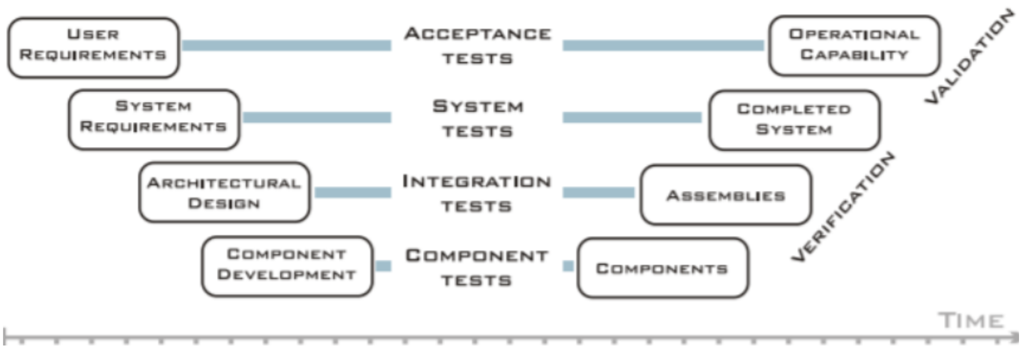

Figure 1.1: Vehicle development V diagram [1]

The Figure 1.1 above shows the product development V diagram [1]. A vehicle life-cycle from conception to launch follows a similar flow. User requirements are set from customer and business point of view and define the market the vehicle is aimed toward. This is followed by the system requirement on the overall vehicle level to achieve these goals. Next is the architectural design of the various subsystems and their connection with each other to fulfill vehicle goals. Finally, on the product definition and design side, the various different components are developed that make up the subsystems. On the verification and validation side, first, the designed components are manufactured and tested to ensure they fulfill component level design requirements. Similarly, subsystem and overall vehicle level assemblies are verified to ensure integration and fulfillment of overall vehicle performance requirements. Finally, the operational capability of the vehicle as a project is validated with respect to initial user requirements.

The work in this project deals specifically with suspension subsystem and thus directly with architectural design, assemblies and integration tests of the product development cycle. But, it also has effect on all the phases of the development as user requirements and operational capability deal with platform thinking choices while system requirements and completed system phases deal with setting vehicle dynamics parameters and types of suspension to be used. Even component level is considered when looking at packaging concerns where component shapes and sizes along with strength and stiffness requirements are looked into for suspension design.

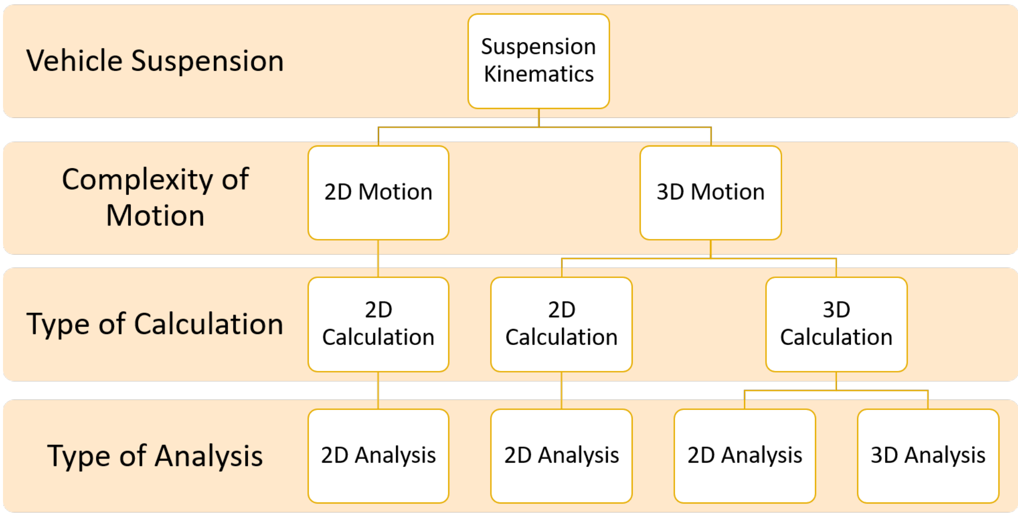

Figure 1.2: Breakdown of Suspension Kinematic Analysis Approaches

In Figure 1.2, the breakdown of the different approaches to analyze suspension kinematics is shown. The suspension geometry can first be classified in terms of its motion which may be in a plane i.e. 2D or in 3D which is to say that they are spatial in nature. For 2D motion, the method of calculation and analysis is in 2D as well. But, for 3D motion, the methods are divided between 2D calculation with 2D analysis and 3D calculation and 2D analysis.

1.4 Delimitations

- This thesis does not quantify or look at the effectiveness and improvement in terms of Multi-link suspensions over other types of suspensions.
- Elastokinematics are not specifically looked into and only kinematics is considered although some methods used can be applicable to both.

1.5 Vehicle Axis System

Due to the usage of various axes and planes to define suspension and vehicle dynamic characteristics in this thesis, a specific coordinate system is followed throughout. The axis or coordinate system used is the ISO8855 standard for defining the vehicle coordinates [2].

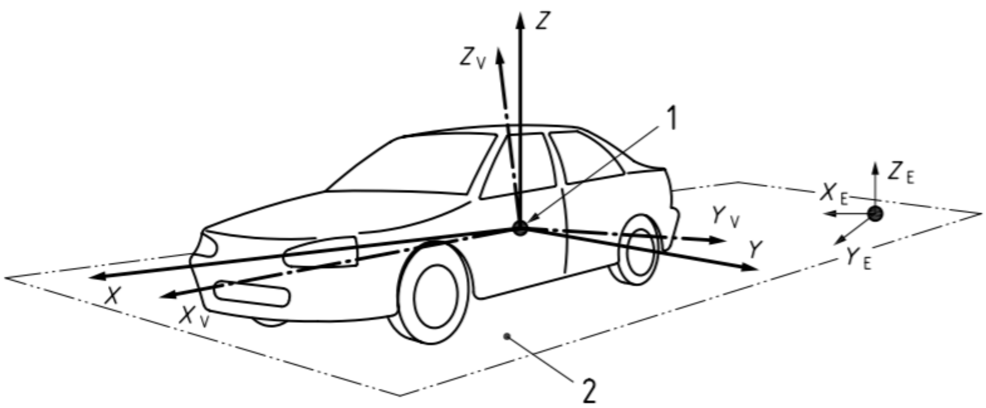

Figure 1.3: Vehicle Axis System [2]

The Figure 1.3 above shows the vehicle axis system used in this thesis. Note that the vehicle coordinate system is considered in this thesis hence, X_V,Y_V,Z_V defined in the ISO system is equivalent to X,Y,Z in this thesis.

Thus, according to this system, positive X axis is pointing to the front of the vehicle, positive Y axis to the left of the vehicle and positive Z axis is pointing upwards. Point 1 in the figure is the reference point for the vehicle, which in the case of this thesis is the centre of gravity of the sprung mass of the vehicle. Also, 2 is the reference plane which here defines the road plane.

In cases where the complete vehicle is not defined and only one suspension or a single axle is defined, a similar axis system is followed with the reference point moving accordingly. Thus, for a suspension, the reference point would move to the wheel center point while for an axle, the reference point would be a point at the center in between the axles at wheel center height. Here, positive X axis is forward from this reference point, positive Y axis is left from this reference point and positive Z is upwards from this reference point.

1.6 Wheel Planes

Apart from the vehicle axis system, another important system used in this thesis is that of wheel planes as shown in Figure 1.4. The suspension can be analyzed about an infinite number of planes but, some planes are more helpful to look at than others as they are easier to comprehend and analyze from a design perspective. In this case, the planes chosen are called the wheel planes. These are the YZ and XZ planes passing through the wheel contact patch i.e. they are the rear view and side view planes respectively. This is because the forces generated by the vehicle are at the contact patches and thus it is logical to look at planes passing through the contact patch. The YZ plane is considered when the roll motion is studied as it occurs around the X axis while the XZ plane is considered when the pitch motion is studied which is defined as the rotation along the Y axis.

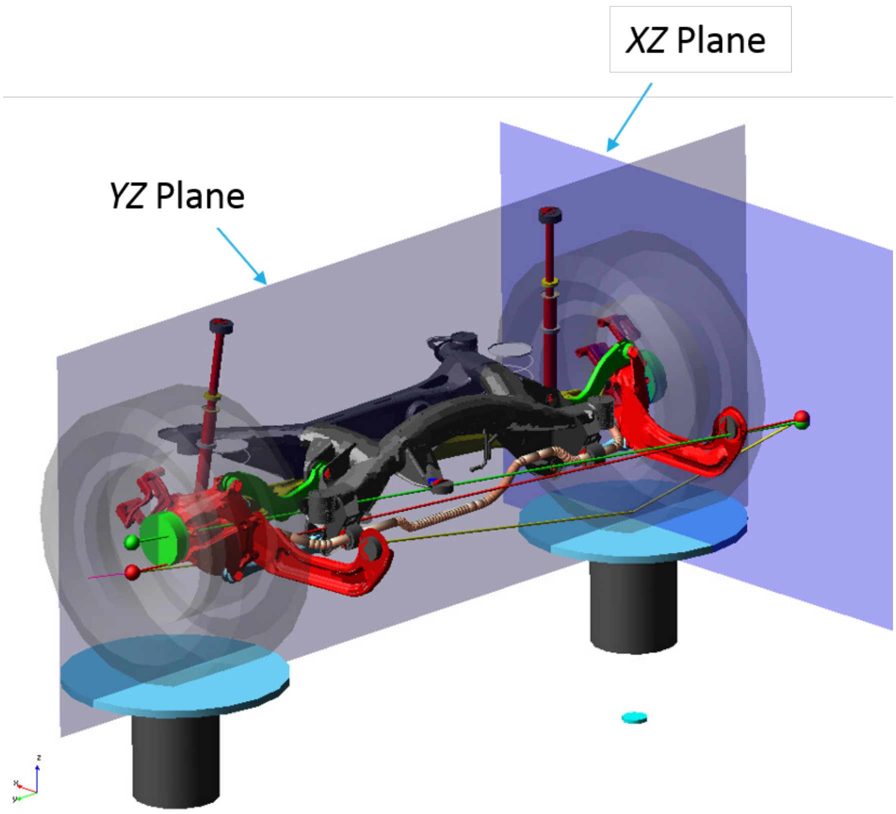

Figure 1.4: Wheel planes depicted for a rear axle [3].

1.7 Types of Suspension Systems

With the focus of this thesis being suspension systems, it is important to establish and explain suspension systems and its types. A suspension system in a vehicle connects the wheels, which are in contact with the ground to the body or chassis and it allows for relative motion between the two [4]. The job of the suspension system is to absorb forces from the road/ground. But, it also controls the orientation of the wheels or the wheel angles as explained in Section 3.3 while the vehicle is in motion to affect the vehicle behaviour.

Suspension systems can be categorized in multiple ways for example with respect to the types of spring used, the configuration of the spring and damper and active or passive suspension to name a few. But, in this report, the categorization deals purely with the kinematic part of the suspension i.e. the different ways the links are connected to the chassis of a vehicle.

Based on the above, there are two types of suspension systems:

- Dependent Suspension - When the motion of one side of the suspension directly influences the motion of the other side of the suspension.
  - Eg: Panhard Rod (Figure 1.5), Watts Linkage
- Independent Suspension - When the motion of one side of the suspension is independent of the motion of the other side of the suspension.
  - Eg: Double Wishbone(Figure 1.6), McPherson's Strut

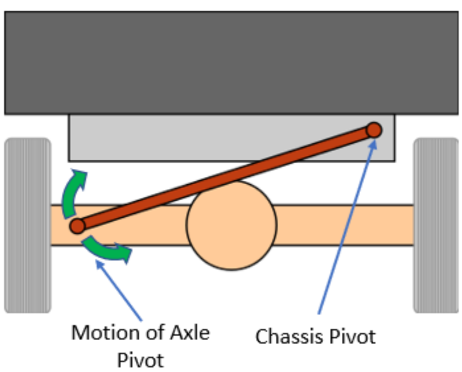

Figure 1.5: Panhard Rod Suspension [5]

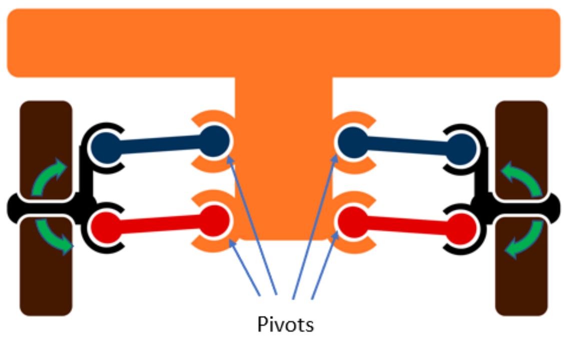

Figure 1.6: Double Wishbone Suspension [6]

The independent suspension system is used more widely in today's cars because of better performance due to the vertical disturbances on each corner of the suspension being mostly isolated from each other. Looking at independent suspension systems in more detail, one way to categorize them is the following [7]:

- Planar Suspension
- Spherical Suspension
- Spatial Suspension

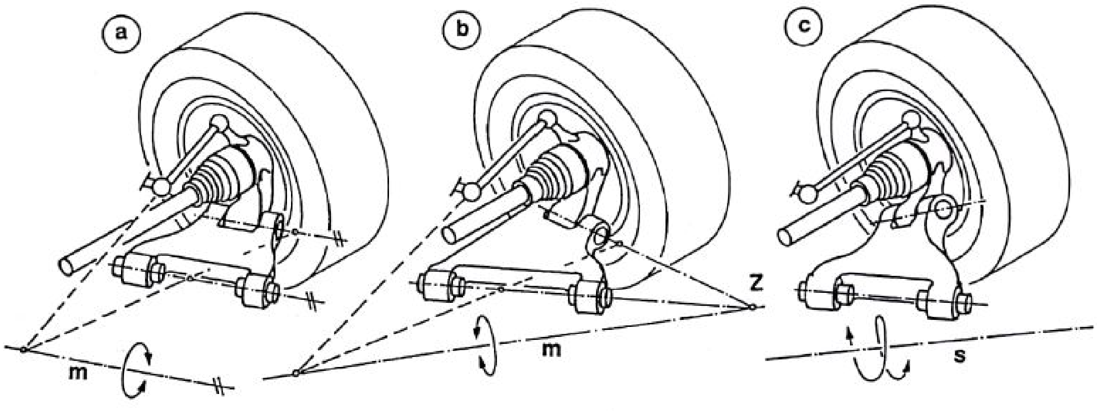

Figure 1.7: Three Types of Independent Suspensions with their Instantaneous Axes of Rotation [7]

1.7.1 Planar Suspension

In this type of independent suspension, the wheel center has an instantaneous axis of rotation which is always directed along its X axis. The wheel centre also does not have any motion(or component of velocity) along the direction of the rotation axis.This means that its instantaneous motion defines a circle. This is illustrated in Figure 1.7 (a).

1.7.2 Spherical Suspension

In this type of independent suspension, the wheel center has an instantaneous axis of rotation which has a component in more than one axis directions. But, similar to the planar suspension, the wheel centre also does not have any motion(or component of velocity) along the direction of the rotation axis. This is illustrated in Figure 1.7 (b).

1.7.3 Spatial Suspension

In this type of independent suspension, the wheel center has an instantaneous axis of rotation which can have an axis of rotation with its component in one or more axis directions. But, in this case, the wheel center has a motion (or component of velocity) in the direction of the rotation axis. This means that its instantaneous motion defines a screw rather than a circle. This is illustrated in Figure 1.7 (c).

2 Theory

2.1 Chebychev–Grübler–Kutzbach criterion

This mobility criterion is used to find the mobility of a kinematic chain or a mechanism [8] where n is number of rigid bodies including the ground as a fixed rigid body, j is the total number of joint pairs, f_i is the number of degrees of freedom (DoF) for the i^{th} joint pair and K is the maximum allowed degrees of freedom for a rigid body or a joint. For any unconstrained rigid body in a spatial motion, there exists 3 translational DoF(s) and 3 rotational DoF(s) leading to total of 6 DoF(s) i.e. $K = 6$. However any rigid body without constraints in planar motion has 2 translational and one rotational summing to 3 DoF(s) or $K = 3$.

Movability of a kinematic system is represented as the $K = 6$ DoF(s) of the system as a whole without being constrained to the ground. However, mobility f, unlike movability, considers only the relative motions of the rigid bodies in the mechanism or kinematic system with respect to ground [9]. $f \leq 0$ represents fully-constrained or over-constrained kinematic chain. Kutzbach criteria for simple closed loop mechanism for planar and spatial motion are mentioned in Equations (2.1) and (2.2). Furthermore, total mobility can be represented as contribution from translational , rotational and screw DoF(s) as in Equation (2.3). Mobilities of joints that are used in suspension system is listed in Table A.1.

$$\text{Planar motion, Mobility: } f = (n-1)K - \sum_{i=1}^{j}(K - f_i) \qquad K = 3 \tag{2.1}$$

$$\text{Spatial motion, Mobility: } f = (n-1)K - \sum_{i=1}^{j}(K - f_i) \qquad K = 6 \tag{2.2}$$

$$\text{Mobilty based on freedom: } f = f_{rot} + f_{tran} + f_{scr} \tag{2.3}$$

2.2 The Instantaneous Center of Rotation of a Rigid Body

Consider a rigid body with planar motion with movability of $K = 3$ DoF(s) as shown in Figure 2.1a. At every instant, there exists instantaneous center of rotation (IC) represented as I in the figure, around which the body rotates with angular velocity $\boldsymbol{\omega}$ perpendicular to the plane. The Equation (2.5) is then solved to find the unknown position vector of the instantaneous center of rotation, $\boldsymbol{r}_I$, if other parameters in the equation are known for a particular instant.

$$\boldsymbol{r}_{IA} = \boldsymbol{r}_A - \boldsymbol{r}_I \tag{2.4}$$

$$\boldsymbol{v}_A = \boldsymbol{\omega} \times \boldsymbol{r}_{IA} \tag{2.5}$$

2.2.1 Based on Angular Momentum

Now assume that the rigid body S_1 is lumped to n identical point masses, S_A, as depicted in Figure 2.1b, such that condition in the Equation (2.6) is satisfied. Consider a point mass on the rigid body at position A as shown in Figure 2.1c. Linear momentum $\boldsymbol{p}_A$ with an arm $\boldsymbol{r}_{IA}$ creates an angular momentum $\boldsymbol{L}_{IA}$ about the center I as represented in Equation (2.7). However, $\boldsymbol{L}_{IA}$ depends on moment of inertia scalar perpendicular to the XY plane [10], I_{IA}, and angular velocity, $\boldsymbol{\omega}$, as mentioned in Equation (2.8). These two relations are then expanded as represented in Equations (2.11) and (2.12). Using the expanded relations, an expression for $\boldsymbol{\omega}$ is derived as shown in Equation (2.13). The numerator signifies the importance of orientation of arm with respect to velocity of the linear momentum. The denominator also denotes the importance of the length of the moment arm. It is also worth considering the fact that the angular velocity vector, $\boldsymbol{\omega}$, passes through the IC, I, perpendicular to the plane of motion. However, since the body is experiencing free motion without constraints, IC, I, is considered only to be instant center of zero velocity but not moment center of zero angular momentum as mentioned in Section 2.3. Here, the angular velocity vector is also the instantaneous screw axis of the body with zero pitch velocity. The instantaneous screw axis will be briefly discussed in Section 2.5.

2.3 Moment center

Contraints as mentioned in Equations (2.14) and (2.15) are incorporated by adding fixed revolute joint at IC, I and constant length link L_1 between the IC and the point mass as shown in Figure 2.2 leading to planar mechanism with $f = 1$. The link is assumed to be massless to ignore its inertial effects. The angular moment becomes zero under the constraints in the following cases:

- When the length of the arm is zero i.e. $|\boldsymbol{r}_{IA}| = 0$
- When the linear momentum, $\boldsymbol{p}_A$ is zero i.e. $\boldsymbol{v}_A = 0$
- the linear momentum, $\boldsymbol{p}_A$, and the arm, $\boldsymbol{r}_{IA}$ are parallel vectors i.e $\boldsymbol{r}_{IA} \times \boldsymbol{p}_A = 0$

In the above mentioned cases of zero angular momentum, the linear momentum $\boldsymbol{p}_A \neq 0$ must act on or directed towards the constrained instantaneous center of rotation, I. Hence the constrained IC, I, qualifies to be a moment center (MC). This implies all fixed IC(s) are fixed MC(s). However some moving IC(s) associated with similar constraints are also instant moment centers and these moments centers will be discussed in Section 2.4.

$$m(S_1) = n \cdot m(S_A) \tag{2.6}$$

$$\boldsymbol{L}_{IA} = \boldsymbol{r}_{IA} \times \boldsymbol{p}_A \tag{2.7}$$
$$\boldsymbol{L}_{IA} = I_{IA} \cdot \boldsymbol{\omega} \tag{2.8}$$

where

$$\text{Linear momentum: } \boldsymbol{p}_A = m(S_A)\boldsymbol{v}_A \tag{2.9}$$
$$\text{Moment of Inertia: } I_{IA} = m(S_A)|\boldsymbol{r}_{IA}|^2 \tag{2.10}$$

The Equations (2.7) and (2.8) expands to:

$$\boldsymbol{L}_{IA} = \boldsymbol{r}_{IA} \times m(S_A)\boldsymbol{v}_A \tag{2.11}$$
$$\boldsymbol{L}_{IA} = m(S_A)|\boldsymbol{r}_{IA}|^2\boldsymbol{\omega} \tag{2.12}$$

Using the above two equations,

$$\boldsymbol{\omega} = \frac{\boldsymbol{r}_{IA} \times \boldsymbol{v}_A}{|\boldsymbol{r}_{IA}|^2} \tag{2.13}$$

Constraints

$$\text{Fixed IC: } \boldsymbol{\Delta r}_I = 0 \qquad \forall\ t \tag{2.14}$$
$$\text{Constant length: } \boldsymbol{\Delta}|\boldsymbol{r}_{IA}| = 0 \qquad \forall\ t \tag{2.15}$$

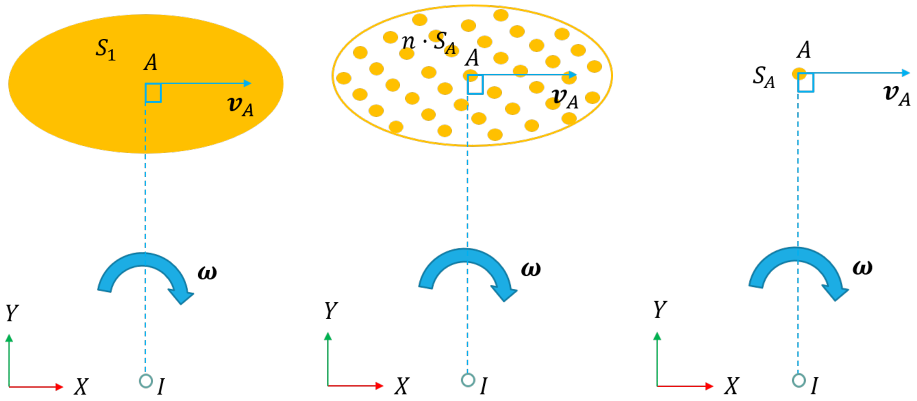

(a) Rigid body (b) Lumped mass (c) Point mass

Figure 2.1: Instantaneous center of rotation for planar motion

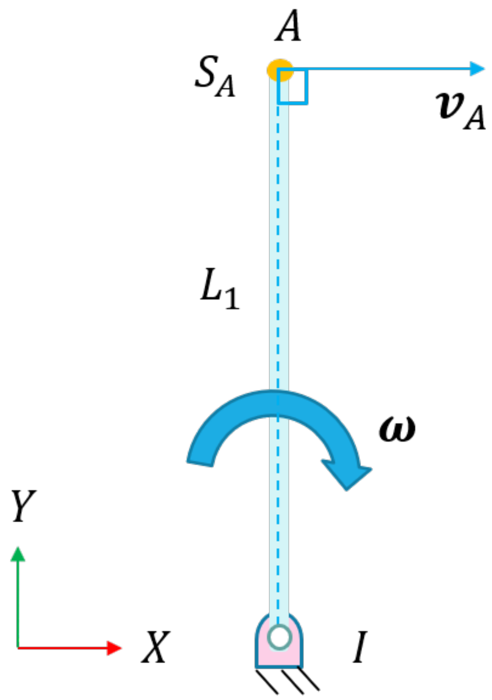

Figure 2.2: Planar motion with constraints

2.4 Arnold Kennedy Theorem

When three rigid bodies are in relative planar motion to each other forming a mechanism, they share instantaneous centers of rotation which lie on the same line. As shown in Figure 2.3, three rigid bodies S_0, S_1 and S_2 are in relative planar motion. S_0 is fixed, S_1 and S_2 are cranks connected to S_0 by revolute joints at fixed IC(s) or MC(s) I_{01} and I_{02} respectively. S_1 and S_2 meets at moving instantaneous center of rotation, I_{12}. The cranks S_1 and S_2 have relative angular velocities with the fixed body S_0 which are $\boldsymbol{\omega}_{01}$ and $\boldsymbol{\omega}_{02}$ respectively. Velocity of I_{12} is found using kinematic Equations (2.17) and (2.18). The relation mentioned in Equation (2.19) is obtained from the kinematic equations. This relation is valid only when the IC(s) I_{01}, I_{12} and I_{02} are collinear. Furthermore, this theorem is applied to estimate the relation between the angular velocities $\boldsymbol{\omega}_{01}$ and $\boldsymbol{\omega}_{02}$, and gear radii $\boldsymbol{r}_{I_{01}I_{12}}$ and $\boldsymbol{r}_{I_{02}I_{12}}$ as shown in Figure 2.4. Here I_{12} is the contact point the rigid gears S_1 and S_2. However, if the contact point is replaced with a physical revolute joint connecting S_1 and S_2, the kinematic chain will be completely constrained with $f = 0$.

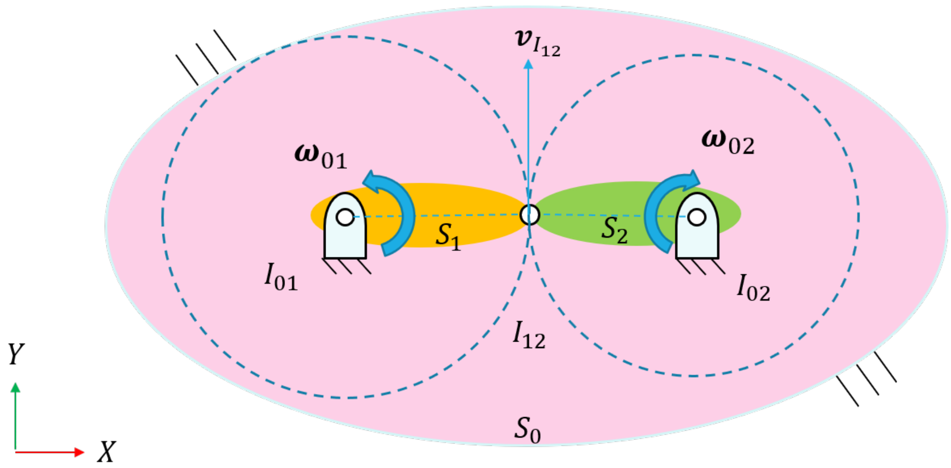

Figure 2.3: Kennedy's theorem illustrated with 3 rigid bodies

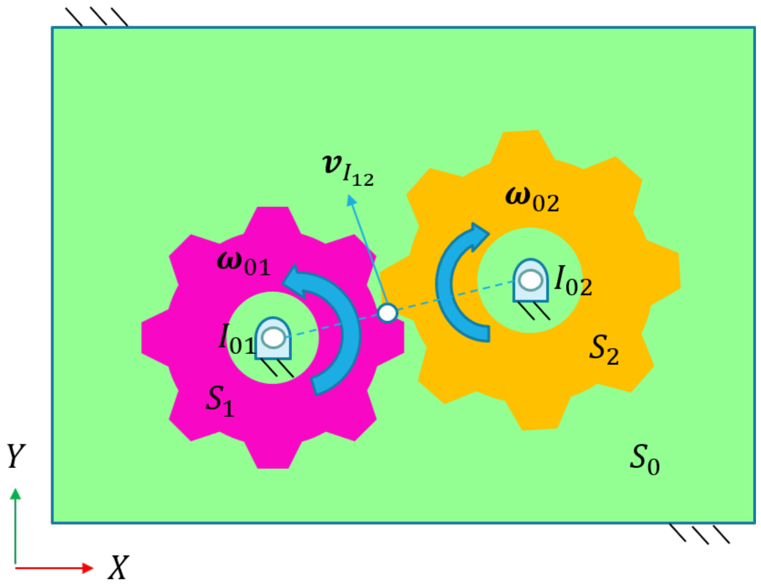

Figure 2.4: Kennedy's theorem in gear coupling

$$\boldsymbol{r}_{I_{02}I_{12}} = \boldsymbol{r}_{I_{12}} - \boldsymbol{r}_{I_{02}} \tag{2.16}$$
$$\boldsymbol{v}_{I_{12}} = \boldsymbol{r}_{I_{02}I_{12}} \times \boldsymbol{\omega}_{02} \tag{2.17}$$
$$\boldsymbol{v}_{I_{12}} = \boldsymbol{r}_{I_{01}I_{12}} \times \boldsymbol{\omega}_{01} \tag{2.18}$$

Using above equations

$$\boldsymbol{r}_{I_{01}I_{12}} \times \boldsymbol{\omega}_{01} = \boldsymbol{r}_{I_{02}I_{12}} \times \boldsymbol{\omega}_{02} \tag{2.19}$$

2.4.1 Four bar mechanism

Consider a four bar mechanism with two cranks, a coupler and a fixed link as shown in Figure 2.5. The cranks S_1 and S_3 are connected to the fixed link S_0 by revolute joints at the fixed IC(s) or MC(s), I_{01} and I_{03} respectively. The coupler is connected to the cranks, S_1 and S_3, with moving revolute joints initially located at the points I_{12} and I_{23}. The cranks and coupler, S_1, S_2 and S_3 have relative angular velocities with the fixed body S_0 which are $\boldsymbol{\omega}_{01}$, $\boldsymbol{\omega}_{02}$ and $\boldsymbol{\omega}_{03}$ respectively. Since the point I_{12} represent the center of relative rotation between the links S_1 and S_2, and the point I_{23} represents the same between the links S_2 and S_3, thus I_{12} and I_{23} can be considered as moving instant centers. But S_2, being a rigid body, also moves in plane relative to the fixed link S_0, thereby, adding an IC, I_{02} as shown in Figure 2.5. The velocities at the moving IC(s) I_{12} and I_{23} are found using the kinematic equation systems, Equations (2.20) and (2.21), and Equations (2.23) and (2.24) respectively. Based on the kinematic equation systems, the relation Equations (2.22) and (2.25) are obtained for each equation system. These relations are valid only if conditions of Kennedy theorem are satisfied, i.e., IC(s) I_{01}, I_{12} and I_{02} are collinear, and I_{02}, I_{23} and I_{03} are also collinear at every instant. Further using Equations (2.22) and (2.25), kinematic Equation (2.26) of the mechanics is obtained. From the Equation (2.26), it is observed that I_{02} is not just a moving IC but also a instant moment center of the coupler S_2, since I_{02} is dependent to the constant length constraints and fixed IC(s) constraints. As a result, mobility of the mechanism becomes $f = 1$.

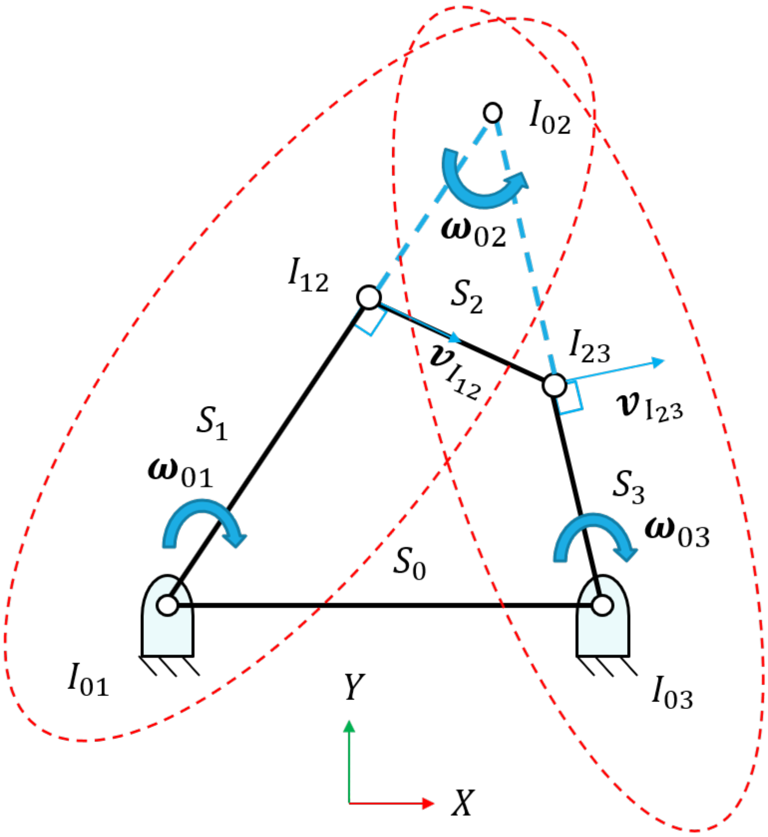

Figure 2.5: Kennedy's theorem explained with 4 bar mechanism

Kinematic equation system for $\boldsymbol{v}_{I_{12}}$:

$$\boldsymbol{v}_{I_{12}} = \boldsymbol{r}_{I_{01}I_{12}} \times \boldsymbol{\omega}_{01} \tag{2.20}$$

$$\boldsymbol{v}_{I_{12}} = \boldsymbol{r}_{I_{02}I_{12}} \times \boldsymbol{\omega}_{02} \tag{2.21}$$

Using the above equation system to obtain the relation

$$\boldsymbol{r}_{I_{01}I_{12}} \times \boldsymbol{\omega}_{01} = \boldsymbol{r}_{I_{02}I_{12}} \times \boldsymbol{\omega}_{02} \tag{2.22}$$

Kinematic equation system for $\boldsymbol{v}_{I_{23}}$:

$$\boldsymbol{v}_{I_{23}} = \boldsymbol{r}_{I_{03}I_{23}} \times \boldsymbol{\omega}_{03} \tag{2.23}$$

$$\boldsymbol{v}_{I_{23}} = \boldsymbol{r}_{I_{02}I_{23}} \times \boldsymbol{\omega}_{02} \tag{2.24}$$

Using the above equation system to obtain the relation

$$\boldsymbol{r}_{I_{03}I_{23}} \times \boldsymbol{\omega}_{03} = \boldsymbol{r}_{I_{02}I_{23}} \times \boldsymbol{\omega}_{02} \tag{2.25}$$

Using Equations (2.22) and (2.25),

$$\boldsymbol{r}_{I_{03}I_{23}} \times \boldsymbol{\omega}_{03} - \boldsymbol{r}_{I_{01}I_{12}} \times \boldsymbol{\omega}_{01} = \boldsymbol{r}_{I_{02}I_{23}} \times \boldsymbol{\omega}_{02} - \boldsymbol{r}_{I_{02}I_{12}} \times \boldsymbol{\omega}_{02} \tag{2.26}$$

Constraints

$$\text{Fixed IC: } \boldsymbol{\Delta r}_{I_{01}} = \boldsymbol{\Delta r}_{I_{03}} = 0 \qquad \forall\, t \tag{2.27}$$

$$\text{Constant length: } \boldsymbol{\Delta}|\boldsymbol{r}_{I_{01}I_{12}}| = \boldsymbol{\Delta}|\boldsymbol{r}_{I_{12}I_{23}}| = \boldsymbol{\Delta}|\boldsymbol{r}_{I_{23}I_{03}}| = \boldsymbol{\Delta}|\boldsymbol{r}_{I_{01}I_{03}}| = 0 \qquad \forall\, t \tag{2.28}$$

2.5 The Instant Screw Theory

Many previous works have defined this theory in different ways. Matschinsky[7] and Suh [11] have comprehensively explained this theory. The theory provides a way to represent any rigid body motion (2D or 3D) with a combination of rotation and translation along the instantaneous screw axis at a particular instant. The instantaneous screw axis represents the angular velocity vector $\boldsymbol{\omega}$ of a rigid body at the particular instant. However, the position of the instantaneous screw axis, $\boldsymbol{r}_I$ and rate of pitch, $\dot{s}$, along the direction of instantaneous screw axis, $\widehat{\boldsymbol{\omega}}$ at the instant are the additional information obtained through instant screw theory as shown in Figure 2.6. The velocity at any location e.g point I on the instantaneous screw axis is the pitch velocity $\boldsymbol{t}$ along the instantaneous screw axis as mentioned in Equations (2.29) and (2.31). However, the velocity at any location A which is not on the instantaneous screw axis is combination of the pitch velocity, $\boldsymbol{t}$ and the circumferential velocity, $\boldsymbol{u}_A$ as represented in Equations (2.30) and (2.32). While analyzing the kinematics of an independent suspension system, this theory can be applied to study the motion of the assembly of upright, wheel and tire (UWT) as a rigid body. In complex spatial suspensions as shown in Figure 1.7, the UWT moves in a screw motion as it rotates and translates about an axis instantaneously. However, like instant moment center mentioned in the Sections 2.3 and 2.4.1 instantaneous screw axis can become instant moment axis if similar constraints are satisfied. Application of this theory will be further discussed in Section 4.2.3 and Chapter 5.

$$\boldsymbol{t} = \dot{s}\boldsymbol{\omega} \tag{2.29}$$

$$\boldsymbol{u}_A = \boldsymbol{\omega} \times (\boldsymbol{r}_A - \boldsymbol{r}_I) \tag{2.30}$$

$$\boldsymbol{v}_I = \boldsymbol{t} \tag{2.31}$$

$$\boldsymbol{v}_A = \boldsymbol{t} + \boldsymbol{u}_A \tag{2.32}$$

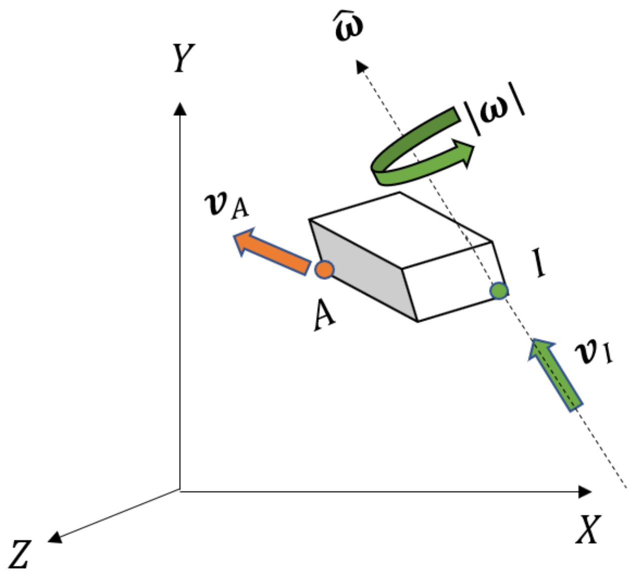

Figure 2.6: A rigid body motion with respect to Instant Screw Theory

3 Vehicle Characteristics

3.1 The Tire

When considering the dynamics of a vehicle, the only contact between the road and the vehicle is through the tires. In fact, the 4 contact patches of a general passenger car have the combined area equivalent to the size of an A4 sheet of paper [12]. But, all the forces between the tire and the road are generated in these patches and they define the vehicle behaviour. Thus, understanding tire characteristics and their effects on the complete vehicle is important.

Tires here are also called pneumatic tires because they are filled with gas, most commonly just air and hence the name. Tires produce forces which accelerate the vehicle in both the lateral and the longitudinal direction. Their elastic properties enable them to deform at and near the contact patch to generate forces that affect the complete vehicle. Longitudinal characteristics are commented on more in Section 3.6 and Appendix B while lateral characteristics are focused in this thesis.

The lateral forces are produced by lateral deformation of the contact patch which are measured in terms of slip angle. The slip angle is the difference in the direction a tire is heading to the direction it is pointing in. This is shown in the Figure 3.1 below. The tire treads deform to form the slip angle and the direction of the treads which is shown along the circumference of the tire at the contact patch is the direction in which the tire travels whereas the direction of the treads not in contact with the ground is the direction in which the tire is pointing.

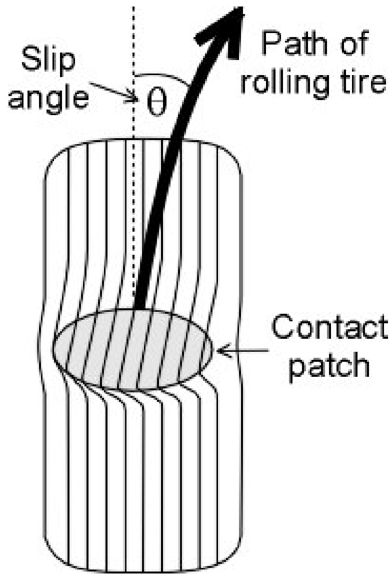

Figure 3.1: Slip Angle for a Pneumatic Tire [13]

Given below are the explanations of tire characteristics with the help of tire curves or graphs[13]. They are in imperial [US] units and are for racing tires (unless otherwise mentioned). But, with the discussion in this section being about understanding the trend of tire behaviour, it should be noted that the behaviour remains similar for racing and passenger car tires as they are both essentially pneumatic tires which have similar property trends. The difference is that racing tires have more lateral and longitudinal grip, higher stiffness and different or no tread patterns. Hence, it is still adequate to look at these graphs for the purpose of understanding tire behaviour.

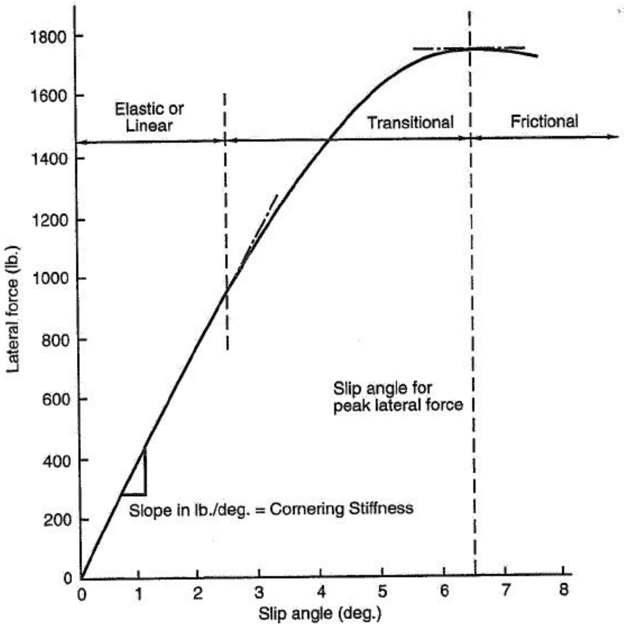

Figure 3.2: Lateral force vs Slip Angle graph for a pneumatic tire [13]

The Figure 3.2 above shows the lateral force (F_y) vs slip angle (α) curve of a tire. It can be seen that the tire has a linearly increasing characteristic at smaller slip angles and becomes non-linear at higher slip angles. It reaches a peak value and then drops off at even higher slip angles. This behaviour is similar for all pneumatic automotive tires. The linear range is of great importance for passenger car applications as it operates in this range most of the time and this is the basis for complete vehicle steady state analysis. This steady state behaviour of the vehicle is the focus in this thesis. Note that the non-linear range does come into effect in sudden manoeuvres for passenger vehicles as well for example evasive action like a double lane change as it usually occurs at higher lateral accelerations putting the tire in its non-linear range.

An important value for a tire for vehicle dynamic considerations in the steady state analysis is the tire cornering stiffness. This is the slope of the tire lateral force vs slip angle at slip angle close to zero i.e. the slope of the linear range of the curve. The mathematical for of this can be seen below in Equation (3.1) where $C_{F\alpha}$ is cornering stiffness.

$$C_{F\alpha} = \left.\frac{\partial F_y}{\partial \alpha}\right|_{\alpha=0} \tag{3.1}$$

There are various factors which affect the tire's characteristics and how they affect the full vehicle dynamics. Two of these are talked about below namely, camber angle and vertical load. Tire pressure, tire temperature and tire wear are some of the other factors in this non-exhaustive list that affect the tire characteristics and performance.

One of the factors affecting the performance of the tires is their angles with respect to the road and the chassis. These angles are described and talked about more in Section 3.3. But, they affect the amount of lateral and longitudinal forces that the tires can generate. The Figure 3.3 below shows the effect of camber angle on the lateral force (F_y) produced versus slip angle(α). The camber angle essentially adds some amount of lateral force to the tire at the same slip angle for negative camber and vice versa for positive camber. This is known as camber thrust. But, this drops off at higher slip angles. This drop off is also greatly affected by amount of negative camber as very high negative camber actually decreases the tires lateral force capacity again(*This phenomenon is not shown in the graph below*). The explanations for this behaviour are mentioned in the Section 3.3.

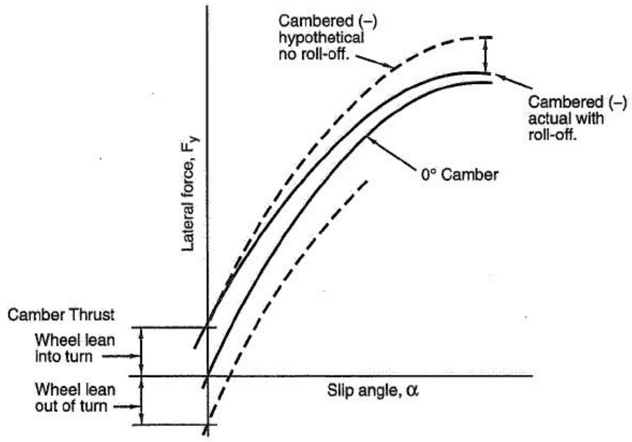

Figure 3.3: Lateral force vs Slip Angle graph for varying camber angle [13]

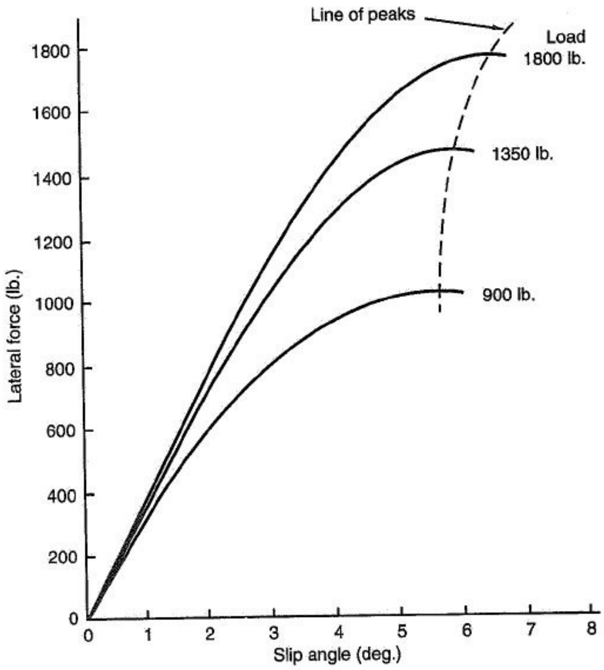

Figure 3.4: Lateral force vs Slip Angle graph for varying vertical loads [13]

The other factor discussed here which affects the tire characteristics is the vertical load. The Figure 3.4 above shows the graph of lateral force(F_y) vs slip angle(α) at various vertical loads(F_z). It can be seen that the absolute value of lateral force increases with increase in vertical load on a tire. But, if the lateral force is normalized with the vertical load i.e. $\frac{F_y}{F_z}$ is plotted against the slip angle as shown in Figure 3.5 below, it gives a different picture.

Here, $\frac{F_y}{F_z}$ which is also called the normalized lateral force or a measure of the tire-road coefficient of friction in the lateral direction can be seen with respect to slip angle at various vertical loads. It shows that the coefficient of friction of the tire-road interface decreases as the load increases. It can also be said that the utilization capacity of the tire decreases. This property of the tire where the normalized lateral force decreases with increase in vertical load is called the tire load sensitivity. Hence, while more load may give higher lateral force, the increase in lateral force diminishes with increasing vertical force. So, for a vehicle where load transfer occurs between the left and the right tires, the increase in lateral force generated by the added vertical load on one side is less than the decrease in lateral force due to decrease in vertical load on the other tire. This means

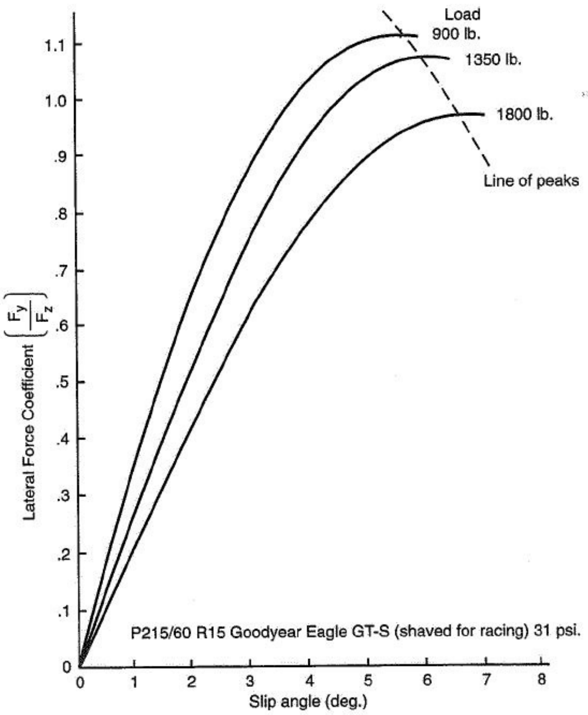

Figure 3.5: Normalized Lateral force vs Slip Angle graph for varying Vertical Loads [13]

that the overall axle lateral force generated will be less due to load transfer occurring. This is explored further at the end of this chapter in Section 3.4.1.

3.2 Vehicle Model

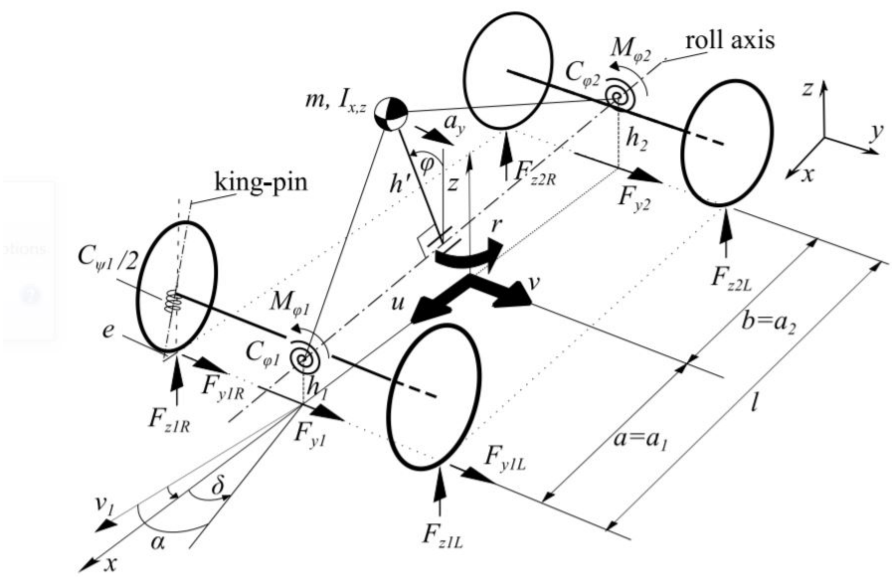

Figure 3.6: Pacejka Two Track Model [14]

Shown above in Figure 3.6 is the representation of a two track model having 4 degrees of freedom namely two degrees for translation in the road plane and also yaw and roll degree of freedom. This model includes vehicle inertial properties, tire characteristics, driver input and suspension characteristics in the form of roll stiffnesses for the two axles [14].

The inertial properties are denoted by m, I_x and I_z at the center of gravity of the sprung mass of the vehicle. These are the sprung mass properties and unsprung masses are neglected. The location of the centre of gravity is defined by a and b. They denote the distance of the centre of gravity from the two axles in the fore-aft direction or along the vehicle X axis.

The roll axis shown is defined as the axis about which the vehicle rolls in the initial instant. This axis passes through the front axle and the rear axle roll centers. Roll center heights are denoted by h_i where the subscript $i = 1, 2$ based on the axle being looked at (*where 1 is front axle and 2 is rear axle*). Another suspension parameter defined is the roll stiffnesses of the front and the rear axles or suspensions. They are denoted by $c_{\phi i}$ where $i = 1, 2$ based on the axle.

The vehicle model can be considered to be geometrically symmetric along both the fore-aft plane (XZ plane) and the left-right plane (YZ plane) except for the steering input which is present in the front axle and not in the rear axle for the static case.

3.3 Wheel Angles

The way in which the wheel is angled with respect to the road and the chassis affects how the tire behaves which in turn affects the vehicle dynamics. The change in these angles in dynamic conditions i.e. as the vehicle is in motion also affects the the tire and vehicle behaviour. Two of the wheel angles are talked about here are camber angle and toe angle.

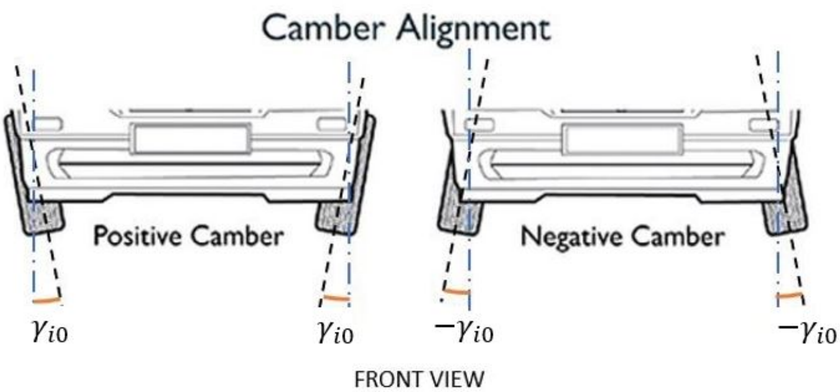

Figure 3.7: Camber angle[15]

The Figure 3.7 above shows the illustration of camber angle. It is the angle of the wheel with respect to the vertical in the front view plane. Like in the figure, it is usually denoted by γ. If the top of the left and right wheels are pointing towards each other, it is called negative camber whereas if their tops are pointing away from each other, it is called positive camber. It is also important to note that sometimes the word inclination angle is used which refers to a single wheels angle with the vertical in front view irrespective of the other wheel. In this case, the sign convention followed is that the right wheel in a negatively cambered axle will have a positive inclination angle while the opposite holds true for the left wheel. This is shown in Equation (3.2) below. Note that static or initial camber angle is denoted as γ_{i0} here.

$$\begin{aligned} \gamma_{iL0} &= -\gamma_{i0} \\ \gamma_{iR0} &= \gamma_{i0} \end{aligned} \tag{3.2}$$

As mentioned in Section 3.1, it affects the tire behaviour both in lateral and longitudinal direction (and hence in combined too). For longitudinal performance, zero camber is the best as it has the largest contact patch area. In terms of lateral performance, it was shown in that section that a small amount of negative camber is beneficial. This is because the negative camber deforms the tire sideways which gives a side force in towards the center of the vehicle. This is called camber thrust and a camber thrust coefficient is denoted by $C_{F\gamma}$. The camber thrust is linear for small camber angles. This adds onto the tires usual lateral force capabilities. Thus, assuming small slip angles and small camber angles, Equation (3.3) below can be used to obtain the lateral force from a tire.

$$F_y = C_{F\alpha}\alpha + C_{F\gamma}\gamma \tag{3.3}$$

Camber thrust exists at static case too but is cancelled out by the camber thrust from the tire on the opposite side (assuming symmetric suspension). As the vehicle turns, due to lateral load transfer, the loaded outer tire is more prominent and provides a thrust into the turn. But, the lateral capabilities of a tire does not increase as the negative camber keeps increasing and it has a peak before decreasing again. This is because with increase in negative camber, the camber thrust may increase, but at a point the decrease in contact patch area due to high camber affects the lateral capability of the tire more than that gained from any camber thrust.

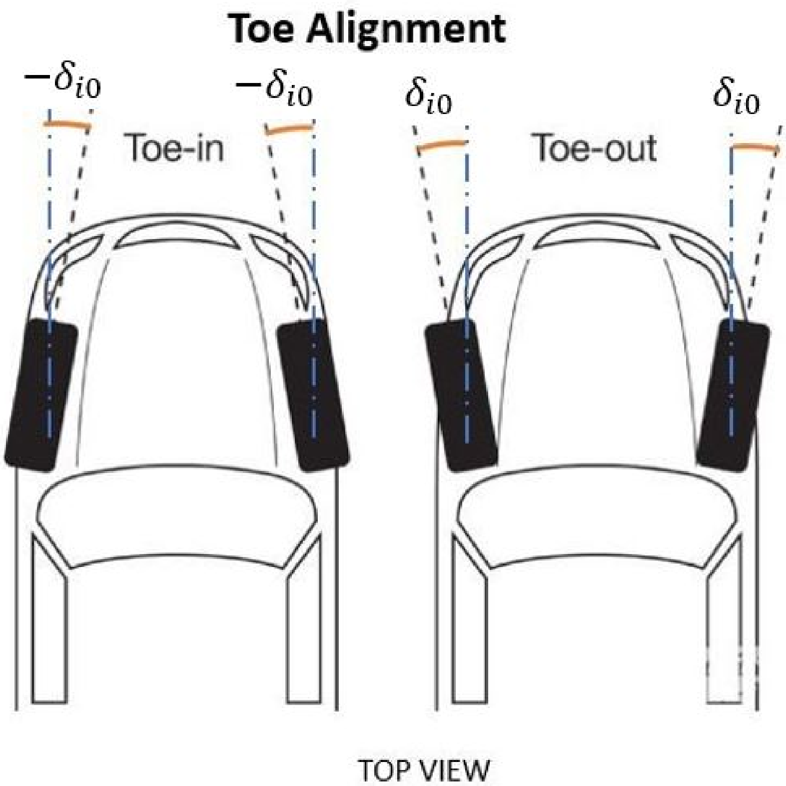

Figure 3.8: Toe angle[16]

The Figure 3.8 above shows the toe angle for a vehicle. It is the angle of the wheels with respect to the centreline of the vehicle in the top view. The case where the front of the left and the right wheels are pointing towards each other is called toe in and when they are pointing away from each other is called toe out. Toe out here is considered positive toe. But, when considering the steer angles, a steer to the left is considered as positive steering regardless of the opposite wheel's steer angle. Thus, in case of static toe angles, the equivalent steer angles of the left and the right wheels are opposite This is seen in Equation (3.4) below where in case of toe out, the right wheel has a negative added steer angle as it points to the right while the left wheel has a positive added steer angle due to it pointing to the left.

$$\begin{aligned} \Psi_{iL0} &= \Psi_{i0} \\ \Psi_{iR0} &= -\Psi_{i0} \end{aligned} \tag{3.4}$$

A toe in angle of 2° would mean that the wheels are toed in and each wheel has an angle of 2° with respect to the vehicle centreline. A toe angle gives slip angles generated on the tires when the vehicle is moving even when there is no steering input. This affects the vehicle behaviour at slow and high speeds. Toe in makes the car more stable at high speeds whereas toe out helps in slow speed turning.

3.4 Steady State Cornering

Having the aforementioned knowledge about the behaviour of the tire under various circumstances and its effect on the axle and vehicle characteristics, it is now useful to know the effect of various vehicle and suspension parameters on these. Here, only the steady state lateral properties are looked into. Steady state lateral motion of a vehicle is defined by very low or zero longitudinal acceleration and very slow changing or constant lateral acceleration. The actual vehicle rarely is in steady state, but it is a useful state to quantify a vehicle's characteristic in. Steady state lateral study is also referred to as Steady State Cornering.

3.4.1 Axle Cornering Stiffness

Static vertical loading of the tires and the lateral load transfer in steady state cornering affects the performance of the axle as a whole. Load transfer occurs from the inner wheel to the outer wheel when a vehicle takes a turn. As mentioned in the subsection regarding tires, the lateral force coefficient of a tire diminishes when the vertical load increases. The effect of this on the axle cornering stiffness is mentioned in this section.

First, the vertical load changes due to lateral acceleration, also known as lateral load transfer is derived. This is shown in Equation (3.5) below.

$$\Delta F_{zi} = \sigma_i m a_y \tag{3.5}$$

here, ΔF_{zi} is the load transferred and i denotes the axle chosen where 1 is front axle and 2 is rear axle. σ_i is the load transfer coefficient of the axle and is given below. The elastic component of the load transfer and the geometric component of the load transfer are differentiated as well in the equation.

$$\sigma_i = \frac{1}{2s_i}\left(\underbrace{\frac{c_{\phi i}}{c_{\phi 1} + c_{\phi 2} - mgh'}h'}_{\text{Elastic Component}} + \underbrace{\frac{l - a_i}{l}h_{RC_i}}_{\text{Geometric Component}}\right) \tag{3.6}$$

It can be seen that c_ϕ which is the roll stiffness is a factor in deciding which axle has more load transfer. The roll center height h_{RC_i} and its distance from the center of gravity h' also affect the load transfer distribution between the axles. This section also explains the effect of vertical load on tire lateral capacity.

$$\begin{aligned} C_{F\alpha} &= C_{F\alpha o} + \zeta_\alpha \Delta F_z \\ C_{F\gamma} &= C_{F\gamma o} + \zeta_\gamma \Delta F_z \end{aligned} \tag{3.7}$$

Here, in Equation (3.7), $C_{F\alpha}$ is the tire cornering stiffness which is given by the initial tire cornering stiffness $C_{F\alpha o}$ added to the product of the change in vertical load and tire cornering stiffness load sensitivity component ζ_{α}. It is similar for the camber stiffness based on vertical load transfer effect as seen too.

The actual camber, steer and slip angles are affected by many factors such as vehicle body roll and compliances to name a few. In Equation (3.8) Ψ_i is the additional steer angle which is the addition of the aligning torque steer (Ψ_{ci}), side force steer (Ψ_{sfi}) and roll steer (Ψ_{ri}). The notation α_i is the average slip angle considering the effect of the additional steer angle mentioned. Finally, the notation γ_i is the additional camber angle which is due to roll camber (γ_{ri}).

$$\begin{aligned} \Psi_i &= \Psi_{ri} + \Psi ci + \Psi sfi \\ \alpha_i &= \alpha_{ai} + \Psi_i \\ \gamma_i &= \gamma_{ri} \end{aligned} \tag{3.8}$$

As shown in the previous equation, a factor affecting the wheel angles is the amount of chassis roll. Equation (3.9) shows the toe angle change and the camber angle change due to roll (ϕ). This is given by ϵ_i and τ_i which represent the roll steer coefficient and the roll camber coefficient respectively for the vehicle and are in degrees of steer/camber per degrees of roll. These are properties of the geometry of the suspension and steering linkages.

$$\begin{aligned} \Psi_{ri} &= \epsilon_i \phi \\ \gamma_{ri} &= \tau_i \phi \end{aligned} \tag{3.9}$$

The aligning torque steer (Ψ_{c1}) is a factor of the steering stiffness about the kingpin axis c_{Ψ}, the sum of the caster trail e and pneumatic trail t_1 and the side force or lateral force F_{y1}. Caster trail is determined by the suspension geometry. This is given in the first equation in Equation (3.10) below. The second equation gives the side force steer Ψ_{sfi} which is the steer angle caused due to deformation of the suspension and steering linkages in the presence of a side force. Both these factors add onto the given steer angle and the initial toe angle and the roll steer angle to give the actual steer angle.

$$\begin{aligned} \Psi_{c1} &= -\frac{F_{y1}(e + t_1)}{c_{\Psi}} \\ \Psi_{sfi} &= c_{sfi} F_{yi} \end{aligned} \tag{3.10}$$

The effective axle cornering stiffness $C_{eff,i}$ is given by the the given axle lateral force and effective axle slip angle shown in Equation (3.11). (*Note that $C_{eff,i}$ is the axle cornering stiffness whereas when $C_{F\alpha i}$ is mentioned, it concerns the tires*)

$$C_{eff,i} = \frac{F_{yi}}{\alpha_{ai}} \tag{3.11}$$

The axle lateral force talked about in the previous effective cornering stiffness equation can be found using Equation (3.12) below for a steady state turn.

$$F_{yi} = \frac{l - a_i}{l} m a_y \tag{3.12}$$

The axle side force is the sum of the forces from the left and the right side of the tire which are given in the Equation (3.13) below for both sides of the axle. The sign notation followed is based on the signs used thus far in this section.

$$\begin{aligned} F_{yiL} &= \big(\frac{1}{2}C_{F\alpha i} + \zeta_{\alpha i}\Delta F_{zi}\big)(\alpha_i - \Psi_{i0}) + \big(\frac{1}{2}C_{F\gamma i} + \zeta_{\gamma i}\Delta F_{zi}\big)(\gamma_i - \gamma_{i0}) \\ F_{yiR} &= \big(\frac{1}{2}C_{F\alpha i} - \zeta_{\alpha i}\Delta F_{zi}\big)(\alpha_i + \Psi_{i0}) + \big(\frac{1}{2}C_{F\gamma i} - \zeta_{\gamma i}\Delta F_{zi}\big)(\gamma_i + \gamma_{i0}) \end{aligned} \tag{3.13}$$

Putting the previous information together, the overall equation for axle lateral capability can be found as shown in Equation (3.15) below with the separate components marked in the equation too. This is got from Equation (3.14) where the $C_{eff,i}$ is a single term encompassing all the small effects that affects the axle effective cornering stiffness and is based on Equation (3.11).

$$\alpha_{ai} = \frac{F_{yi}}{C_{eff,i}} \tag{3.14}$$

$$\alpha_{ai} = \frac{Fyi}{C_{F\alpha i}}\left[1 + \underbrace{\frac{l(\epsilon_i C_{F\alpha i} + \tau_i C_{F\gamma i})h'}{(l-a_i)(c_{\phi 1} + c_{\phi 2} - mgh')}}_{\text{Suspension}} + \underbrace{\frac{C_{F\alpha i}(e_i + t_i)}{c_{\Psi i}}}_{\text{Aligning Torque}} - \underbrace{C_{F\alpha i} c_{sfi}}_{\text{Side Force Steer}} + \underbrace{\frac{2l\sigma_i}{l-a_i}(\zeta_{\alpha i}\Psi i0 + \zeta_{\gamma i}\gamma_{i0})}_{\text{Load Transfer}}\right] \tag{3.15}$$

Thus, it can be seen from the above equation that the roll center height which is part of σ_i in this equation is a factor in the expression for effective axle characteristics.

3.4.2 Complete Vehicle Understeer Gradient

In the previous subsections, the tire characteristics were explained, followed by the axle level characteristics. With that information, it is possible to look at the complete vehicle lateral characteristics as they define the final vehicle behaviour taking all the effects into account.

One of the vehicle lateral characteristic indicators is the understeer gradient. Understeer in general is the state when a vehicle has less lateral grip in the front axle than the rear axle. Grip here refers to lateral force generating capacity. For information, oversteer is the exact opposite where the rear axle has less lateral grip than the front. It is important to note that understeer and oversteer have multiple definitions but in this case, only the steady state conditions are considered. In that case, the amount of understeer can be characterized by comparing the axle cornering stiffnesses to determine which axle has more grip. The understeer gradient is a quantification of the amount of understeer in a vehicle. The value is positive for understeered vehicle and negative for oversteered vehicles. Equation (3.16) below gives the expression for understeer gradient which is denoted by η.

$$\eta = \frac{F_{z10}}{C_{eff,1}} - \frac{F_{z20}}{C_{eff,2}} \tag{3.16}$$

The above equation shows that the understeer gradient is a factor of the initial vehicle load on each axle and the axle effective cornering stifnesses. the larger the value, the greater the amount of steady state understeer in the vehicle and the signs ensure that the value is negative for oversteer.

Finally, here it can be seen that the complete vehicle understeer gradient is a factor of the effective axle cornering stiffnesses. These were seen in the previous subsection to be affected by suspension parameters such as wheel angles and dynamic wheel angle changes, suspension stiffness and geometric parameters such as the roll center height. Thus, it is important to consider the suspension design while designing for the complete vehicle characteristics.

3.5 The Roll Center of a Vehicle Suspension

The previous section explained that the suspension design has a large role to play in the overall vehicle dynamic characteristics. Roll center is one of the key factors in these calculations and it is a parameter of the suspension system. SAE defines roll center as "The point in the transverse vertical plane through any pair of wheel centers at which lateral forces may be applied to the sprung mass without producing suspension roll" [17]. This can be interpreted as being the moment center (MC) of the sprung mass in the YZ or rear view plane considering a lateral force. It can also be considered as the instantaneous center of rotation of the sprung mass considering one axle. Refer to Section 2.2 for explanation of Moment Center and Instantaneous Centers of Rotation. If the velocity vectors of the sprung mass were to be checked for and the perpendiculars of these vectors are taken, they would meet at the roll center.

The roll center is a point that is found for a single axle. But, for a two axle passenger car, if the front and the rear roll centers are joined, the roll axis is obtained. This is the axis through which, if a lateral force passes, no chassis roll occurs. Thus, it is the zero moment axis of the chassis or sprung mass. Under the assumption of soft suspensions which are symmetric to each other, then the roll axis also represents the axis about which the chassis physically roll about at the initial instants. This is also shown in the Section 3.2 in the vehicle model. Note that from the Instant Screw Theory, the instantaneous screw axis for the chassis for pure lateral force also defines the roll axis of the vehicle.

Due to the importance of this parameter in deciding crucial vehicle factors, it is of great interest to understand methods to accurately calculate and analyze the roll center of passenger vehicle suspensions of different complexities. Calculation and analysis of both the roll center and roll axis enables the use of it as a design variable to reach complete vehicle requirements. This is the focus of the next chapter.

3.6 Longitudinal and Combined Properties of the Vehicle

The vehicle characteristics explained in this chapter cover solely the lateral characteristics of tire, axle, suspension and complete vehicle. Pure longitudinal properties are also of importance to the vehicle dynamics and suspension designer. Apart from pure longitudinal effects, the addition of longitudinal effects with lateral effects also creates a different challenge of understanding vehicle characteristics in this combined loading case. However, this is not the focus of the study regarding suspension analysis in the further chapters. Hence, it is not discussed here. But, characteristics such as longitudinal and combined tire properties and the pitch center are mentioned in the Appendix B.

4 Suspension Kinematics

4.1 Planar Suspension Kinematics

Planar suspensions are ones which move in a single plane as mentioned before. Thus, they have a 2D only motion and can be calculated and analyzed by 2D approaches. In this case a simple planar double wishbone suspension is used to show the approach. It is useful to first know the method to calculate instantaneous center of a suspension as it is used to calculate the roll center of the vehicle. The concepts used here such as the instantaneous center of rotation of the suspension and the moment center of the suspension are based on explanations in Section 2.2 wherein the mechanism in question is the suspension system.

4.1.1 Instantaneous Center of a Planar Suspension

A planar double wishbone suspension as shown in Figure 4.1, can be represented as four bar mechanism in YZ wheel plane as mentioned in Section 2.4. The chassis which is fixed is considered as fixed link S_0. The upper and lower arms are the cranks S_1 and S_3. UWT is the coupler S_2 of the mechanism. As a result, according to Kennedy's theory for single closed loop four mechanism mentioned in Section 2.4.1, I_{02}, the instantaneous center of the coupler, UWT, becomes the moment center (MC) of the suspension or Instantaneous Center of rotation (IC) of the suspension. Furthermore, the mechanism has mobility, $f = 1$.

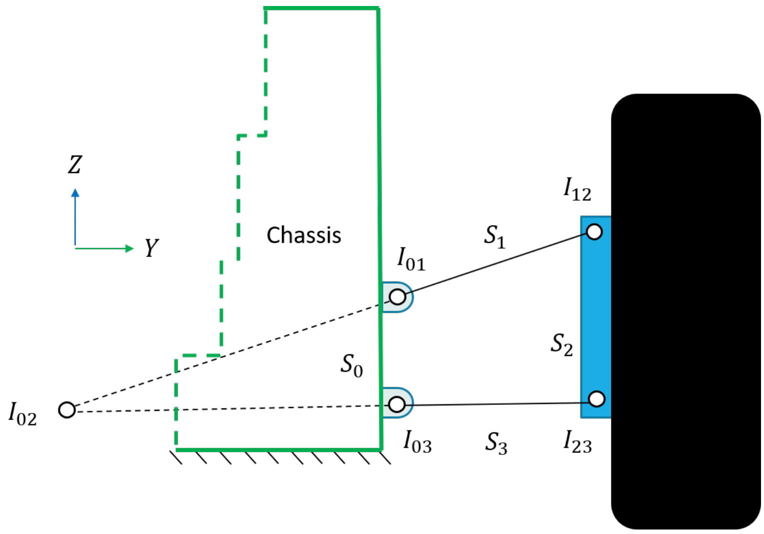

Figure 4.1: Single closed loop mechanism for planar suspension kinematics

4.1.2 Roll Center of a Vehicle with Planar Suspension

The interaction between chassis and left and right suspension subsystems at an axle in YZ wheel plane as depicted in Figure 4.2 is considered to estimate roll center location at a particular instant for a given constraint conditions. As discussed in Figure 4.1.1, four bar mechanisms of left and right suspension subsystems results in the left and right IC(s) I_{02l} and I_{02r} of couplers S_{2l} and S_{2r} represents left and right UWT(s) at the extreme ends of the axle. Unlike in Section 4.1.1, ground is considered as the fixed link S_G. Left and right contact patches are the fixed IC(s) I_{G2l} and I_{G2r}. The moving IC(s) I_{02l} and I_{02r} and the fixed IC(s) I_{G2l} and I_{G2r} leads to an instant four bar mechanism for relative planar motion of three rigid bodies i.e the left and right UWT(s), and the chassis based on the idea given in the previous work by Madhusudan[18]. The instantaneous center of rotation, I_{G0} of the coupler S_0, the chassis, of this instant mechanism is the moment center (MC) of the chassis or popularly known as roll center in automotive industry as mentioned in Section 3.5. Using Equation (2.1), the mobility for this kinematic system of closed loop mechanisms is estimated to be $f = 1$.

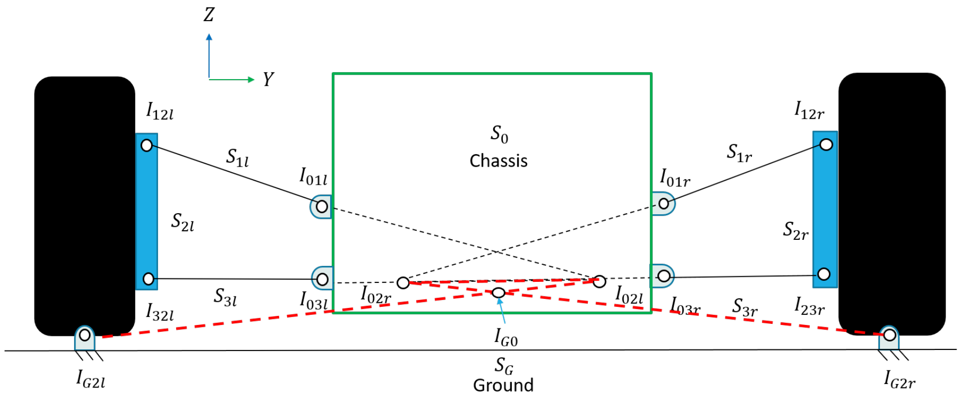

Figure 4.2: Multiple closed loop mechanisms for planar roll kinematics

4.1.3 Reduced Instant Single Closed Loop Mechanism

A complex kinematic system with multiple kinematic closed loops can be simplified to fewer closed loops. A closed loop four-bar mechanism with same mobility $f = 1$ as shown in the Figure 4.3 is a good way to explain the reduction of loops. A chassis with suspension systems on either sides of it can be depicted by a four bar linkage . The virtual coupler, V_0, is represented as a link connecting the left and right MC(s) or IC(s) of the suspensions. The virtual cranks, V_{02l} and V_{02r}, are connected by corresponding MC(s) of the suspensions and tire-contact patches, I_{G2l} and I_{G2r}. The fixed link is considered to be the ground. Unlike the four bar mechanism mentioned in Section 2.4, the cranks and the coupler in this instant mechanism are virtual links with varying lengths at different instants and thus the model is only valid for a certain instant and the links change in the next instant. Also MC(s) of the suspensions, I_{02l} and I_{02r}, act as the virtual revolute joints connecting the cranks and the coupler [18]. The MC or IC of the coupler, I_{G0}, is roll center of the vehicle for the axle at the wheel plane. It is easy to see from this model, the reason the Roll center is the MC of the chassis since, a force on the coupler directed to the MC of coupler will not generate any angular moment to the mechanism.

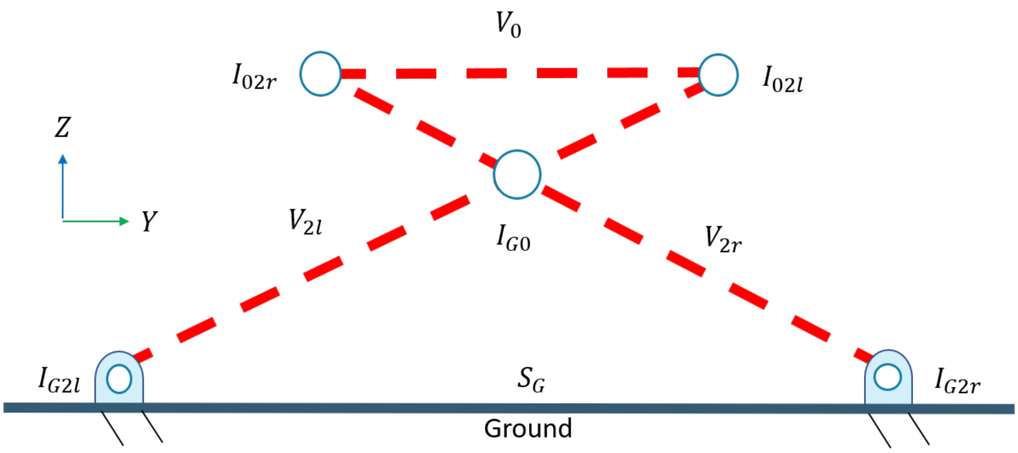

Figure 4.3: Reduced instant single closed loop mechanism for planar roll kinematics

4.2 Spatial Suspension Kinematics

In the Section 1.7 the 3 different types of independent suspensions are mentioned. The spatial suspension is the most complex type of independent suspension because it exhibits a three dimensional screw motion. Studying this motion is more difficult to do than planar or spherical suspensions. But, there are methods to either calculate and analyze suspensions in three dimensions or convert it into a two dimensional problem and analyze it which is talked about in this chapter. Thus, here 3D motion is being looked into which may be calculated in 2D or 3D and then analyzed in 2D.

4.2.1 Roll center location from $\Delta Y/\Delta Z$ Method

One method to analyze a spatial suspension by looking at it in a specific plane is the $\Delta Y/\Delta Z$ Method. This is a method of calculating the suspension motion in 2D as the motion along X axis is ignored. Considering the wheel planes mentioned in Section 1.6, a spatial suspensions roll characteristics can be studies solely by looking in the YZ wheel plane.

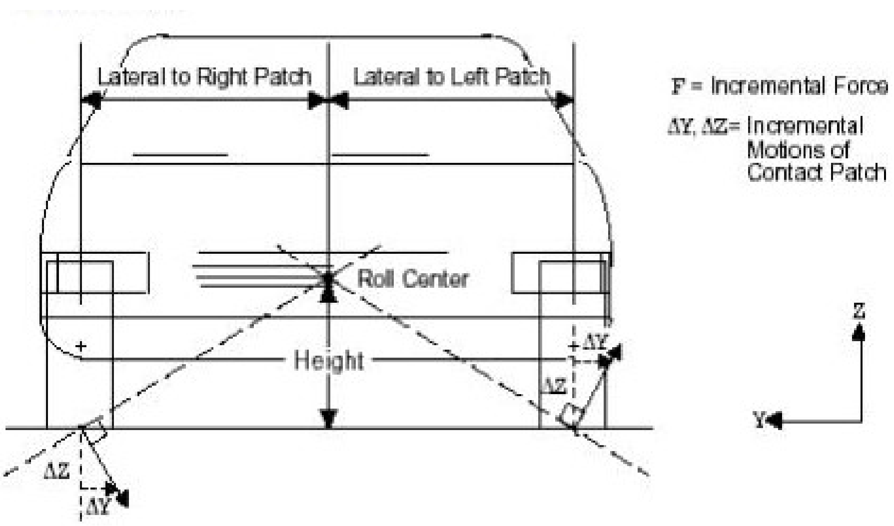

Figure 4.4: Roll center location estimated in MSC Adams Car [19]

Figure 4.4 above shows the use of this method. A incremental 2D force is given to tire contact patches (TCP(s)) at both sides to incrementally displace them in opposite directions in YZ plane. The 2D displacement vector of each tire contact patch is considered and the perpendiculars to these vectors are taken. The intersection points of the perpendiculars is the roll center location.

A few things to note here are that this calculation can be done with multiple types of inputs based on compliance matrix at TCP(s) and location at TCP(s). A force can be given to the tire contact patch and the instantaneous displacement vectors can be recorded. Or, a small force vector can be given and the displacement vector from the initial to the final position of the tire contact patch can be considered which approximately represents the instantaneous velocity vector integrated over time for the instant of the displacement under the influence of the force.

Based on the explanation of instantaneous center of rotation (IC), the perpendiculars from the displacement vectors essentially point towards the IC of that side of the wheel in the YZ wheel plane. This method is used by a many commercial kinematic softwares most notably, MSC ADAMS Car where it considers an incremental 2D force on the TCP(s) and calculates the displacements of the TCP(s) [19].

It is also used in the industry to check the roll centers for actual vehicles on the Kinematics and Compliance (K & C) rig or a Suspension Parameter Measurement Machine (SPMM). Here, a small known planar force is given in the vertical direction and the displacement in lateral and vertical direction (ΔY and ΔZ) of the contact patch is measured. The vector $[\Delta Y, \Delta Z]$ is planar incremental displacement vector and the perperdicular of this vector can be now be used to calculate the roll center using the method described above.

4.2.2 Virtual Position using Kennedy's approach

Another 2D calculation method being discussed here is the Virtual Position using Kennedy's approach. The concept of instantaneous center of rotation and Kennedy's theory as discussed in Sections 2.2 and 2.4 can be even applied to spatial suspension mechanisms. Virtual positions, $\boldsymbol{pl_x r}$, are the projection of actual positions $\boldsymbol{r}$ at an instant on the YZ wheel plane with normal, $\boldsymbol{n} = [1, 0, 0]$, at the contact patch is found using Equations (4.1) and (4.4). Velocities of these virtual points, $\boldsymbol{v}(pl_{\boldsymbol{n}}\boldsymbol{r})$, are found by placing markers at virtual points in case of Adams View simulations. Furthermore, planar velocities of these virtual positions, $pl_{\boldsymbol{n}}(\boldsymbol{v}(pl_{\boldsymbol{n}}\boldsymbol{r}))$, are found using the Equations (4.2) and (4.5). For a right side suspension, as depicted in Figure 4.5, the planar lines perpendicular to velocity of the virtual positions of the moving joints/ points in the plane can be estimated. These lines must intersect at the MC of the suspension or instantaneous center of rotation (IC) of the mechanism in the plane. The line passing through the contact patch and MC/ IC of suspension intersect with the corresponding line from the opposite suspension in a similar way as shown in Figure 4.4 at MC of the chassis or roll center (RC) in the plane. IC(s) and RC is this method are approximately in par with the results from $\Delta Y/\Delta Z$ Method shown in Section 4.2.1. Unlike the previous method based on compliance and displacements, this kinematic method is based on instant velocity and can be used determine MC of chassis and, left and right MC(s) of the suspension at an instant.

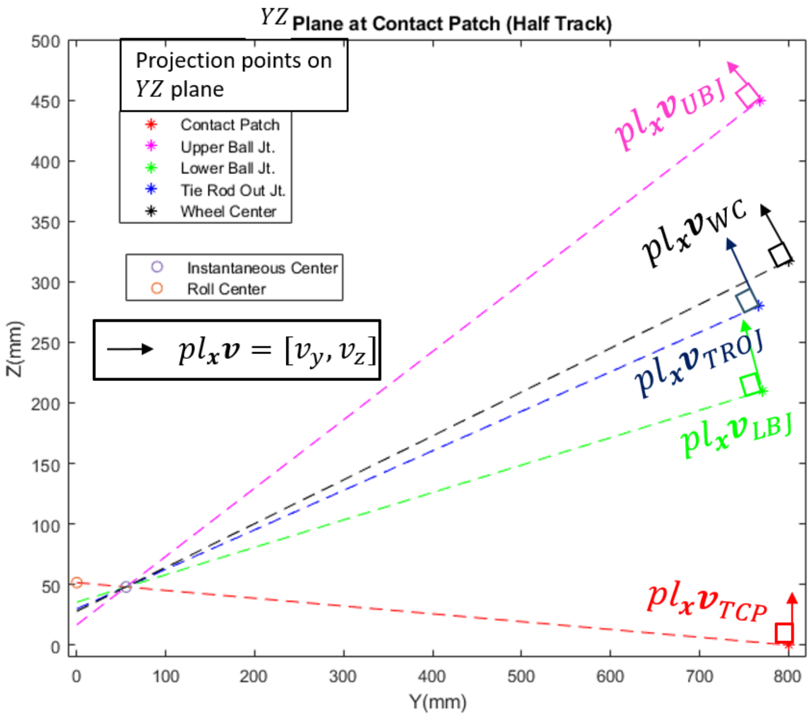

Figure 4.5: MC estimation for a spatial double wishbone suspension at static equilibrium

$$pl_{\boldsymbol{n}}\boldsymbol{r} = \frac{\boldsymbol{n} \times (\boldsymbol{r} \times \boldsymbol{n})}{|\boldsymbol{n}|^2} \tag{4.1}$$

$$pl_{\boldsymbol{n}}(\boldsymbol{v}(pl_{\boldsymbol{n}}\boldsymbol{r})) = \frac{\boldsymbol{n} \times (\boldsymbol{v}(pl_{\boldsymbol{n}}\boldsymbol{r}) \times \boldsymbol{n})}{|\boldsymbol{n}|^2} \tag{4.2}$$

since

$$\boldsymbol{n} = \boldsymbol{e}_x = \boldsymbol{x} = [1, 0, 0] \quad \text{normal vector for } YZ \text{ plane} \tag{4.3}$$

Then Equations (4.1) and (4.2) becomes

$$pl_{\boldsymbol{x}}\boldsymbol{r} = [0, r_y, r_z] = [r_y, r_z] \tag{4.4}$$

$$pl_{\boldsymbol{x}}(\boldsymbol{v}(pl_{\boldsymbol{x}}\boldsymbol{r})) = [0, v_y, v_z] = [v_y, v_z] \tag{4.5}$$

4.2.3 Screw Axis Offset Method

Another method looked into in this thesis to analyze a spatial suspension is calculating the motion of the suspension in three dimensions and using this data to analyze the suspension in two dimensional wheel planes. Thus, this is the 3D calculation of a 3D motion and then it is analyzed in 2D. This is based on the one proposed by Wolfgang Matschinsky [7] and uses the Instant Screw Theory explained in Section 2.5. Here the wheel suspension motion is first defined assuming a perfectly kinematic suspension without compliance. The definition of motion explains the translation velocities and rotational velocities in all three dimensions. This data is then used to look at the wheel plane and find the MC. It is a general method of analyzing the wheel travel of a vehicle suspension and is not just specific to spatial suspensions.

4.2.4 Motion Analysis of a Wheel Carrier

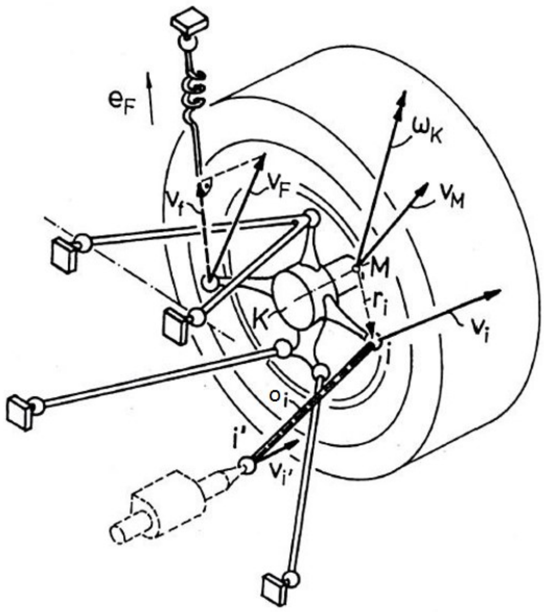

Figure 4.6: Motion Analysis of a Wheel Carrier [7]

One way to find the roll center of the chassis, as mentioned previously, is to find the instantaneous center of rotation of each suspension. Thus, the motion analysis of each wheel carrier is important. Wheel carrier here refers to the Upright, Wheel and Tire (UWT) assembly which is considered as a single rigid body.

Figure 4.6 shows the wheel carrier and the suspension linkages including the steering link 'i' and spring link 'f'. It has 5 links where the top two links are joined at the wheel end to make a triangle. But, they are considered as two separate links. Thus, a double wishbone suspension would basically be a five link suspension with its top two and bottom two links joined at the upper and lower ball joints respectively. The spring can be considered a very compliant link and be used to find the velocity of the spring motion. For this analysis though, the spring link 'f' is ignored as it does not affect the kinematic motion of the wheel carrier.

M is the wheel center whose motion is defined by its angular velocity $\boldsymbol{\omega}$ and its translational velocity $\boldsymbol{v}_M$. $\boldsymbol{v}_i$ and $\boldsymbol{r}_i$ are the velocity and connecting radius of one of the other links with respect to the wheel center. i' signifies the other end of the link.

The following Equation (4.6) holds for the velocity of the links:

$$\boldsymbol{v}_i = \boldsymbol{v}_M + \boldsymbol{\omega} \times \boldsymbol{r}_i \tag{4.6}$$

Considering velocity of a link along its axis which is non zero for example in steering inputs, the following Equation (4.7) is found (where $\boldsymbol{o}_i$ refers to the direction of the link vector pointing from i to i' in Figure 4.6).

$$\boldsymbol{v}_i \cdot \boldsymbol{o}_i = \boldsymbol{v}_{i'} \cdot \boldsymbol{o}_i \tag{4.7}$$

From, Equation (4.6) and Equation (4.7), the following Equation (4.8) can be written.

$$(\boldsymbol{v}_M + \boldsymbol{\omega} \times \boldsymbol{r}_i) \cdot \boldsymbol{o}_i = \boldsymbol{v}_{i'} \cdot \boldsymbol{o}_i \tag{4.8}$$

So, from the above, there are 5 equations if $\boldsymbol{r}_i$, $\boldsymbol{v}_{i'}$ and $\boldsymbol{o}_i$ for the 5 links excluding the spring are substituted. And there are six unknowns.
The unknowns are the components of $\boldsymbol{v}_M$ and $\boldsymbol{\omega}$

- v_{M_x}, v_{M_y}, v_{M_z}, ω_x, ω_y and ω_z

If one of them is considered as input, the 5 equations can be solved for the 5 remaining unknowns. This is better understood by looking at the MATLAB code mentioned at the very end of this chapter.

For bump and roll analysis, a vertical input at the wheels with respect to the chassis is needed. Thus, v_{M_z} is taken as a input vertical velocity. Now, only 5 unknowns remain and there are 5 equations, hence, the system of equations can be solved for v_{M_x}, v_{M_y}, ω_x, ω_y and ω_z.

From the values of $\boldsymbol{\omega}$ and $\boldsymbol{v}_M$, a lot of other information can be derived about the motion of the body.

- A body with spatial motion not only rotates about an axis but also translates along it. This translation velocity is called pitch velocity and denoted by $\boldsymbol{t}$. The magnitude is denoted by $\dot{s}$. The pitch velocity is the component of $\boldsymbol{v}_M$ in the direction of $\boldsymbol{\omega}$. $\widehat{\boldsymbol{\omega}}$ is the direction vector of $\boldsymbol{\omega}$. Equation (4.9) and Equation (4.10) below show the calculations for $\boldsymbol{t}$ and $\dot{s}$.

$$\dot{s} = \boldsymbol{v}_M \cdot \widehat{\boldsymbol{\omega}} \tag{4.9}$$

$$\boldsymbol{t} = \dot{s} \cdot \widehat{\boldsymbol{\omega}} \tag{4.10}$$

- Apart from the pitch velocity component the other component of $\boldsymbol{v}_M$ is the tangential velocity at which the body is rotating about the axis of rotation. This is called circumferential velocity and is denoted by $\boldsymbol{u}$ and its magnitude is denoted by $|\boldsymbol{u}|$. It is the remaining velocity component excluding the pitch velocity. Equation (4.11) below show the calculations for $\boldsymbol{u}$ and $|\boldsymbol{u}|$.

$$\boldsymbol{u} = \boldsymbol{v}_M - \boldsymbol{t} \tag{4.11}$$

- Another parameter that is important is the distance from the wheel center to the instantaneous axis of rotation. It is denoted by r. The calculation of r is given in Equation (4.12)

$$r = \frac{|\boldsymbol{u}|}{|\boldsymbol{\omega}|} \tag{4.12}$$

The value of $\boldsymbol{t}$ is null for non spatial suspensions as they do not translate along the rotation axis.

Note that both pitch velocity $\boldsymbol{t}$ and circumferential velocity $\boldsymbol{u}$ have their components along the three axes and are represented as t_x, t_y and t_z for pitch velocity components and u_x, u_y and u_z for circumferential velocity components.

Now, the equations are solved to get the data of the wheel carrier motion. The concept introduced in the first chapter regarding the three different types of independent suspension is important to consider henceforth.

Also, let the axis of rotation of the wheel carrier be called $\boldsymbol{\omega}$. $\boldsymbol{\omega}$ gives the information about the location of this axis about which the wheel rotates instantaneously and also gives its direction. This axis $\boldsymbol{\omega}$ is just the instantaneous axis of rotation for planar or spherical motion and the instantaneous screw axis for spatial motion. According to the explanation in Section 2.2 the MC at any given plane lies on the instantaneous axis of rotation. According to the definition of MC of a rigid body, if a force passes through it, the body will not undergo any angular displacement or angular moment. But, it is more complicated for screw motions as the instantaneous screw axis is not the moment equilibrium axis always. The mechanism with a screw motion is only in moment equilibrium for a force passing through its axis of rotation (which in this case is the instantaneous screw axis) only if the force is perpendicular to this axis. This is because the pitch velocity is perpendicular to the force and cannot give a power to the body and does not give a moment to it as shown in Equation (4.13). On the other hand, for a force passing through the instantaneous screw axis but not perpendicular to it, the force and the pitch velocity are not perpendicular to each other thereby giving a power to the body and giving it a moment as shown in Equation (4.13) where, P is Power, $\boldsymbol{F}$ is Force and $\boldsymbol{v}$ is velocity

$$P = \boldsymbol{F} \cdot \boldsymbol{v} \tag{4.13}$$

A good way to understand this is if a nut and bolt mechanism is considered. If a force is given to the nut perpendicular to the bolt and passing through its primary axis, the nut will not move. But if the same force passing through the nut primary axis is at an angle not perpendicular to the axis, the nut will rotate on the bolt.

But, a moment equilibrium point or moment center (MC) may still exist in a particular plane for a force that is not directed perpendicular to the instantaneous screw axis as it is a rigid body with a constrained motion. Let this moment equilibrium point be a length, $|\boldsymbol{a}|$, away from the instantaneous screw axis. This offset, $\boldsymbol{a}$, needs to be defined in mathematical terms so that it can be found for spatial suspensions.

The explanation on how to find the compenents of $\boldsymbol{a}$ is given below. Note that when referring to velocity pole, it defines the point of zero velocity of a mechanism, on a particular plane.

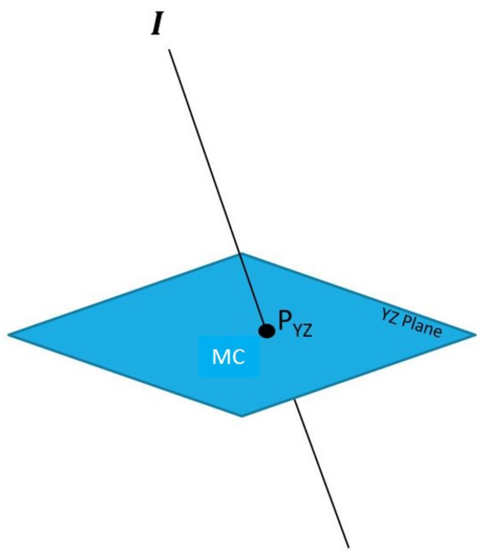

Figure 4.7: Finding the velocity pole of a non spatial (spherical) suspension

Figure 4.7 shows the YZ plane and instantaneous axis of rotation I of a spherical suspension. P_{yz} shows the point of zero velocity on that plane. In this case, it is the MC of the body undergoing motion in that plane. In case of non spatial suspensions, as mentioned above, it only has a radial component of velocity and hence, its velocity about the axis of this radial motion i.e. the instantaneous axis of rotation has to be zero. Thus, P_{yz} is the point of zero velocity in the plane. The idea behind point P_{yz} is that it must not have any velocity in the plane and can only have a velocity perpendicular to it. Thus, any force in the plane passing through the point P_{yz} will not give any power to the body thus keeping it in moment equilibrium.

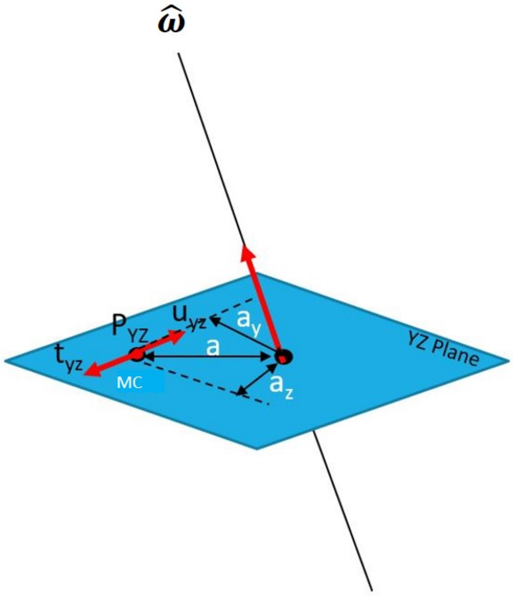

Figure 4.8: Finding the velocity pole of a spatial suspension

Figure 4.8 shows the YZ plane and instantaneous screw axis $\widehat{\boldsymbol{\omega}}$. Notations u_{xy} and t_{xy} are the components of the circumferential velocity and the pitch velocity respectively, in the YZ plane. P_{yz} shows the point of zero velocity on that plane. In this case too, it would be MC of the body undergoing screw motion in that plane. But, here it is offset from the instantaneous screw axis by $\boldsymbol{a}$ unlike the spherical suspension above which lies on the instantaneous axis of rotation. This is due to the fact that for spatial suspensions, pitch velocity is non zero and thus, a point in the instantaneous screw axis still has a velocity component which is non zero i.e. the pitch velocity component. Thus, the zero velocity point which is the MC is offset from the axis. The zero velocity in the plane will be due to the circumferential velocity component u_{xy} canceling out the pitch velocity component t_{xy}.

Using the above theory, the value of a_y (lateral offset of $\boldsymbol{a}$ in rear view) and a_z (vertical offset of $\boldsymbol{a}$ in rear view) can be found to be the following shown in Eq.4.14 and Eq.4.15.

$$a_y = \frac{t_y}{\omega_x} \tag{4.14}$$

$$a_z = \frac{t_y}{\omega_x} \tag{4.15}$$

This calculation from hardpoints to roll center location can be done for rigid suspensions. For flexible or suspensions with included elastokinematic effects of components like bushings, if the velocity and angular velocity data of the wheel carrier can be found, it can be used as a direct input in this method to get the roll center location. Due to the easy calculations required in this method, it can be done in simple softwares like excel. For the purpose of this thesis, MATLAB was used to create a code for this. The code can be found in Chapter D.

5 Chassis kinematics

This chapter aims to analyze the effects of steering on roll axis or the chassis' instantaneous screw axis (also called chassis screw axis in the texts that follow) in steady state cornering without braking at low speed. Simulations are done using a multibody model developed in the CAE package, MSC Adams View. Planar double wishbone, spatial double wishbone and spatial multi-link suspension are considered for this analysis. However, it is important to note that this simulation is not similar to a full-vehicle simulation done in MSC Adams Car, a CAE package also from MSC Softwares but rather a simulation of a multibody model on MSC Adams View with the required constraints in place.

5.1 Chassis Screw Axis Analysis Method

5.1.1 Assumption

Friction circle or ellipse of the tire at its contact patch is represented as inline primitive joint at the road tire contact. Primitive joint has 3 rotational DoF(s) and one translational DoF accounting to $f = 4DoF(s)$ [20]. The $f_{tran} = 1$ of joint represents negligible rolling resistance of the tire in longitudinal direction while cornering without braking. Two other translational DoF(s) are fixed while considering one DoF for high lateral friction and other translational DoF(s) for weight of the vehicle. Elasto- kinematics is not considered in this model. Lateral acceleration or centrifugal acceleration a_{centri} is constant. Since this analysis is for steady state cornering, total simulation need not exceed 0.3[s] and the steering angle is considered to be small.

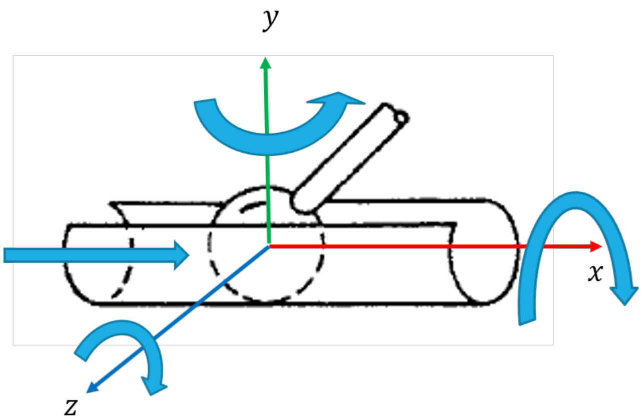

Figure 5.1: Physical representation of inline-primitive joint [20]

5.1.2 Initial Vehicle Parameters

Design parameters presented in Table 5.1 are considered based on rough values for common small sedans and hatchbacks available in the market. Limited packaging space is accounted to develop the three different types of suspensions and their initial parameters are also mentioned in Table 5.2. The idea is to have a suspension that is plausible in the real world case.

Table 5.1: Design Parameter

Parameter	mm
L	1800
l_f	900
w	1650
h	500

Table 5.2: Initial Suspension Parameters

	h_{RC} [mm]	$\widehat{\omega}_x$	$\widehat{\omega}_y$	$\widehat{\omega}_z$
Planar Double Wishbone	50.7692	1	0	0
Spatial Double Wishbone	65.3217	-0.4165	-0.9050	-0.0861
Spatial Multi Link	59.3553	-0.181	-0.798	-0.573

5.1.3 Boundary conditions

Two different kinematic models as shown in Figures 5.2 and 5.3 are considered for each type of suspension. The model without steering input has zero steering rack displacement, hence the primitive joint has translational DoF parallel to local X-axis of the chassis. However, the model which considers steering input has a given 4mm steering rack displacement, thereby obtaining the steered state of UWT and the corresponding orientation of steered primitive joint. The steering angles acquired through the rack displacement is mentioned in Table 5.3. It is to be noted that, in this case, unlike the double wishbone suspension, $\delta_l \neq \delta_r$ for multi-link suspension. This means that the ackermann % is different for the three suspensions looked at. Although it is possible to have similar ackermann % in both double wishbone and multilink suspensions, they were not considered here and thus need to be taken into account for any inferences. Mobility for the model representing multi-link suspension has 22 DoF(s) and the ones depicting double wishbone suspension have 6 DoF(s). Hovever there exists only 2 active DoF(s) which enable the instantaneous screw motion of the chassis. The rotational along the axis of links with spherical joints at both ends account remaining passive DoF(s). Centrifugal acceleration of $a_{centri} = 0.1g\ m/s^2$ is considered for both models. All four suspensions are considered be identical in terms of boundary conditions while analyzing them.

Table 5.3: Steering Angles

	δ_l	δ_r
Planar Double Wishbone	1.52803	1.52809
Spatial Double Wishbone	1.52809	1.52815
Spatial Multi Link	2.30592	2.27971

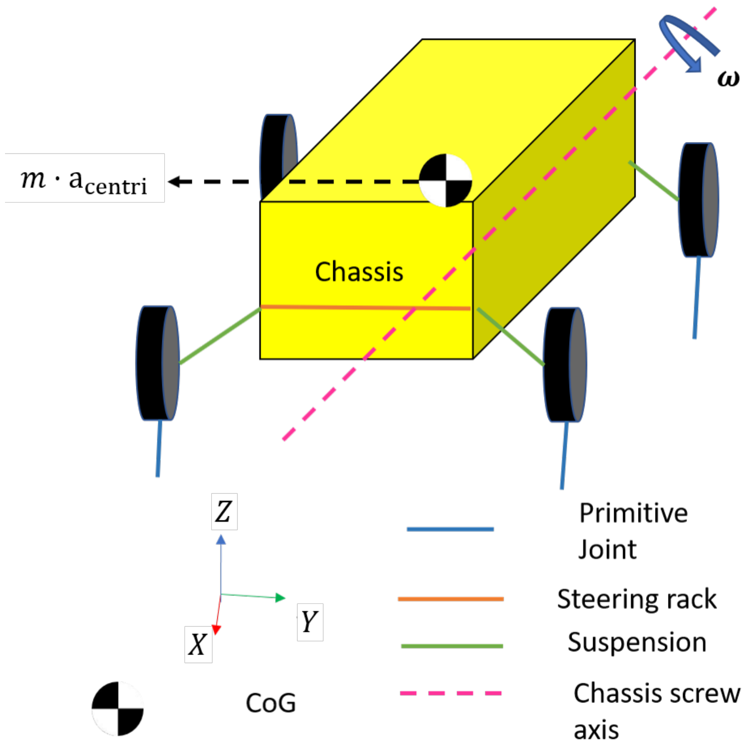

Figure 5.2: Boundary conditions of the kinematic model without steering input

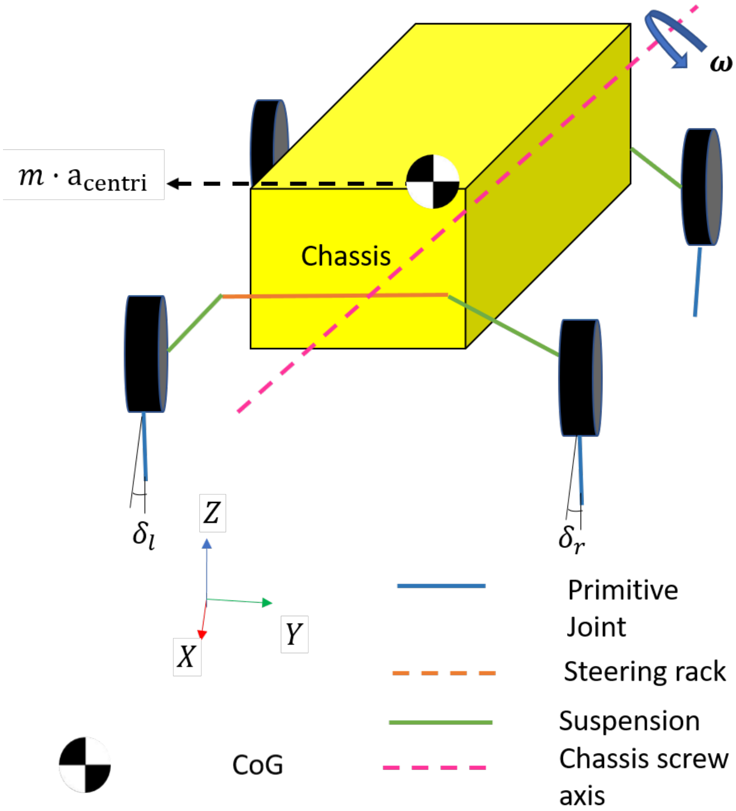

Figure 5.3: Boundary conditions of the kinematic model with steering input

6 Result

In this chapter, the results from using the methods in Section 4.2 are found for various suspensions. The values of MC from the $\Delta Y/\Delta Z$ method and Virtual Position using Kennedy's approach were the same and they also matched with the Screw Axis Offset method. Here, only the Screw Axis offset method is verified with the multibody model which implies that they also match with the other two methods.

6.1 Suspension Analysis - Multibody Model vs Screw Axis Offset Method

The multibody models can be used to find the Moment Center (MC) of a suspension or the chassis depending on which model is used. A force is applied at various heights on the body whose MC is to be found. The height at which the body does not undergo any angular displacement is the height of the MC as the force passes through it. For finding the instantaneous center of rotation of a suspension, a single suspension model is used with the force being applied at the upright link. For finding the roll center of one side, the one axle model is used and the force is applied on the chassis at various heights. This is then compared with the results from the Screw Axis Offset method to check if its calculated value matches the MC from the multibody model. Here, $\widehat{\boldsymbol{\omega}}$ is mostly used in figures and explanations which defines the direction and location of $\boldsymbol{\omega}$.

6.1.1 Planar Suspension

For a planar suspension, the planar single suspension multibody model was used which is talked about in Section C.1.1. The MC was found from this model and compared with the results from the Screw Axis Offset calculations. Please refer to Figure 4.6 for information about the variables.

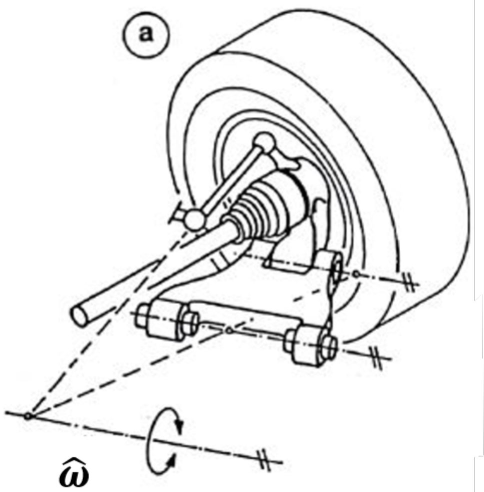

Figure 6.1: Planar Suspension with $\widehat{\boldsymbol{\omega}}$ [7]

Figure 6.1 above shows the same as Figure 1.7 (a) but $\widehat{\boldsymbol{\omega}}$ is shown as the rotation axis as mentioned in the previous subsection.

The following are the features of a planar suspension as defined by the terms v_{M_x}, v_{M_y}, v_{M_z}, ω_x, ω_y and ω_z:

- $\widehat{\boldsymbol{\omega}}$ is parallel to the X axis of the vehicle.
- $\boldsymbol{v}_M$ has no component in the direction of $\boldsymbol{\omega}$.

- So, example of planar suspension is,

$$\boldsymbol{v}_M = \left[0, v_{M_y}, v_{M_z}\right]$$
$$\boldsymbol{\omega} = \left[\omega_x, 0, 0\right]$$

As discussed earlier in Section 1.6, the wheel planes are looked at now. The intersection of $\widehat{\boldsymbol{\omega}}$ with the wheel planes give a point. Let this point be called $\widehat{\boldsymbol{\omega}}$ intersection point.

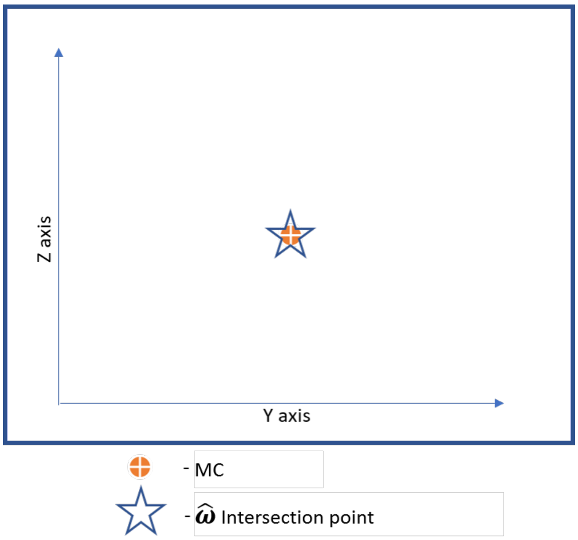

Figure 6.2: $\widehat{\boldsymbol{\omega}}$ intersection point vs MC in rear wheel plane for a planar suspension

Figure 6.4 shows the $\widehat{\boldsymbol{\omega}}$ intersection point and the MC in the rear wheel plane found from the multibody model. It can be seen that the two points coincide as expected and the point on the instantaneous rotation axis is also the MC in the wheel plane.
Also, note that, considering this is a planar suspension, pitch velocity, $t = 0$ hence, Equation (4.14) and Equation (4.15) give values of zero for the offsets a_y and a_z.

6.1.2 Spherical Suspension

For a spherical suspension, the spherical single suspension multibody model was used which is talked about in Section C.1.1. Please refer to Figure 4.6 for information about the variables. Figure 6.3 shows the same as Figure 1.7 (b) but $\widehat{\boldsymbol{\omega}}$ is shown as the rotation axis as mentioned in the previous subsection.

The following are the features of a spherical suspension as defined by the terms v_{M_x}, v_{M_y}, v_{M_z}, ω_x, ω_y and ω_z:

- $\boldsymbol{v}_M$ has no component in the direction of $\widehat{\boldsymbol{\omega}}$.
- So, example of spherical suspension is,

$$\boldsymbol{v}_M = \left[v_{M_x}, v_{M_y}, v_{M_z}\right]$$
$$\boldsymbol{\omega} = \left[\omega_x, \omega_y, \omega_z\right]$$

Where $\boldsymbol{v}_M$ does not have a component in the direction of $\boldsymbol{\omega}$ or in numerical form is the same as follows.

$$\boldsymbol{\omega} \cdot \boldsymbol{v}_M = 0$$

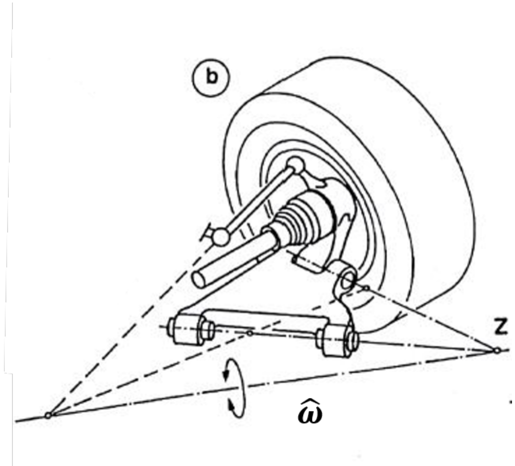

Figure 6.3: Spherical Suspension with $\widehat{\boldsymbol{\omega}}$ [7]

A similar method as that used for the Planar suspension above was followed to find the $\widehat{\boldsymbol{\omega}}$ intersection point and the MC.

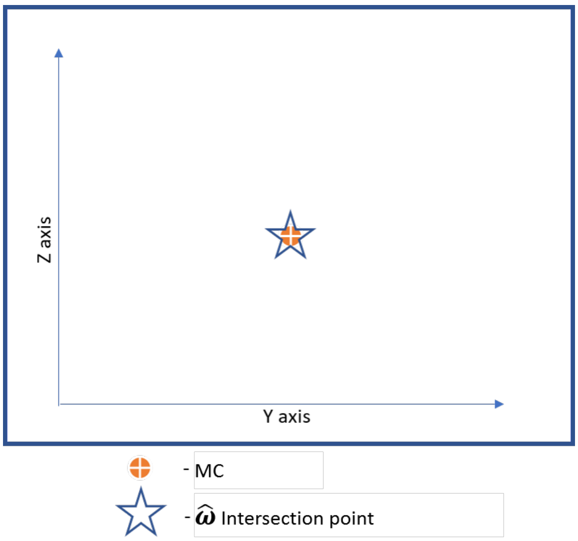

Figure 6.4: $\widehat{\boldsymbol{\omega}}$ intersection point vs MC in rear wheel plane for a spherical suspension

Figure 6.4 shows the $\widehat{\boldsymbol{\omega}}$ intersection point and the MC in the rear wheel plane. It can be seen that the two points coincide as expected similar to the planar suspension case.
Also, note that, considering this is a planar suspension, pitch velocity, $t = 0$ hence, Equation (4.14) and Equation (4.15) give values of zero for the offsets a_y and a_z.

6.1.3 Spatial Suspension

For a spatial suspension, the spatial single suspension multibody model was used which is talked about in Section C.1.2. The MC was found from this model and compared with the results from the Screw Axis Offset calculations. Please refer to Figure 4.6 for information about the variables.

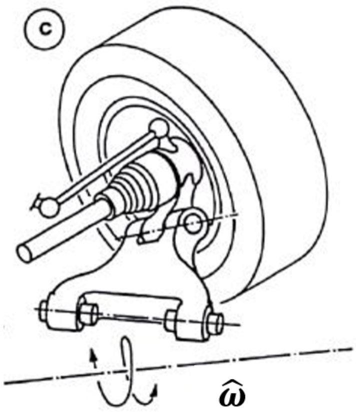

Figure 6.5: Spatial Suspension with $\widehat{\boldsymbol{\omega}}$ and t [7]

Figure 6.5 above shows the same as Figure 1.7 (c) but $\widehat{\boldsymbol{\omega}}$ is shown as the rotation axis and pitch velocity t is also shown.

The following are the features of a spatial suspension as defined by the terms v_{M_x}, v_{M_y}, v_{M_z}, ω_x, ω_y and ω_z:

- $\boldsymbol{v}_M$ has a component in the direction of $\widehat{\boldsymbol{\omega}}$ i.e. the wheel carrier translates along the rotation axis giving a screw motion.

- So, example of spatial suspension is,

$$\boldsymbol{v}_M = \left[v_{M_x}, v_{M_y}, v_{M_z}\right]$$

$$\boldsymbol{\omega} = \left[\omega_x, \omega_y, \omega_z\right]$$

  Where $\boldsymbol{v}_M$ does have a component in the direction of $\widehat{\boldsymbol{\omega}}$

$$\boldsymbol{\omega} \cdot \boldsymbol{v}_M \neq 0$$

Here two cases are looked into:

Spatial Suspension - Case 1

In this case the rotation axis is along the vehicle X axis like the planar suspension while the suspension is still spatial i.e. it has a velocity component in X axis.

- So, the vectors look like the following

$$\boldsymbol{v}_M = \left[v_{M_x}, v_{M_y}, v_{M_z}\right]$$

$$\boldsymbol{\omega} = \left[\omega_x, \omega_y, \omega_z\right]$$

- Where $\boldsymbol{v}_M$ has a component in $\boldsymbol{\omega}$.

A similar method as that used for the Planar suspension above was followed to find the $\widehat{\boldsymbol{\omega}}$ intersection point and the MC.

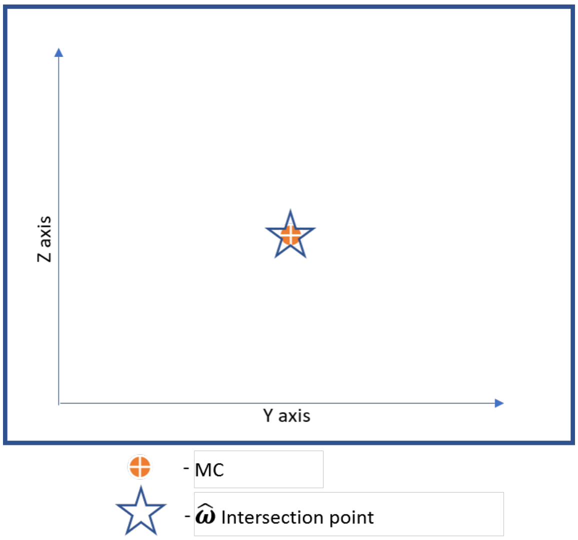

Figure 6.6: $\widehat{\boldsymbol{\omega}}$ intersection point vs MC in rear wheel plane for spatial suspension case 1

Figure 6.4 shows the $\widehat{\boldsymbol{\omega}}$ intersection point and the MC in the rear wheel plane. Here too, it can be seen that the two points coincide which is similar to planar and spherical suspension.
Note that, in this case pitch velocity t is non zero but it only has a component in the direction of t_x. t_y and t_z are zero. Hence, in Equation (4.14) and Equation (4.15) components of offset vector a_y and a_z are zero.

Spatial Suspension - Case 2

In this case the rotation axis is not along the vehicle X axis but is a 3D axis like a spherical suspension while the suspension is still spatial i.e. it has a velocity component along the rotation axis.

- So, the vectors look like the following

$$\boldsymbol{v}_M = \left[v_{M_x}, v_{M_y}, v_{M_z}\right]$$
$$\boldsymbol{\omega} = \left[\omega_x, 0, 0\right]$$

- Where v_{M_x} is non zero.

A similar method as that used for the Planar suspension above was followed to find the $\widehat{\boldsymbol{\omega}}$ intersection point and the MC.

Figure 6.7 shows the $\widehat{\boldsymbol{\omega}}$ intersection point and the MC in the rear wheel plane.

It is interesting to note that in this case the $\widehat{\boldsymbol{\omega}}$ intersection point and the MC do not match. There is an offset of $\boldsymbol{a}$ as discussed previously in Section 4.2.3. Thus, the instantaneous screw axis does not directly define the MC in this type of suspension. Note that, in this case pitch velocity t is non zero. Since t_y and t_z are non zero, Equation (4.14) and Equation (4.15) give non zero offsets a_y and a_z.

6.1.4 Roll Center Calculation

Now, with the information about the MC in the rear wheel plane, a Planar Instantaneous Link Model can be created like the one mentioned in chapter 2. The point of intersection between the lines drawn between the contact patch and the MC's give the roll center. The same can be done in the side view to find the pitch center.

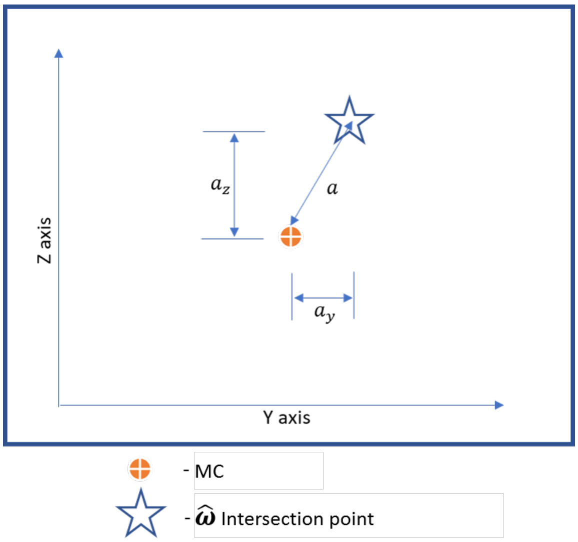

Figure 6.7: $\hat{\omega}$ intersection point vs MC in rear wheel plane for spatial suspension case 2

This was checked with the one axle model explained in Section C.2 and it correlated with the MC found from that multibody model.

6.2 Effect of steering on the chassis screw axis

As shown in Figure 6.8, for planar double wishbone very little deviation in $\boldsymbol{\omega}$ components are observed in planar double wishbone suspension in case of steering. Visible deviations as depicted in Figure 6.10 for spatial double wishbone suspension upon steering. However, for multi-link suspension deviations of $\boldsymbol{\omega}$ components are much significant as shown in Figure 6.12 while comparing with the two models. Since the deviations are enormous 0.15 [s], end time for simulations with multi-linked is considered to be 0.15[s].

Locus of the intercept of the chassis screw axis on a particular plane defines the location of the instantaneous screw axis. The YZ plane at x=900mm where CoG lies is considered as the reference plane. In Figure 6.9, loci of the intercepts from two models perfectly coincides for planar double wishbone suspension. In case of spatial double wishbone suspension, initially coinciding the loci deviates to end of the simulation as depicted in Figure 6.11. For the multi-link suspension, as shown in Figure 6.13, two loci never coincides through the simulation and there exists a great deviation between the loci.

Spatial multi-link suspension becomes asymmetric upon steering due to changes in moving hardpoints which include all spherical balljoint on the upright. Considerable deviations in steering angles of multi-link suspension mentioned in Table 5.3 also supports the inference of the asymmetry. Negligible asymmetry of planar suspension upon steering does not affect instantaneous screw axis parameters. However, for spatial wishbone suspension, unlike the planar suspension, it becomes slightly asymmetric upon steering. But, translational DoF of the steered primitive joints affects the spatial motion of the steered suspensions, thereby affecting all moving hardpoint leading to asymmetric suspension. Furthermore, for a spatial multi-link suspension, there exists initial asymmetry due to steering and asymmetric enhances further with steered primitive joint like spatial double wishbone suspension. As a result, there exists huge deviations both in the instantaneous screw axis $\boldsymbol{\omega}$ and its location upon steering.

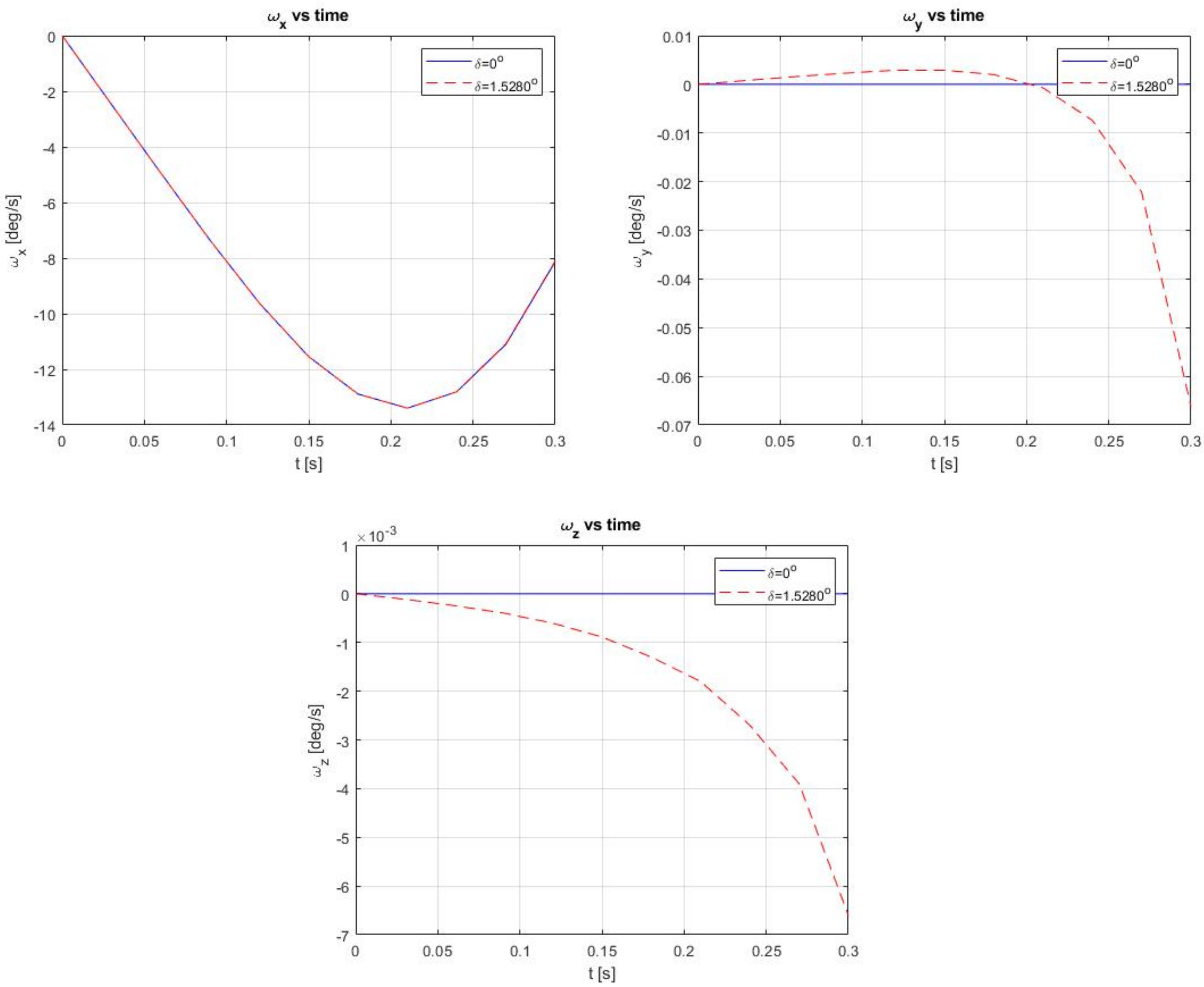

Figure 6.8: $\boldsymbol{\omega}$ components chassis with planar double wishbone suspensions

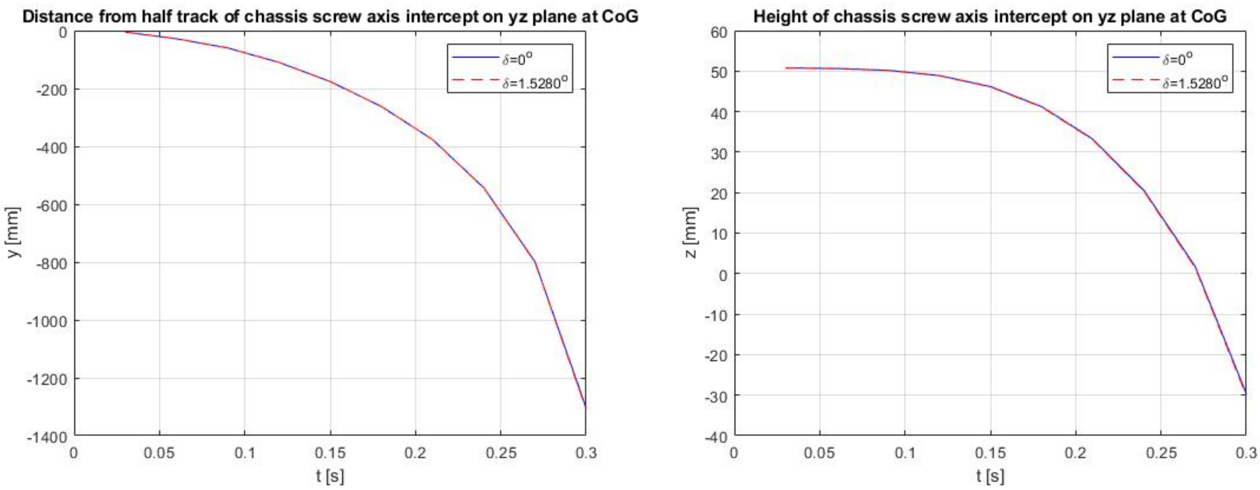

Figure 6.9: Chassis screw axis intercept locus of planar double wishbone suspension

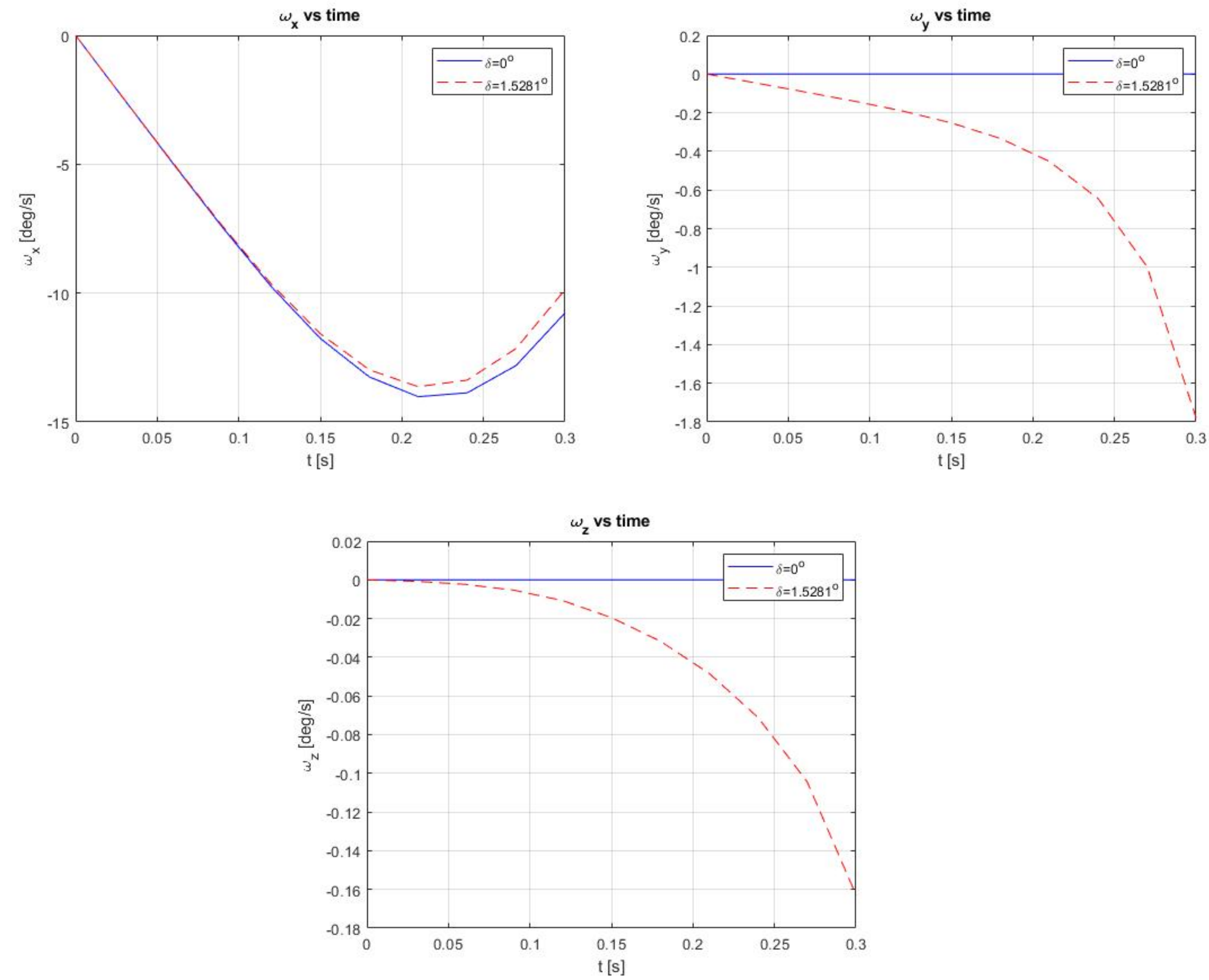

Figure 6.10: $\boldsymbol{\omega}$ components chassis with spatial double wishbone suspensions

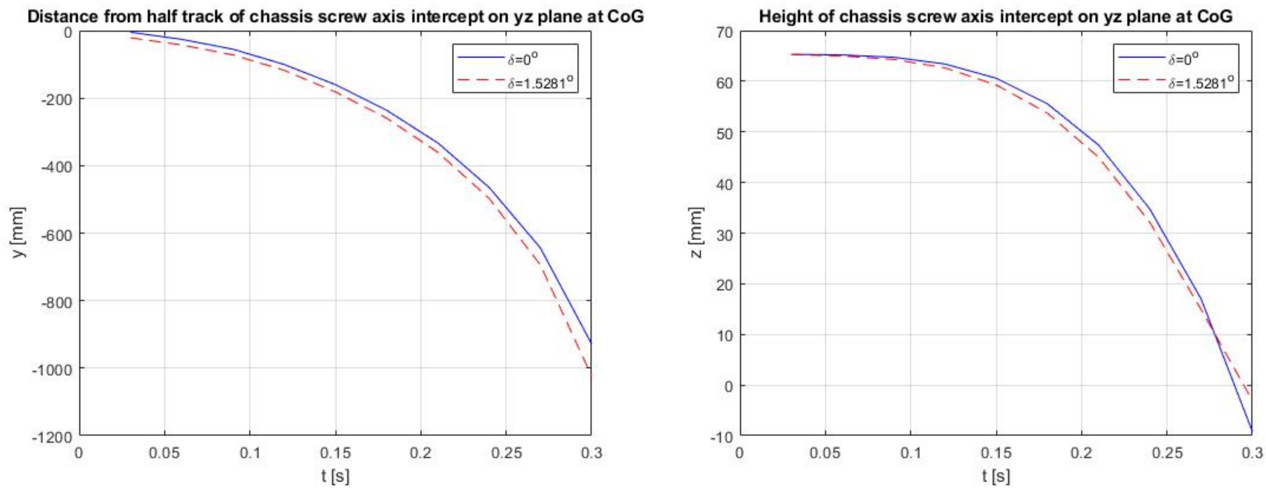

Figure 6.11: Chassis screw axis intercept locus of spatial double wishbone suspension

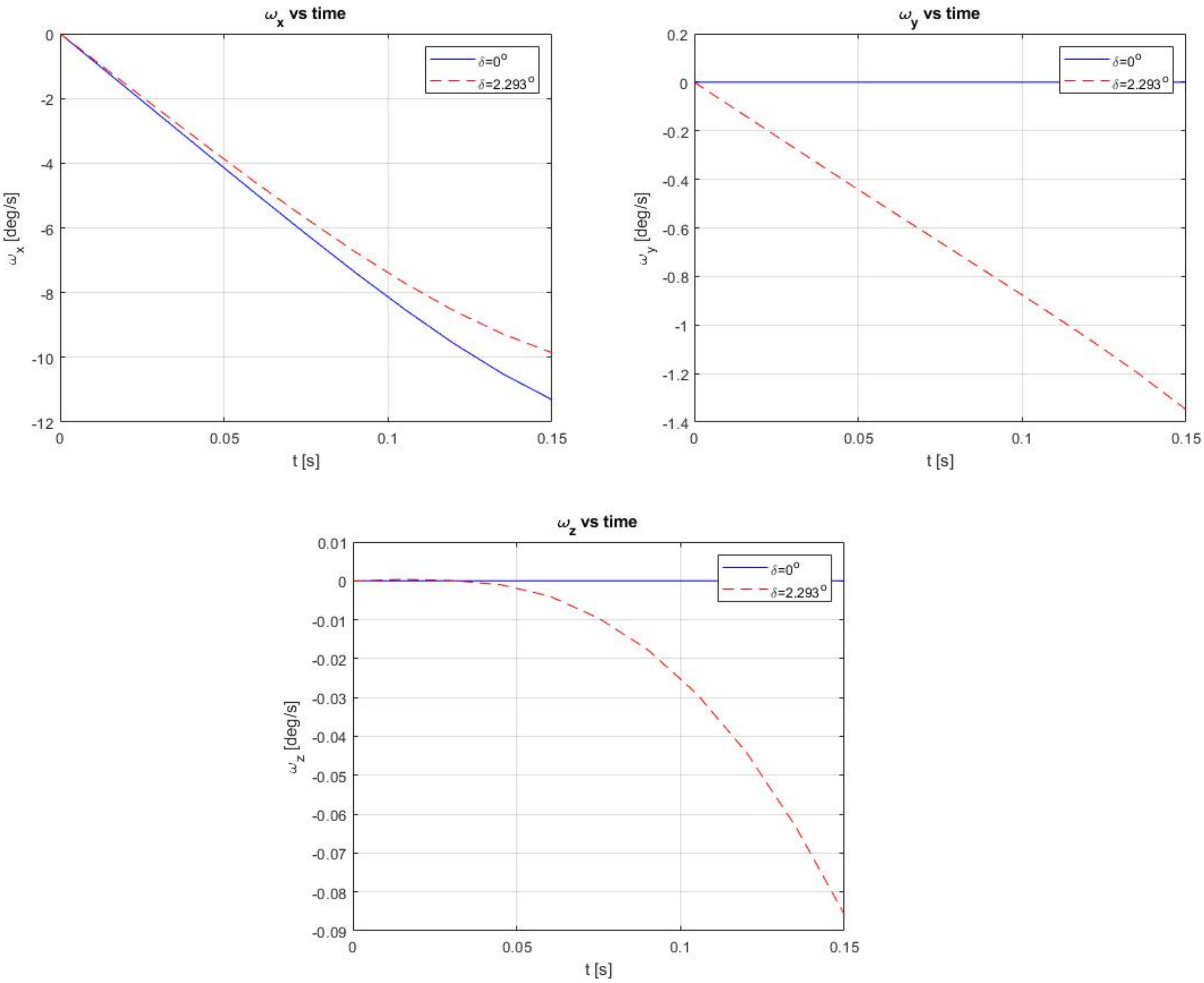

Figure 6.12: $\boldsymbol{\omega}$ components chassis with spatial multi-link suspensions

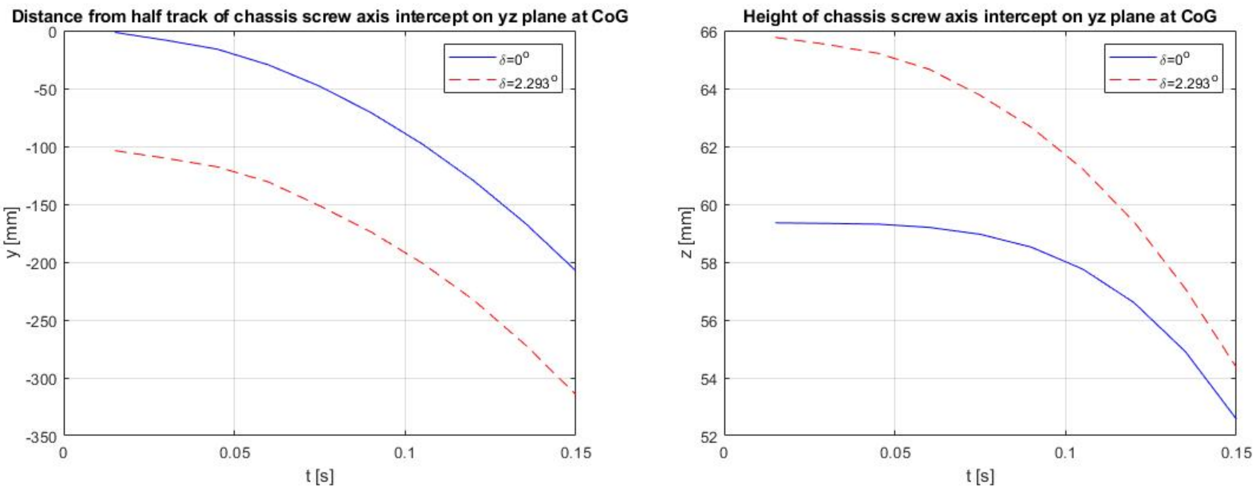

Figure 6.13: Chassis screw axis intercept locus of spatial multi-link suspension

7 Discussion

7.1 Comparison of Suspension Analysis Methods

The suspension analysis methods explained in Section 4.2 can be compared to each other.

First thing to be noted is that the Roll Center and Instantaneous Center of rotation values from all the three methods give the same result which also correlates with the multibody models. This is true not only for spatial suspensions, but also spherical and planar suspensions. The difference is in the approaches used.

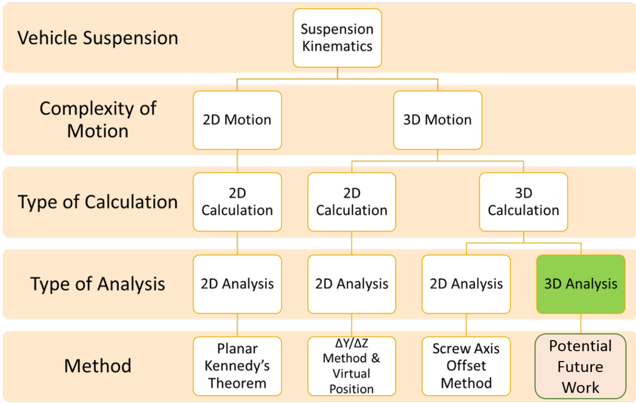

Figure 7.1: Categorisation of methods used in the thesis

As seen in Figure 7.1, although the results obtained are the same, the methods vary in the way they calculate and analyze suspensions. The conversion of a 3D motion to a 2D calculation is better from a computational point of view whereas calculating in 3D helps understand the complex motion better and understand effect of design changes easily and tune the suspension more efficiently. The analysis in 2D is also helpful to visualize the suspension. Thus, they complement each other and it also gives a more complete idea of the screw motion and its effects and helps understand spatial suspensions better.

7.2 Use case in Production Vehicle

The Screw Axis Offset Method was also used on a production vehicle suspension to check its roll center heights. This was done in collaboration with CEVT AB on one of their platforms.

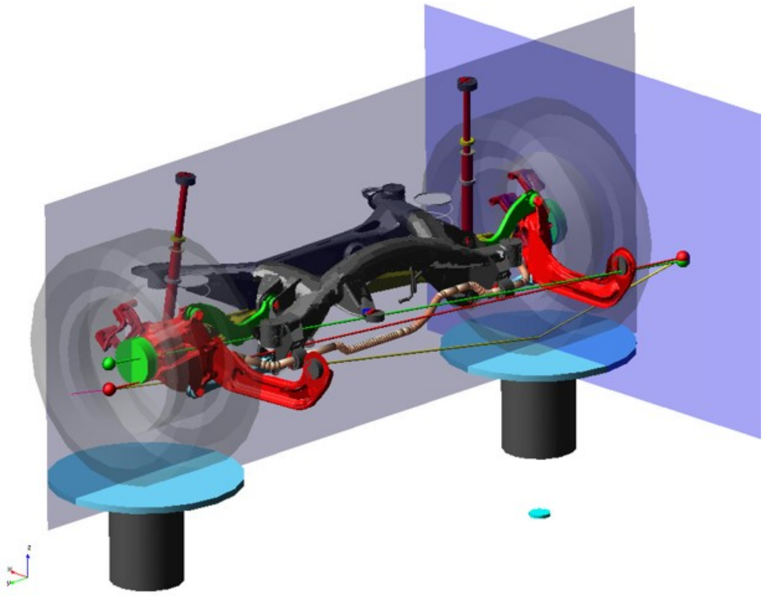

Figure 7.2: MSC ADAMS Model of the production vehicle suspension used to verify Screw Axis Offset Method (courtesy CEVT AB)

In the image above i.e. Figure 7.2, the MSC ADAMS model of the suspension discussed is shown. When the roll center height of this suspension is derived using the assumption that the rotation axis of this spatial suspension contains the location of the moment center in a given plane, an incorrect roll center height is found. When the screw axis offset is taken into consideration to calculate the MC of the suspension and subsequently the roll center, the value matches with that from MSC ADAMS Car. In the image, the green line indicates the initial value of the instantaneous center of rotation that was considered based on the rotation axis of the suspension without consideration for offset. The red line corresponds to the offset which gives the correct value for the instantaneous center of rotation denoted by the red dots in the two wheel planes. Finally, the yellow line joins the contact patch to the correct instantaneous center of rotation and is used for calculating the roll center. Thus, the Screw Axis Offset method was checked with an actual production vehicle suspension and verified.

7.3 Steering Effect

Steered suspensions becomes asymmetric compared to unsteered suspension for multi-link suspension. Steered primitive joints used in the steady steady cornering analysis affects the spatial motion and moving hardpoint of any spatial suspensions, thereby summing the asymmetric. When the kinematic model considers this asymmetry and changes in the contraints of the primitive joints, the model provides more accurate chassis screw axis parameters. These parameters could possibly be used in developing better load transfer models for steady state cornering. These load transfer models are extensively used during the designing phase in the automotive industry and are useful to develop further. But, as mentioned in the methodology section, it is important to note that the ackermann % of the three suspensions were not aligned to make them similar in the static or at some dynamic conditions and the effect of this is not looked into. Thus, it is important to note that each suspension and steering system here is different and should not be compared with each other but rather within themselves in the steered vs. non steered cases. Any other inferences found by comparing them to each other could be incorrect owing to the differences in their steering design parameters.

8 Future Work

A more thorough theoretical treatment of the roll center and its effect on load transfer and overall characteristics can be studied with equations derived for the same. This is currently difficult to find, in an understandable form, for linear and non linear cases. The equations should help understand the extent of effect that the roll center has and its sensitivity with respect to various other vehicle parameters and different manoeuvres.

The value of the offset found from the Screw Axis Offset Method was seen to be closely related to the amount of bump steer present in the axle. The higher the value of the offset, the higher the bump steer. This was not studied further and thus is not talked about in this thesis. But, it can be quantified and looked into as a tool for suspension design in spatial suspensions.

The Screw Axis Offset Method can be turned into a tool in itself with graphical axes and offsets being represented and changing with change in hardpoints to make the design process more intuitive.

Elasto-kinematics can be implemented to consider the effects of bushings and elastomer on the instantaneous screw axes of suspensions and chassis.

The steering analysis done can be furthered with more simulations to look at the possibility to understand and derive better vehicle properties while it can also be done for other steering simulation with equivalent steering parameters for each type of suspension to compare the effects of various suspensions which is not done here. Completely 3D methods have not been looked into in this thesis but could be interesting to study and understand if they give any extra or important information. Multibody models can be used to understand the 3D motion of the chassis for different inputs. The idea is to get a instantaneous screw axis for the chassis to check two specific characteristics. Firstly, the relation between the four suspension screw axes and the chassis screw axis. Secondly, the effect of this chassis screw axis on the vehicle behaviour can be evaluated in both an objective sense to define load transfer characteristics for example and also in a subjective sense to use as a tool to understand driver feedback from testing.

Appendices

A Joints

Illustration	Description	Mobility
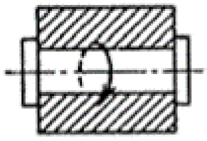	**Revolute Joint** Axis of rotation passes through the center of the joint at which two bodies rotate relatively.	$f_{rot} = 1$ $f_{tran} = 0$ $f = 1$
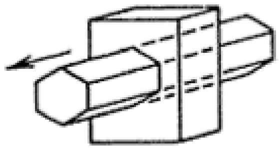	**Translation Joint** Two bodies translate relatively in one direction defined by the joint.	$f_{rot} = 0$ $f_{tran} = 1$ $f = 1$
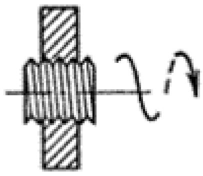	**Screw Joint** Two bodies moves relatively in a screw or helical motion along the axis passing through the joint center.	$f_{scr} = 1$ $f = 1$
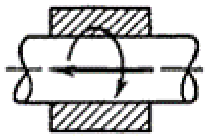	**Cylindrical Joint** Two bodies translate and rotate relatively according to the axis passing through the joint center.	$f_{rot} = 1$ $f_{tran} = 1$ $f = 1$
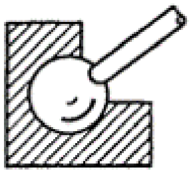	**Spherical Joint/ Ball Joint** Two bodies rotate relatively based on spherical contact surfaces in the joint.	$f_{rot} = 3$ $f_{tran} = 0$ $f = 3$
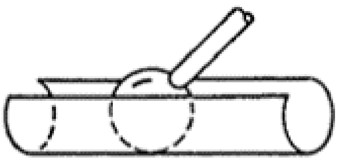	**Inline Primitive Joint** Two bodies can move relatively free in all rotational DoF(s) and also translates in direction defined by the joint.	$f_{rot} = 3$ $f_{tran} = 1$ $f = 4$

Table A.1: Common joints being utilised in suspension kinematics model [20]

B Vehicle Longitudinal and Combined Characteristics

This appendix gives some details about the vehicle longitudinal characteristics and combined longitudinal and lateral characteristics. As the thesis deals primarily with steady state lateral dynamics, longitudinal characteristics have not been mentioned in the contents but rather in this appendix for readers that may be interested.

B.1 Tire Longitudinal Characteristics

The longitudinal forces are produced by the longitudinal deformation of the contact patch which is measured in terms of the slip ratio. This can be defined as the ratio of the longitudinal velocity of the tire with respect to the expected longitudinal velocity of the tire based on the rotational velocity considering pure rolling. Thus, to produce longitudinal forces, the tire cannot be in pure rolling. Longitudinal forces can be in acceleration and in braking as well. The definition of slip ratio is not universally agreed upon and various equations are used to define it although most of them mean the same thing. Here, it is defined as is mentioned in the "Vehicle Dynamics Compendium for Course MMF062" by Bengt Jacobson et al [21].

$$s_x = \frac{R_e \cdot \omega - v_x}{R_e \cdot \omega} \tag{B.1}$$

where R_e is effective rolling radius of the tire, ω is the rotational velocity of the tire, v_x is the longitudinal translational velocity of the tire.

The Equation (B.1) above shows the slip ratio calculation for a case where the tire is accelerating forward. This equation has to be changed slightly to make it compatible for braking case and this is shown in Equation (B.2) below

$$s_x = \frac{R_e \cdot \omega}{R_e \cdot \omega - v_x} \tag{B.2}$$

The longitudinal behaviour of the tire has similarities with the lateral in some aspects. The longitudinal force F_x vs slip ratio SR curve looks the same as the one for lateral force and slip angle shown in Figure 3.4 above. Looking at the factors affecting the longitudinal behaviour, in case of vertical loading, the normalized longitudinal force $\frac{F_x}{F_z}$ is similar to the behaviour of the normalized lateral force where the longitudinal tire-road coefficient decreases with increase in vertical loading. In terms of camber, the highest longitudinal force is produced at zero camber and drops off as the camber changes to either positive or negative. This is explained in Section 3.3.

Finally, the tire also has characteristics for combined longitudinal and lateral forces. The tire cannot utilize the maximum possible tire-road coefficient for both longitudinal and lateral directions together. If the tire is using part of its maximum lateral capabilities, then the longitudinal force it can produce is less than the maximum pure longitudinal force capability. If maximum lateral capacity of the tire is being used, then it cannot generate any longitudinal force and vice versa. This is illustrated using a concept called the friction circle. Here the normalized lateral force is plotted on one axis and the normalized longitudinal force is plotted on another axis. The limits of the tire appear as a circle on this graph which shows the maximum combined capability a tire can reach. Most of the times, the actual tire characteristics and limits are not equivalent in lateral and longitudinal direction and hence the actual plot it is more of a friction ellipse than a friction circle. In the Figure B.1 below shows a graph of a friction circle of a tire. In the case below, only the right half of the circle is shown as it is only showing the data for a right handed turn. Also note that this graph is not from racing tire but from a normal small passenger car tire.

B.2 The Pitch Center

The concept of pitch center is the exact same as roll center except for longitudinal forces. It also exists in the XZ plane or side view plane of the vehicle. This is the zero moment point for a longitudinal force. It is important to note that the front and the rear suspension of regular passenger cars may be different but the left and the right sides are always the same and hence it does not affect the steady state longitudinal load transfer characteristics of the vehicle. But, the height of the pitch center affects the amount of anti dive and anti squat in the vehicle. The anti effects can be compared to the effect of the suspension links being the path of load transfer which causes a jacking force. Anti is similar to the jacking effect. Anti dive refers to the front suspension links taking the forces instead of the springs when the car "dives" which is when it decelerates the front of the chassis tries to pitch down. Anti squat is similar but occurs for the rear suspension when the vehicle accelerates and tries to pitch the rear of the chassis downward. Anti values are mentioned in percentages so, 100 percent anti would mean that the suspension links take all the forces and the spring takes none. The value of anti depends not only on the height of the pitch center with respect to the sprung mass center of gravity height, but also the brake and drive torque distribution between the front and the rear axles.

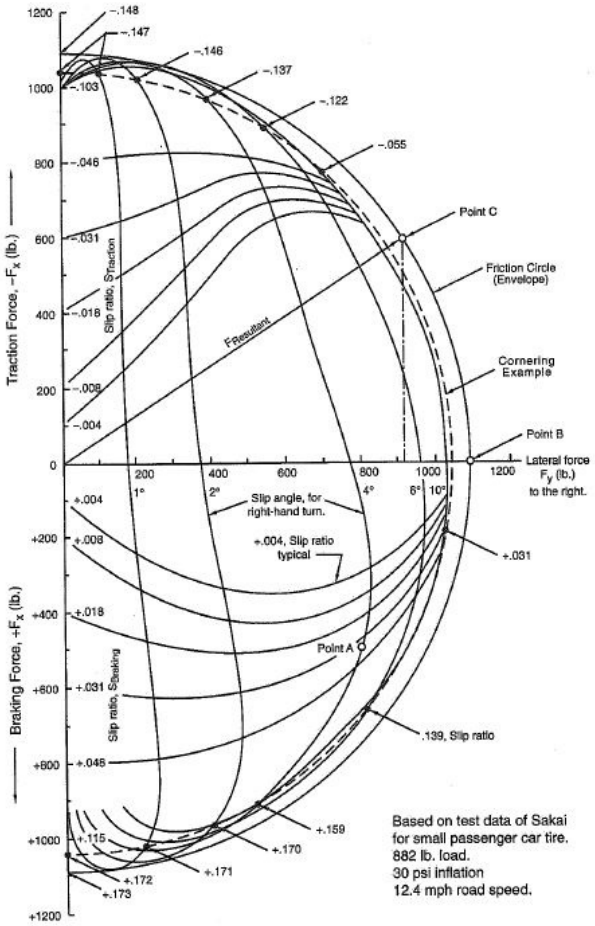

Figure B.1: Friction Circle for a right hand turn of a small passenger car tire [13]

C Multibody Systems Vehicle Modelling and Simulation

For the purpose of understanding the vehicle suspension and the kinematics, and also to validate and verify the results from the different theoretical methods used, multibody models are very helpful. For this thesis MSC ADAMS software was used extensively to made multibody models. This chapter looks at these models. Further details about the model are also included in the Appendix.

C.1 Single Suspension Model

A single suspension model is one which has a fixed chassis and one side of the suspension attached to it. The purpose of doing this was to understand the ZMP of the suspension.

C.1.1 Planar and Spherical Suspension

Figure C.1 above shows the parts of the multibody model to create a single planar suspension. Figure C.2 shows the constraints used in the model. It can be seen that the links are connected to the chassis by revolute joints with their axis of rotation perpendicular to the view plane making it purely planar motion. the links are also connected to the upright link by similar revolute joints defined in the plane. The chassis is fixed to the ground.

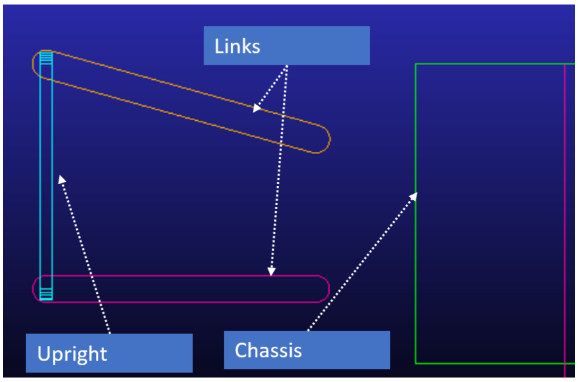

Figure C.1: Planar Suspension ADAMS View Model

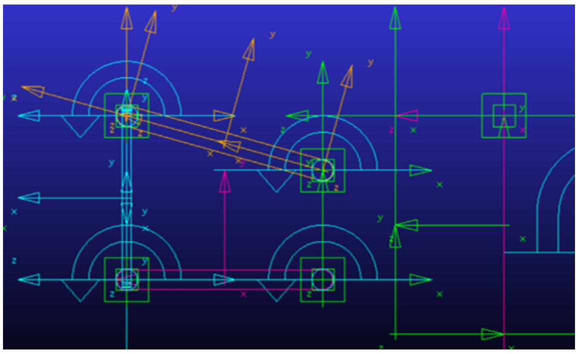
Figure C.2: Constraints of the Planar Suspension ADAMS View Model

Forces can now be given to the upright in this model to study its motion. Since, only the suspension kinematic effects and motions are looked into, the spring was not modeled. Hence, no gravity was added during simulations either as it would collapse the free body. Only lateral forces are being looked into which means that gravity is not required either.

The multibody model of a single spherical suspension created was almost identical to the planar suspension above with the only difference being the definition of the joints. The same revolute joints were used in the same locations as the planar model but with the slight difference of changing the axis of rotation of the spherical joint between the links and the chassis. This axis is now defined in three dimensions instead of being perpendicular to the view plane.

C.1.2 Spatial Suspension

For the multibody model of a spatial suspension a a fixed chassis with a complete 5 link mechanism was constructed on ADAMS. The Figure C.3 above shows the model of the suspension. It was created using 5 links that are connected to the chassis by spherical joints and the other ends joined to a plate representing the upright by spherical joints as well. The chassis was kept fixed as in the case for planar and spherical suspensions above.

C.2 Single Axle Model

A single axle model is one that has a complete axle with two sides of the suspension connected by a chassis. The chassis in this case in not fixed and the wheels are fixed to the ground. Planar and Spatial Single Axle models were made for the purpose of this thesis. The single axle model helps find the ZMP for the chassis which as has been discussed earlier is the roll center point. Thus, this model gives the location of the roll center for an axle.

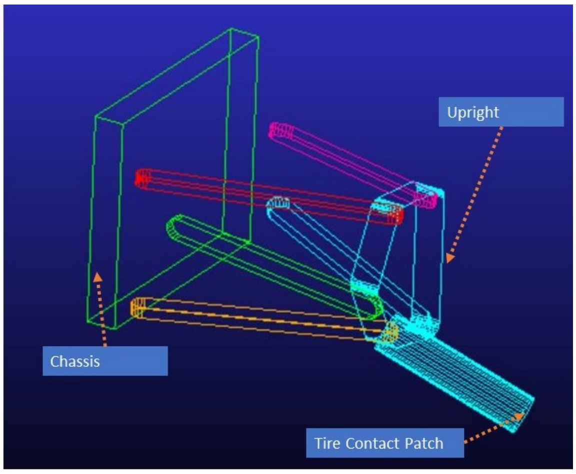

Figure C.3: Spatial Suspension ADAMS View Model (Isometric View)

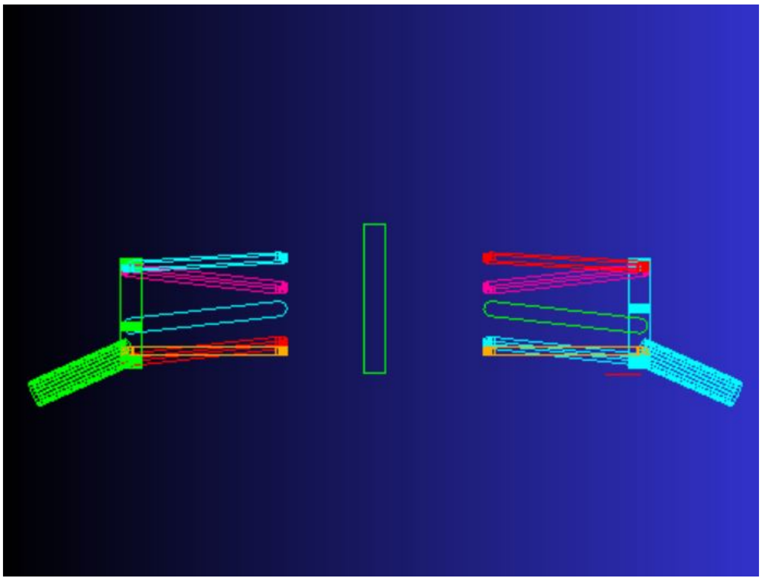
Figure C.4: Spatial Suspension One Axle ADAMS View Model

The Figure C.4 shows the model for a spatial suspension.

The constraints used for both the planar and the spatial were similar to the ones used for the single suspension model described previously. The addition being that the upright link was extended to a contact patch point which was constrained to the ground using spherical joints and making the chassis free. Again, no gravity is given to make sure that the chassis does not collapse.

C.3 Two Axle Model

A two axle model contains all four corners of the vehicle and the chassis. This is useful for understanding the roll axis which is defined by both the front and rear suspension. It can also be used to understand the pitching behaviour of the vehicle when the complete suspension links are modeled.

The above Figure C.5 shows the full vehicle model for 4 spatial suspensions. The front and the rear suspensions are the same type to simplify the modeling although they can be made different and the model would still be valid and working. The constraints between the chassis and the suspension links and the links and the upright are identical to the ones in the aforementioned single axle model. The difference is in the way the tire contact patch link is connected to the ground.

The idea behind this model is to understand the angular motion of the chassis. Hence, the chassis needs to

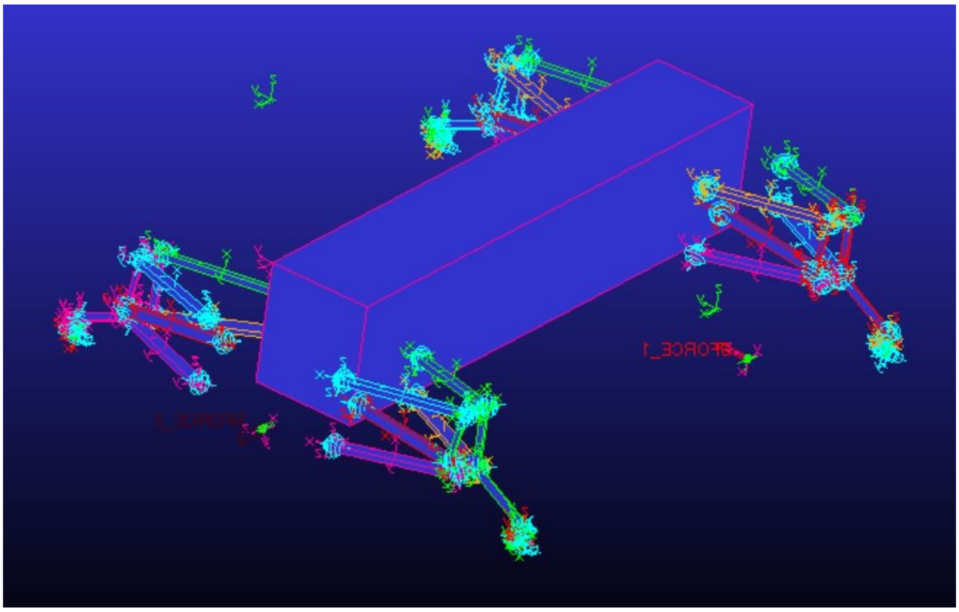

Figure C.5: Spatial Suspension Two Axle Model

be kept free and the tires need to be connected to the ground. Initially the attempt was to connect the four tire contact patches to the ground using spherical joints similar to the single axle model. It is interesting to note that the mechanism or the model had no degree of freedom left in this case and it was locked. This makes sense as in the real world, during chassis roll, the tires can rotate or roll on the ground forward and backward while during pitch, the contact patch can change with respect to each other and change the track width.

Thus, for the model to check for roll, a new constraint was used. Here, the contact patched were connected to the ground via a dummy part. The dummy part is just to have two joints in series. First, the contact patch was connected to the dummy part by a spherical joint and then the dummy part was connected to the ground by a planar sliding joint in the direction of the vehicle X axis. This now allows for the roll of the chassis similar to a real vehicle. This can also be done by using Primitive joints which give the same result.

To simulate pitching, the same model cannot be used and it needs to be altered slightly. Here, the sliding joint is changed to slide along the vehicle Y axis.

C.4 Double Axle Planar Instantaneous Link Model

The final model created was a simplified model representing a full vehicle. It is called the Double Axle Planar Instantaneous Link Model. It is the complete vehicle version of the "Planar Instantaneous Link Model" written about in Chapter 2.

The Figure C.6, Figure C.7,Figure C.8 above show this model. It is a combination of the Planar Instantaneous Link Model and the Two Axle Model discussed in the previous section. The instantaneous links are similar to the Planar Instantaneous Link Model but are now present in for both the front and the rear axle while the chassis coupler link is now a plate. It also has links to define the Pitch Center point which is exactly the same as the one created in rear view, but now in side view. These are combined together in this model.

The constraint at the Tire Contact Patch though is not the same as the Planar Instantaneous Link Model. It is discussed in the previous section that four spherical joints lock the mechanism. Hence, like the Two Axle model, a combination of a spherical joint and a planar joint is used to create the model.

With this model, it is possible to check the instantaneous behaviour of the chassis with the suspension Tire Contact Patch and ZMP points know in both side view and rear view. But, to check for roll, the planar sliding joint needs to be directed in the vehicle X axis and to check for picth, the sliding jpint needs to be directed along the vehicle Y axis.

Note that this model is only instantaneous and any large motions no longer define the behaviour of an actual vehicle.

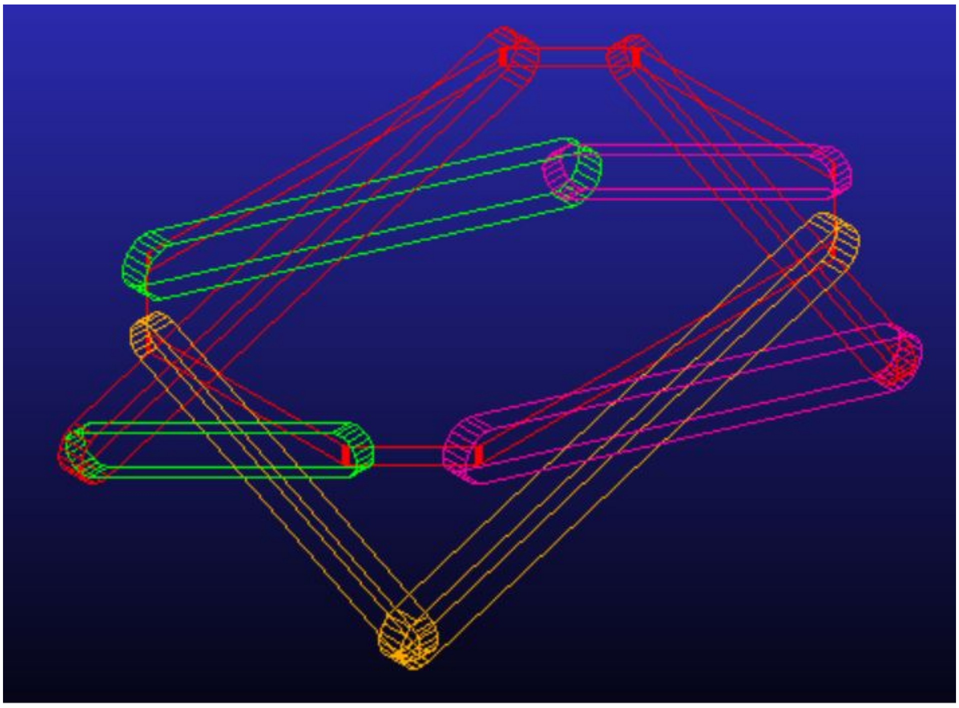

Figure C.6: Double Axle Planar Instantaneous Link Model (Isometric View)

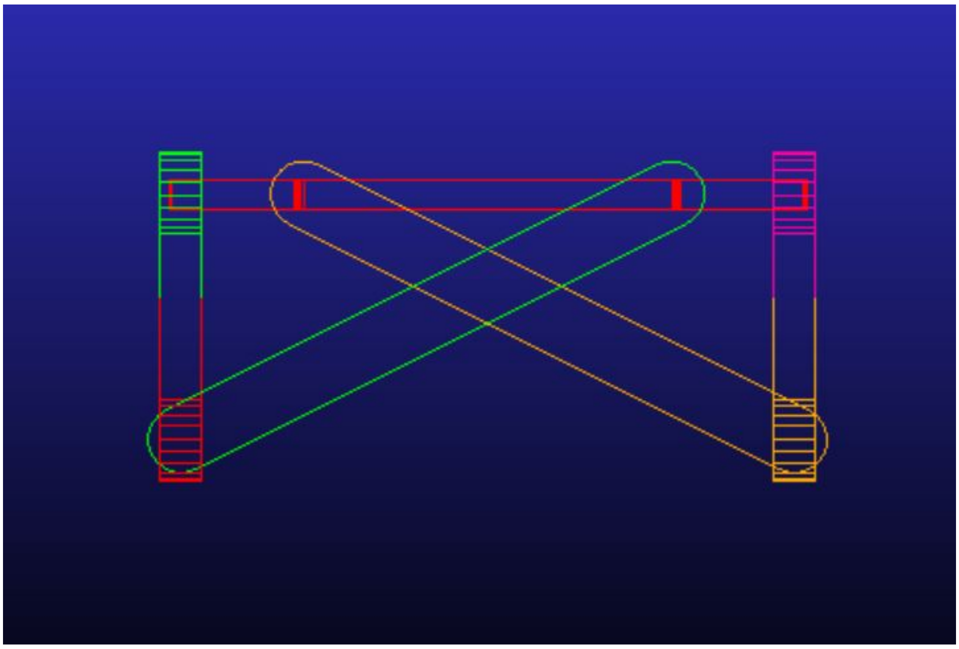

Figure C.7: Double Axle Planar Instantaneous Link Model (Front View)

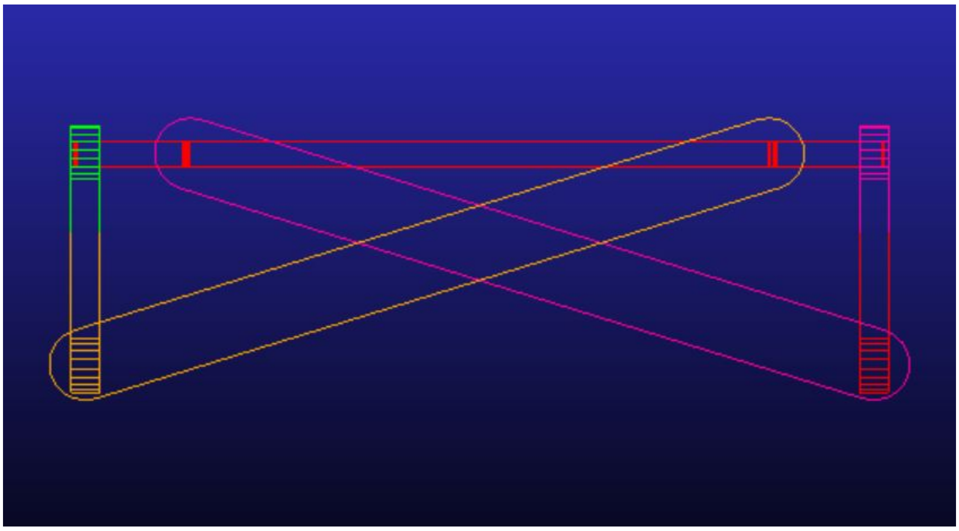

Figure C.8: Double Axle Planar Instantaneous Link Model (Side View)

D MATLAB Code - Screw Axis Offset Method

Contents


```
clear all
close all
clc
```

INPUT SUSPENSION PARAMETERS

```
L=2675; %Wheelbase [mm]

% Front (Left)
ShiftVecFL=[-267, 760, -330];
Afl =[67 -450 180]+ShiftVecFL;
Gfl =[467 -450 180]+ShiftVecFL;
Pfl =[367 -490 560]+ShiftVecFL;
Qfl=[517 -490 560]+ShiftVecFL;
B1_1fl=[267 -750 130]+ShiftVecFL;
B1_2fl=[267 -750 130]+ShiftVecFL;
C1_1fl=[307 -675 555]+ShiftVecFL;
C1_2fl=[307 -675 555]+ShiftVecFL;
Tfl=[467 -400 365.224]+ShiftVecFL;
H1fl=[417 -750 330]+ShiftVecFL;
E1fl=[267 -760 330]+ShiftVecFL;
cpfl=[267 -760 0]+ShiftVecFL;

% Rear (Left)
```

```
ShiftVecRL=[0,825,-0.5*457];
Arl =[200 -250 100]+ShiftVecRL;
Grl =[-200 -250 120]+ShiftVecRL;
Prl =[200 -250 320]+ShiftVecRL;
Qrl=[-200 -250 250]+ShiftVecRL;
B1_1rl=[50 -600 100]+ShiftVecRL;
B1_2rl=[-50 -600 80]+ShiftVecRL;
C1_1rl=[50 -600 300]+ShiftVecRL;
C1_2rl=[-50 -600 290]+ShiftVecRL;
Trl=[100 -250 200]+ShiftVecRL;
H1rl=[100 -600 260]+ShiftVecRL;
E1rl=[0,-825,0.5*457]+ShiftVecRL;
cprl=[0,-825,0]+ShiftVecRL;

% Velocity Input for steering link (If steering input is given)

V1e_x_fl= 0;
V1e_y_fl= 0;
V1e_z_fl= 0;

V1e_x_fr= 0;
V1e_y_fr= 0;
V1e_z_fr= 0;

V1e_x_rl= 0;
V1e_y_rl= 0;
V1e_z_rl= 0;

V1e_x_rr= 0;
V1e_y_rr= 0;
V1e_z_rr= 0;

% Input Wheel Velocity (Z component velocity input for bump analysis)

Vm_z_fl= 10;
Vm_z_fr= 10;
Vm_z_rl= 10;
Vm_z_rr= 10;

% Wk_z_fl= 0;
% Wk_z_fr= 0;
% Wk_z_rl= 0;
% Wk_z_rr= 0;
```

Mirror Calculation

```
Afr=mirrory(Afl);
Gfr=mirrory(Gfl);
Pfr=mirrory(Pfl);
Qfr=mirrory(Qfl);
B1_1fr=mirrory(B1_1fl);
B1_2fr=mirrory(B1_2fl);
C1_1fr=mirrory(C1_1fl);
C1_2fr=mirrory(C1_2fl);
Tfr=mirrory(Tfl);
H1fr=mirrory(H1fl);
```

```
E1fr=mirrory(E1fl);
cpfr=mirrory(cpfl);
ShiftVecFR=mirrory(ShiftVecFL);

Arr=mirrory(Arl);
Grr=mirrory(Grl);
Prr=mirrory(Prl);
Qrr=mirrory(Qrl);
B1_1rr=mirrory(B1_1rl);
B1_2rr=mirrory(B1_2rl);
C1_1rr=mirrory(C1_1rl);
C1_2rr=mirrory(C1_2rl);
Trr=mirrory(Trl);
H1rr=mirrory(H1rl);
E1rr=mirrory(E1rl);
cprr=mirrory(cprl);
ShiftVecRR=mirrory(ShiftVecRL);
```

MOTION CALCULATION

```
% Link No. 1 - Steer Link, 2 - Upper Forward, 3 - Upper Rearward, 4 - Lower Forward, 5 - Lower
% Rearward

% Front Left

[x1fl,y1fl,z1fl]=vecsplit(H1fl);
[x1_efl,y1_efl,z1_efl]=vecsplit(Tfl);

[x2fl,y2fl,z2fl]=vecsplit(C1_1fl);
[x2_efl,y2_efl,z2_efl]=vecsplit(Pfl);

[x3fl,y3fl,z3fl]=vecsplit(C1_2fl);
[x3_efl,y3_efl,z3_efl]=vecsplit(Qfl);

[x4fl,y4fl,z4fl]=vecsplit(B1_1fl);
[x4_efl,y4_efl,z4_efl]=vecsplit(Afl);

[x5fl,y5fl,z5fl]=vecsplit(B1_2fl);
[x5_efl,y5_efl,z5_efl]=vecsplit(Gfl);

[xmfl,ymfl,zmfl]=vecsplit(E1fl);

syms Vm_x_fl Vm_y_fl Wk_x_fl Wk_y_fl Wk_z_fl

eq1_1= (Vm_x_fl + Wk_y_fl*(z1fl-zmfl)-Wk_z_fl*(y1fl-ymfl))*(x1fl-x1_efl)+...
    (Vm_y_fl + Wk_z_fl*(x1fl-xmfl)-Wk_x_fl*(z1fl-zmfl))*(y1fl-y1_efl)+...
    (Vm_z_fl + Wk_x_fl*(y1fl-ymfl)-Wk_y_fl*(x1fl-xmfl))*(z1fl-z1_efl);
eq1_2= V1e_x_fl*(x1fl-x1_efl)+V1e_y_fl*(y1fl-y1_efl)+V1e_z_fl*(z1fl-z1_efl);

eq2_1= (Vm_x_fl + Wk_y_fl*(z2fl-zmfl)-Wk_z_fl*(y2fl-ymfl))*(x2fl-x2_efl)+...
    (Vm_y_fl + Wk_z_fl*(x2fl-xmfl)-Wk_x_fl*(z2fl-zmfl))*(y2fl-y2_efl)+...
    (Vm_z_fl + Wk_x_fl*(y2fl-ymfl)-Wk_y_fl*(x2fl-xmfl))*(z2fl-z2_efl);
eq2_2= 0;

eq3_1= (Vm_x_fl + Wk_y_fl*(z3fl-zmfl)-Wk_z_fl*(y3fl-ymfl))*(x3fl-x3_efl)+...
    (Vm_y_fl + Wk_z_fl*(x3fl-xmfl)-Wk_x_fl*(z3fl-zmfl))*(y3fl-y3_efl)+...
```

```
    (Vm_z_fl + Wk_x_fl*(y3fl-ymfl)-Wk_y_fl*(x3fl-xmfl))*(z3fl-z3_efl);
eq3_2= 0;

eq4_1= (Vm_x_fl + Wk_y_fl*(z4fl-zmfl)-Wk_z_fl*(y4fl-ymfl))*(x4fl-x4_efl)+...
    (Vm_y_fl + Wk_z_fl*(x4fl-xmfl)-Wk_x_fl*(z4fl-zmfl))*(y4fl-y4_efl)+...
    (Vm_z_fl + Wk_x_fl*(y4fl-ymfl)-Wk_y_fl*(x4fl-xmfl))*(z4fl-z4_efl);
eq4_2= 0;

eq5_1= (Vm_x_fl + Wk_y_fl*(z5fl-zmfl)-Wk_z_fl*(y5fl-ymfl))*(x5fl-x5_efl)+...
    (Vm_y_fl + Wk_z_fl*(x5fl-xmfl)-Wk_x_fl*(z5fl-zmfl))*(y5fl-y5_efl)+...
    (Vm_z_fl + Wk_x_fl*(y5fl-ymfl)-Wk_y_fl*(x5fl-xmfl))*(z5fl-z5_efl);
eq5_2= 0;

S_fl = vpasolve([eq1_1== eq1_2, eq2_1== eq2_2, eq3_1== eq3_2, eq4_1== eq4_2, eq5_1== eq5_2],...
    [Vm_x_fl, Vm_y_fl, Wk_x_fl, Wk_y_fl, Wk_z_fl]);


% Front Right

[x1fr,y1fr,z1fr]=vecsplit(H1fr);
[x1_efr,y1_efr,z1_efr]=vecsplit(Tfr);

[x2fr,y2fr,z2fr]=vecsplit(C1_1fr);
[x2_efr,y2_efr,z2_efr]=vecsplit(Pfr);

[x3fr,y3fr,z3fr]=vecsplit(C1_2fr);
[x3_efr,y3_efr,z3_efr]=vecsplit(Qfr);

[x4fr,y4fr,z4fr]=vecsplit(B1_1fr);
[x4_efr,y4_efr,z4_efr]=vecsplit(Afr);

[x5fr,y5fr,z5fr]=vecsplit(B1_2fr);
[x5_efr,y5_efr,z5_efr]=vecsplit(Gfr);

[xmfr,ymfr,zmfr]=vecsplit(E1fr);

syms Vm_x_fr Vm_y_fr Wk_x_fr Wk_y_fr Wk_z_fr

eq1_1= (Vm_x_fr + Wk_y_fr*(z1fr-zmfr)-Wk_z_fr*(y1fr-ymfr))*(x1fr-x1_efr)+...
    (Vm_y_fr + Wk_z_fr*(x1fr-xmfr)-Wk_x_fr*(z1fr-zmfr))*(y1fr-y1_efr)+...
    (Vm_z_fr + Wk_x_fr*(y1fr-ymfr)-Wk_y_fr*(x1fr-xmfr))*(z1fr-z1_efr);
eq1_2= V1e_x_fr*(x1fr-x1_efr)+V1e_y_fr*(y1fr-y1_efr)+V1e_z_fr*(z1fr-z1_efr);

eq2_1= (Vm_x_fr + Wk_y_fr*(z2fr-zmfr)-Wk_z_fr*(y2fr-ymfr))*(x2fr-x2_efr)+...
    (Vm_y_fr + Wk_z_fr*(x2fr-xmfr)-Wk_x_fr*(z2fr-zmfr))*(y2fr-y2_efr)+...
    (Vm_z_fr + Wk_x_fr*(y2fr-ymfr)-Wk_y_fr*(x2fr-xmfr))*(z2fr-z2_efr);
eq2_2= 0;

eq3_1= (Vm_x_fr + Wk_y_fr*(z3fr-zmfr)-Wk_z_fr*(y3fr-ymfr))*(x3fr-x3_efr)+...
    (Vm_y_fr + Wk_z_fr*(x3fr-xmfr)-Wk_x_fr*(z3fr-zmfr))*(y3fr-y3_efr)+...
    (Vm_z_fr + Wk_x_fr*(y3fr-ymfr)-Wk_y_fr*(x3fr-xmfr))*(z3fr-z3_efr);
eq3_2= 0;

eq4_1= (Vm_x_fr + Wk_y_fr*(z4fr-zmfr)-Wk_z_fr*(y4fr-ymfr))*(x4fr-x4_efr)+...
    (Vm_y_fr + Wk_z_fr*(x4fr-xmfr)-Wk_x_fr*(z4fr-zmfr))*(y4fr-y4_efr)+...
    (Vm_z_fr + Wk_x_fr*(y4fr-ymfr)-Wk_y_fr*(x4fr-xmfr))*(z4fr-z4_efr);
```

```
eq4_2= 0;

eq5_1= (Vm_x_fr + Wk_y_fr*(z5fr-zmfr)-Wk_z_fr*(y5fr-ymfr))*(x5fr-x5_efr)+...
    (Vm_y_fr + Wk_z_fr*(x5fr-xmfr)-Wk_x_fr*(z5fr-zmfr))*(y5fr-y5_efr)+...
    (Vm_z_fr + Wk_x_fr*(y5fr-ymfr)-Wk_y_fr*(x5fr-xmfr))*(z5fr-z5_efr);
eq5_2= 0;

S_fr = vpasolve([eq1_1== eq1_2, eq2_1== eq2_2, eq3_1== eq3_2, eq4_1== eq4_2, eq5_1== eq5_2],...
    [Vm_x_fr, Vm_y_fr, Wk_x_fr, Wk_y_fr, Wk_z_fr]);


% Rear Left

[x1rl,y1rl,z1rl]=vecsplit(H1rl);
[x1_erl,y1_erl,z1_erl]=vecsplit(Trl);

[x2rl,y2rl,z2rl]=vecsplit(C1_1rl);
[x2_erl,y2_erl,z2_erl]=vecsplit(Prl);

[x3rl,y3rl,z3rl]=vecsplit(C1_2rl);
[x3_erl,y3_erl,z3_erl]=vecsplit(Qrl);

[x4rl,y4rl,z4rl]=vecsplit(B1_1rl);
[x4_erl,y4_erl,z4_erl]=vecsplit(Arl);

[x5rl,y5rl,z5rl]=vecsplit(B1_2rl);
[x5_erl,y5_erl,z5_erl]=vecsplit(Grl);

[xmrl,ymrl,zmrl]=vecsplit(E1rl);

syms Vm_x_rl Vm_y_rl Wk_x_rl Wk_y_rl Wk_z_rl

eq1_1= (Vm_x_rl + Wk_y_rl*(z1rl-zmrl)-Wk_z_rl*(y1rl-ymrl))*(x1rl-x1_erl)+...
    (Vm_y_rl + Wk_z_rl*(x1rl-xmrl)-Wk_x_rl*(z1rl-zmrl))*(y1rl-y1_erl)+...
    (Vm_z_rl + Wk_x_rl*(y1rl-ymrl)-Wk_y_rl*(x1rl-xmrl))*(z1rl-z1_erl);
eq1_2= V1e_x_rl*(x1rl-x1_erl)+V1e_y_rl*(y1rl-y1_erl)+V1e_z_rl*(z1rl-z1_erl);

eq2_1= (Vm_x_rl + Wk_y_rl*(z2rl-zmrl)-Wk_z_rl*(y2rl-ymrl))*(x2rl-x2_erl)+...
    (Vm_y_rl + Wk_z_rl*(x2rl-xmrl)-Wk_x_rl*(z2rl-zmrl))*(y2rl-y2_erl)+...
    (Vm_z_rl + Wk_x_rl*(y2rl-ymrl)-Wk_y_rl*(x2rl-xmrl))*(z2rl-z2_erl);
eq2_2= 0;

eq3_1= (Vm_x_rl + Wk_y_rl*(z3rl-zmrl)-Wk_z_rl*(y3rl-ymrl))*(x3rl-x3_erl)+...
    (Vm_y_rl + Wk_z_rl*(x3rl-xmrl)-Wk_x_rl*(z3rl-zmrl))*(y3rl-y3_erl)+...
    (Vm_z_rl + Wk_x_rl*(y3rl-ymrl)-Wk_y_rl*(x3rl-xmrl))*(z3rl-z3_erl);
eq3_2= 0;

eq4_1= (Vm_x_rl + Wk_y_rl*(z4rl-zmrl)-Wk_z_rl*(y4rl-ymrl))*(x4rl-x4_erl)+...
    (Vm_y_rl + Wk_z_rl*(x4rl-xmrl)-Wk_x_rl*(z4rl-zmrl))*(y4rl-y4_erl)+...
    (Vm_z_rl + Wk_x_rl*(y4rl-ymrl)-Wk_y_rl*(x4rl-xmrl))*(z4rl-z4_erl);
eq4_2= 0;

eq5_1= (Vm_x_rl + Wk_y_rl*(z5rl-zmrl)-Wk_z_rl*(y5rl-ymrl))*(x5rl-x5_erl)+...
    (Vm_y_rl + Wk_z_rl*(x5rl-xmrl)-Wk_x_rl*(z5rl-zmrl))*(y5rl-y5_erl)+...
    (Vm_z_rl + Wk_x_rl*(y5rl-ymrl)-Wk_y_rl*(x5rl-xmrl))*(z5rl-z5_erl);
eq5_2= 0;
```

```
S_rl = vpasolve([eq1_1== eq1_2, eq2_1== eq2_2, eq3_1== eq3_2, eq4_1== eq4_2, eq5_1== eq5_2],...
    [Vm_x_rl, Vm_y_rl, Wk_x_rl, Wk_y_rl, Wk_z_rl]);

% Rear Right

[x1rr,y1rr,z1rr]=vecsplit(H1rr);
[x1_err,y1_err,z1_err]=vecsplit(Trr);

[x2rr,y2rr,z2rr]=vecsplit(C1_1rr);
[x2_err,y2_err,z2_err]=vecsplit(Prr);

[x3rr,y3rr,z3rr]=vecsplit(C1_2rr);
[x3_err,y3_err,z3_err]=vecsplit(Qrr);

[x4rr,y4rr,z4rr]=vecsplit(B1_1rr);
[x4_err,y4_err,z4_err]=vecsplit(Arr);

[x5rr,y5rr,z5rr]=vecsplit(B1_2rr);
[x5_err,y5_err,z5_err]=vecsplit(Grr);

[xmrr,ymrr,zmrr]=vecsplit(E1rr);

syms Vm_x_rr Vm_y_rr Wk_x_rr Wk_y_rr Wk_z_rr

eq1_1= (Vm_x_rr + Wk_y_rr*(z1rr-zmrr)-Wk_z_rr*(y1rr-ymrr))*(x1rr-x1_err)+...
    (Vm_y_rr + Wk_z_rr*(x1rr-xmrr)-Wk_x_rr*(z1rr-zmrr))*(y1rr-y1_err)+...
    (Vm_z_rr + Wk_x_rr*(y1rr-ymrr)-Wk_y_rr*(x1rr-xmrr))*(z1rr-z1_err);
eq1_2= V1e_x_rr*(x1rr-x1_err)+V1e_y_rr*(y1rr-y1_err)+V1e_z_rr*(z1rr-z1_err);

eq2_1= (Vm_x_rr + Wk_y_rr*(z2rr-zmrr)-Wk_z_rr*(y2rr-ymrr))*(x2rr-x2_err)+...
    (Vm_y_rr + Wk_z_rr*(x2rr-xmrr)-Wk_x_rr*(z2rr-zmrr))*(y2rr-y2_err)+...
    (Vm_z_rr + Wk_x_rr*(y2rr-ymrr)-Wk_y_rr*(x2rr-xmrr))*(z2rr-z2_err);
eq2_2= 0;

eq3_1= (Vm_x_rr + Wk_y_rr*(z3rr-zmrr)-Wk_z_rr*(y3rr-ymrr))*(x3rr-x3_err)+...
    (Vm_y_rr + Wk_z_rr*(x3rr-xmrr)-Wk_x_rr*(z3rr-zmrr))*(y3rr-y3_err)+...
    (Vm_z_rr + Wk_x_rr*(y3rr-ymrr)-Wk_y_rr*(x3rr-xmrr))*(z3rr-z3_err);
eq3_2= 0;

eq4_1= (Vm_x_rr + Wk_y_rr*(z4rr-zmrr)-Wk_z_rr*(y4rr-ymrr))*(x4rr-x4_err)+...
    (Vm_y_rr + Wk_z_rr*(x4rr-xmrr)-Wk_x_rr*(z4rr-zmrr))*(y4rr-y4_err)+...
    (Vm_z_rr + Wk_x_rr*(y4rr-ymrr)-Wk_y_rr*(x4rr-xmrr))*(z4rr-z4_err);
eq4_2= 0;

eq5_1= (Vm_x_rr + Wk_y_rr*(z5rr-zmrr)-Wk_z_rr*(y5rr-ymrr))*(x5rr-x5_err)+...
    (Vm_y_rr + Wk_z_rr*(x5rr-xmrr)-Wk_x_rr*(z5rr-zmrr))*(y5rr-y5_err)+...
    (Vm_z_rr + Wk_x_rr*(y5rr-ymrr)-Wk_y_rr*(x5rr-xmrr))*(z5rr-z5_err);
eq5_2= 0;

S_rr = vpasolve([eq1_1== eq1_2, eq2_1== eq2_2, eq3_1== eq3_2, eq4_1== eq4_2, eq5_1== eq5_2],...
    [Vm_x_rr, Vm_y_rr, Wk_x_rr, Wk_y_rr, Wk_z_rr]);
```

OUTPUT CALCULATIONS

```
% Front Left
```

```
Vm_fl = [S_fl.Vm_x_fl S_fl.Vm_y_fl Vm_z_fl]; % WLC Velocity
Wk_fl = [S_fl.Wk_x_fl S_fl.Wk_y_fl S_fl.Wk_z_fl]; % WLC Angular Velocity
eW_fl = Wk_fl/norm(Wk_fl); % WLC Angular Velocity Direction Vector
t_fl = dot(Vm_fl,eW_fl); % Shift Velocity (scalar)
t_fl_vec = t_fl*eW_fl; % Shift Velocity Vector
u_vec_fl = Vm_fl-t_fl_vec; % Circumferential Velocity Vector
u_fl = norm(u_vec_fl); % Circumferential Velocity Scalar
alpha_fl = atan(t_fl/u_fl); % Helix angle of screw
r_m_fl = u_fl/norm(Wk_fl); % Radius from WLC to screw axis
H_fl = 2*pi*r_m_fl*tan(alpha_fl); % Pitch of screw

% Front Right
Vm_fr = [S_fr.Vm_x_fr S_fr.Vm_y_fr Vm_z_fr]; % Same as Front Left
Wk_fr = [S_fr.Wk_x_fr S_fr.Wk_y_fr S_fr.Wk_z_fr];
eW_fr = Wk_fr/norm(Wk_fr);
t_fr = dot(Vm_fr,eW_fr);
t_fr_vec = t_fr*eW_fr;
u_vec_fr = Vm_fr-t_fr_vec;
u_fr = norm(u_vec_fr);
alpha_fr = atan(t_fr/u_fr);
r_m_fr = u_fr/norm(Wk_fr);
H_fr=2*pi*r_m_fr*tan(alpha_fr);

% Rear Left

Vm_rl = [S_rl.Vm_x_rl S_rl.Vm_y_rl Vm_z_rl]; % Same as Front Left
Wk_rl = [S_rl.Wk_x_rl S_rl.Wk_y_rl S_rl.Wk_z_rl];
eW_rl = Wk_rl/norm(Wk_rl);
t_rl = dot(Vm_rl,eW_rl);
t_rl_vec = t_rl*eW_rl;
u_vec_rl = Vm_rl-t_rl_vec;
u_rl = norm(u_vec_rl);
alpha_rl = atan(t_rl/u_rl);
r_m_rl = u_rl/norm(Wk_rl);
H_rl=2*pi*r_m_rl*tan(alpha_rl);

% Rear Right

Vm_rr = [S_rr.Vm_x_rr S_rr.Vm_y_rr Vm_z_rr]; % Same as Front Left
Wk_rr = [S_rr.Wk_x_rr S_rr.Wk_y_rr S_rr.Wk_z_rr];
eW_rr = Wk_rr/norm(Wk_rr);
t_rr = dot(Vm_rr,eW_rr);
t_rr_vec = t_rr*eW_rr;
u_vec_rr = Vm_rr-t_rr_vec;
u_rr = norm(u_vec_rr);
alpha_rr = atan(t_rr/u_rr);
r_m_rr = u_rr/norm(Wk_rr);
H_rr=2*pi*r_m_rr*tan(alpha_rr);
```

OUTPUT

```
% Screw Axis Intersection with Wheel Planes Calculation

% Front Left
syms r1 r2 r3
```

```
R_fl=vpasolve([u_vec_fl(1)==Wk_fl(2)*r3-Wk_fl(3)*r2, u_vec_fl(2)==Wk_fl(3)*r1-Wk_fl(1)*r3, u_vec_fl(3)=
r_m_fl_vec = [R_fl.r1, R_fl.r2, R_fl.r3]+ShiftVecFL;

y_yz_fl= -(r_m_fl_vec(2)*eW_fl(1)-r_m_fl_vec(1)*eW_fl(2))/eW_fl(1);
z_yz_fl= -(r_m_fl_vec(3)*eW_fl(1)-r_m_fl_vec(1)*eW_fl(3))/eW_fl(1);

yz_fl = [y_yz_fl z_yz_fl]; % Y and Z coordinates of Front Left Susp Screw Axis intersection with YZ whe

x_xz_fl= (r_m_fl_vec(1)*eW_fl(2)-r_m_fl_vec(2)*eW_fl(1))/eW_fl(2);
z_xz_fl= (r_m_fl_vec(3)*eW_fl(2)-r_m_fl_vec(2)*eW_fl(3))/eW_fl(2);

xz_fl = [x_xz_fl z_xz_fl]; % X and Z coordinates of Front Left Susp Screw Axis intersection with XZ whe

% Front Right
clear r1 r2 r3
syms r1 r2 r3
R_fr=vpasolve([u_vec_fr(1)==Wk_fr(2)*r3-Wk_fr(3)*r2, u_vec_fr(2)==Wk_fr(3)*r1-Wk_fr(1)*r3, u_vec_fr(3)=
r_m_fr_vec = [R_fr.r1, R_fr.r2, R_fr.r3]+ShiftVecFR;

y_yz_fr= -(r_m_fr_vec(2)*eW_fr(1)-r_m_fr_vec(1)*eW_fr(2))/eW_fr(1);
z_yz_fr= -(r_m_fr_vec(3)*eW_fr(1)-r_m_fr_vec(1)*eW_fr(3))/eW_fr(1);

yz_fr = [y_yz_fr z_yz_fr];

x_xz_fr= (r_m_fr_vec(1)*eW_fr(2)-r_m_fr_vec(2)*eW_fr(1))/eW_fr(2);
z_xz_fr= (r_m_fr_vec(3)*eW_fr(2)-r_m_fr_vec(2)*eW_fr(3))/eW_fr(2);

xz_fr = [x_xz_fr z_xz_fr];

% Rear Left
clear r1 r2 r3
syms r1 r2 r3
R_rl=vpasolve([u_vec_rl(1)==Wk_rl(2)*r3-Wk_rl(3)*r2, u_vec_rl(2)==Wk_rl(3)*r1-Wk_rl(1)*r3, u_vec_rl(3)=
r_m_rl_vec = [R_rl.r1, R_rl.r2, R_rl.r3]+ShiftVecRL;

y_yz_rl= (r_m_rl_vec(2)*eW_rl(1)-r_m_rl_vec(1)*eW_rl(2))/eW_rl(1);
z_yz_rl= (r_m_rl_vec(3)*eW_rl(1)-r_m_rl_vec(1)*eW_rl(3))/eW_rl(1);

yz_rl = [y_yz_rl z_yz_rl];

x_xz_rl= (r_m_rl_vec(1)*eW_rl(2)-r_m_rl_vec(2)*eW_rl(1))/eW_rl(2);
z_xz_rl= (r_m_rl_vec(3)*eW_rl(2)-r_m_rl_vec(2)*eW_rl(3))/eW_rl(2);

xz_rl = [x_xz_rl z_xz_rl];

% Rear Right
clear r1 r2 r3
syms r1 r2 r3
R_rr=vpasolve([u_vec_rr(1)==Wk_rr(2)*r3-Wk_rr(3)*r2, u_vec_rr(2)==Wk_rr(3)*r1-Wk_rr(1)*r3, u_vec_rr(3)=
r_m_rr_vec = [R_rr.r1, R_rr.r2, R_rr.r3]+ShiftVecRR;

y_yz_rr= (r_m_rr_vec(2)*eW_rr(1)-r_m_rr_vec(1)*eW_rr(2))/eW_rr(1);
z_yz_rr= (r_m_rr_vec(3)*eW_rr(1)-r_m_rr_vec(1)*eW_rr(3))/eW_rr(1);

yz_rr = [y_yz_rr z_yz_rr];
```

```
x_xz_rr= (r_m_rr_vec(1)*eW_rr(2)-r_m_rr_vec(2)*eW_rr(1))/eW_rr(2);
z_xz_rr= (r_m_rr_vec(3)*eW_rr(2)-r_m_rr_vec(2)*eW_rr(3))/eW_rr(2);

xz_rr = [x_xz_rr z_xz_rr];
```

ROLL CENTRE CALCULATION

```
ICz_fr=(yz_fr(2)-(t_fr_vec(2)/Wk_fr(1))); % Instant Center point including "transition vector" or offse
ICy_fr=(yz_fr(1)+(t_fr_vec(3)/Wk_fr(1))); % Instant Center point including "transition vector" or offse

ICz_fl=(yz_fl(2)-(t_fl_vec(2)/Wk_fl(1)));
ICy_fl=(yz_fl(1)+(t_fl_vec(3)/Wk_fl(1)));

cpfl=cpfl-ShiftVecFL;
cpfr=cpfr-ShiftVecFR;

% Roll centre calculation from Instant centers found above
syms rcy_f rcz_f
eq1=(ICy_fl-cpfl(2))*(rcz_f-cpfl(3))-(rcy_f-cpfl(2))*(ICz_fl-cpfl(3));
eq2=(ICy_fr-cpfr(2))*(rcz_f-cpfr(3))-(rcy_f-cpfr(2))*(ICz_fr-cpfr(3));

RCf=vpasolve([eq1==0,eq2==0],[rcy_f,rcz_f]);
RC_Front=[RCf.rcy_f, RCf.rcz_f]

ICz_rr=(yz_rr(2)-(t_rr_vec(2)/Wk_rr(1)));
ICy_rr=(yz_rr(1)+(t_rr_vec(3)/Wk_rr(1)));

ICz_rl=(yz_rl(2)-(t_rl_vec(2)/Wk_rl(1)));
ICy_rl=(yz_rl(1)+(t_rl_vec(3)/Wk_rl(1)));

cprl=cprl-ShiftVecRL;
cprr=cprr-ShiftVecRR;

syms rcy_r rcz_r
eq1=(ICy_rl-cprl(2))*(rcz_r-cprl(3))-(rcy_r-cprl(2))*(ICz_rl-cprl(3));
eq2=(ICy_rr-cprr(2))*(rcz_r-cprr(3))-(rcy_r-cprr(2))*(ICz_rr-cprr(3));

RCr=vpasolve([eq1==0,eq2==0],[rcy_r,rcz_r]);
RC_Rear=[RCr.rcy_r, RCr.rcz_r]

debug_fl=[t_fl_vec(2),Wk_fl(1),(t_fr_vec(2)/Wk_fr(1)),yz_fl(2),ICz_fr]'
```

```
RC_Front =

[ 0, 158.75879547631391603065540535451]


RC_Rear =

[ 0, 127.25374098395952201528689848208]


debug_fl =

 0.00000000091785938859863100368466131043141
      -0.0032905283334976389740895407380607
```

```
  -0.0000002789398222938260524881014326686 4
          634.8314172217677800558086341068 9
          634.8314175007076023496346865949 9
```

PLOT

```
figure(1)
plot(RC_Front(1),RC_Front(2),'*')
hold on
plot(ICy_fr,ICz_fr,'*r')
plot(ICy_fl,ICz_fl,'*r')
plot(cpfr(2),cpfr(3),'*g')
plot(cpfl(2),cpfl(3),'*g')
plot([cpfr(2),ICy_fr],[cpfr(3),ICz_fr])
plot([cpfl(2),ICy_fl],[cpfl(3),ICz_fl])
axis equal
```

References

[1] Harold Mooz Kevin Forsberg. "Relationship of System Engineering to the Project Cycle". In: *Center for Systems Management* (1995).

[2] International Standards Organisation. "ISO 8855:2011, Road Vehicles - Vehicle Dynamics and Road Holding Ability - Vocabulary". In: *International Standards Organisation* ().

[3] China Euro Vehicle Technology AB. *MSC Adams Car model of a rear wheel suspension system with subframe*. 2018.

[4] Reza N. Jazar. *Vehicle Dynamics: Theory and Applications*. 2008, p. 455.

[5] Gede. *Panhard rod*. 2. April 2011. URL: http://commons.wikimedia.org/wiki/File:Panhard_rod.svg.

[6] Arnero. *Typical car suspension seen from behind. Omitted for clarity: springs, steering, breaks, shaft*. 2. June 2009. URL: http://commons.wikimedia.org/wiki/File:Panhard_rod.svg.

[7] Wolfgang Matschinsky. *Road Vehicle Suspension*. Professional Engineering Publishing Limited, 2000. ISBN: 1 86058 202 8.

[8] J. M. McCarthy and G. S. Soh. *Geometric Design of Linkages*. Springer, New York, NY, 2010. ISBN: 978-1-4419-7892-9.

[9] G. R. Pennock J. J. Uicker and J. E. Shigley. *Theory of Machines and Mechanisms, Third Edition*. Oxford University Press, 2003. ISBN: 9780195155983.

[10] Levinson D. A Kane T. R. *Dynamics, Theory and Applications*. McGraw-Hill, New York, 1985. ISBN: 0-07-037846-0.

[11] C.H.Suh. "Suspension Analysis using Instant Screw Theory". In: *SAE International* (1991), pp. 143–151.

[12] Société de Technologie Michelin. *The Tire,Grip*. 2001.

[13] Douglas L. Milliken William F. Milliken. *Race Car Vehicle Dynamics*. SAE International, 1994. ISBN: 978-1-56091-526-3.

[14] Igo Besselink Hans B. Pacejka. *Tire and Vehicle Dynamics*. SAE International, 2012, p. 8. ISBN: 1 86058 202 8.

[15] Wheel Alignment Center. *Camber Alignment*. URL: http://www.wheelalignmentcentrebirmingham.co.uk/what-is-wheel-alignment.html.

[16] Wheel Alignment Center. *Toe Alignment*. June 2009. URL: http://www.wheelalignmentcentrebirmingham.co.uk/what-is-wheel-alignment.html.

[17] SAE International. "Vehicle Dynamics Terminology J670$_2$00801". In: *SAE International* (2008).

[18] Madhusudan Raghavan. "Design Innovation". In: *Journal of Mechanical Design* 2 (July 2005), pp. 673–678.

[19] Roll Center Location. "Output of Suspension Analysis". In: *MSC Adams Car Help* (2018).

[20] Harold Rothbart and Thomas H. Brown. *Mechanical Design Handbook, Measurement, Analysis, and Control of Dynamic Systems*. The McGraw-Hill Companies, Inc, 2006. ISBN: 9780071466363.

[21] Bengt Jacobson. *Vehicle Dynamics Compendium for Course MMF062*. 2017.